Online Analysis of Microbial γ-Polyglutamic Acid Production and Plant Defense Priming in Small-Scale Cell Culture

Onlineanalyse der mikrobiellen γ-Polyglutaminsäureproduktion und des Abwehr-Primings in Zellkulturen im Kleinkulturmaßstab

Von der Fakultät für Maschinenwesen der Rheinisch-Westfälischen Technischen Hochschule Aachen zur Erlangung des akademischen Grades einer Doktorin der Naturwissenschaften genehmigte Dissertation

vorgelegt von

Kyra Hoffmann, geb. Bratz

Berichter: Universitätsprofessor Dr.-Ing. Dr. h. c. (Osaka) Jochen Büchs
Universitätsprofessor Dr. rer. nat. Uwe Conrath

Tag der mündlichen Prüfung: 14. Februar 2024

Diese Dissertation ist auf den Internetseiten der Universitätsbibliothek online verfügbar.

Danksagung

Ganz herzlich bedanke ich mich bei Herrn Büchs für seine wissenschaftliche Unterstützung in den letzten Jahren. Seine Begeisterung für die Wissenschaft und Forschung waren ansteckend und haben über so manche Durststrecke hinweggeholfen.

Auch den Kolleg*innen und Projektpartner*innen gilt mein besonderer Dank. Ihr stehts offenes Ohr und ihre Hilfsbereitschaft, das Diskutieren von unerwarteten Versuchsergebnissen und die vielen konstruktiven Besprechungen haben mich immer wieder motiviert. Der Teamgeist und die freundschaftliche, respektvolle Atmosphäre am Lehrstuhl für Bioverfahrenstechnik haben meine Promotionszeit bereichert.

Den Studierenden, insbesondere Simon Briel, danke ich für ihr Engagement in der Forschung und die vielen interessanten Gespräche und Ideen.

Meiner Familie danke ich ganz besonders. Sie hat mich getragen und motiviert durchzuhalten.

Abstract

The development of online analytical tools significantly accelerates research of bioprocesses in small shaken cultures. This thesis demonstrates the application of online analytics for two processes. Firstly for the production of poly-γ-glutamic acid (γ-PGA) in shake flasks and secondly for the detection of priming-active compounds with parsley cell cultures in microtiter plates. These two diverse research topics demonstrate the power of online analytic tools in small culture scale.

The first chapter of this thesis is about the online screening of γ-PGA, a biopolymer with a wide range of applications. The γ-PGA was produced with genetically modified *Bacillus subtilis* 168 strains. The formation and concomitant secretion of γ-PGA increase the culture broth viscosity, while enzymatic depolymerization and degradation of γ-PGA by native depolymerases decrease the viscosity. The viscosity monitoring online system (ViMOS) was applied for optical online measurements of broth viscosity in shake flasks. This online monitoring enabled the analysis of the promoter P_{pst} in combination with different γ-PGA depolymerase and by-product knockout mutants in genetically modified *B. subtilis* 168 strains. The different single depolymerase knockout mutants were Δ*ggt,* Δ*pgdS,* Δ*cwlO,* and a triple knockout mutant. Additionally, to the P_{pst} promoter, the γ-PGA production under the control of the P_{xyl} promoter was analyzed. An increase in γ-PGA yield in $g_{\gamma\text{-PGA}}/g_{glucose}$ of 190% could be achieved with the triple knockout mutant compared to the P_{pst} reference strain. The strain with the P_{xyl} promoter produced even 8.4 $g_{\gamma\text{-PGA}}/mol_{carbon}$. This is a higher γ-PGA yield than achieved using the glutamic acid-dependent γ-PGA producer *Bacillus licheniformis* ATCC 9945. Therefore, *Bacillus subtilis* P_{xyl} is a promising candidate for γ-PGA production with glucose as the sole carbon source.

The second chapter of this thesis presents a biochemical approach to detect defense priming in parsley cell cultures in microtiter plates. Conventional crop protection has major drawbacks, such as developing pest and pathogen insensitivity to pesticides and low environmental compatibility. Therefore, alternative crop protection strategies are needed. One approach treats crops with chemical compounds that induce a primed state of enhanced defense. Online identification of priming-inducing chemistry by recording breathing activity with the oxygen transfer rate (OTR) represents a highly informative approach to spot priming-activating chemistry. This thesis shows the online measurement of the dissolved oxygen tension (DOT) in microtiter plates (MTPs) and the calculation of the OTR from the DOT to be a valid tool to draw conclusions regarding priming-inducing activity. Furthermore, the fluorescence of the priming-active reference compound salicylic acid (SA) and furanocoumarins was simultaneously monitored online in MTPs. Determining the OTR, fluorescence of the priming-active chemical compound SA, and furanocoumarins in parsley suspension cultures in MTPs by online measurement allows an in-depth screening for priming compounds and a better understanding of the priming process induced by a given substance.

Zusammenfassung

Die Entwicklung von Online-Analytik vereinfacht und beschleunigt die Erforschung von Bioprozessen im Kleinkulturmaßstab erheblich. Diese Arbeit demonstriert die Möglichkeiten der Online-Analytik anhand zweier Prozesse. Zum einen für die Herstellung von Poly-γ-glutaminsäure (γ-PGA) in Schüttelkolben und zum anderen für die Erforschung von priming-induzierenden Komponenten unter Verwendung von Petersilienzellkulturen in Mikrotiterplatten. Diese beiden unterschiedlichen Forschungsthemen demonstrieren die Bedeutung von Online-Analysetools für die Forschung im Kleinkulturmaßstab

Das erste Kapitel dieser Arbeit befasst sich mit dem Online-Screening der Poly-γ-Glutaminsäure (γ-PGA) Produktion in gentechnisch veränderten *B. subtilis* 168-Stämmen. γ-PGA ist ein vielseitig einsetzbares Biopolymer. Durch die Sekretion von γ-PGA wird die Viskosität der Fermentationsbrühe erhöht, während enzymatische Hydrolyse von γ-PGA die Viskosität verringert. Das *viscosity monitoring online system* (ViMOS) wurde für optische online Messungen der Viskosität in Schüttelkolben eingesetzt. Damit wurde die γ-PGA-Produktion unter Kontrolle des P_{pst} und P_{xyl} Promotors analysiert. Zusätzlich wurden der Effekt von γ-PGA-Depolymerasen- und Nebenprodukt-Deletionsmutanten untersucht. Mit der Dreifach-Knockout-Mutante Δggt, ΔpgdS, ΔcwlO konnte im Vergleich zum P_{pst}-Referenzstamm eine Steigerung des γ-PGA-Ertrags von 190 % erzielt werden. Mit dem P_{xyl}-Promotor wurden sogar 8,4 $g_{\gamma\text{-PGA}}/mol_{Kohlenstoff}$ erreicht. Das entspricht einer höheren γ-PGA-Ausbeute als mit dem Glutamat abhängigen Wildtypproduzenten *B. licheniformis* ATCC 9945 erreicht wurde. Daher ist *B. subtilis* P_{xyl} ein vielversprechender Kandidat für die γ-PGA-Produktion mit Glucose als einziger Kohlenstoffquelle.

Im zweiten Kapitel dieser Arbeit wird ein biochemischer Ansatz zum Nachweis der Abwehrreaktionen von Petersilienzellkulturen in Mikrotiterplatten vorgestellt. Der konventionelle Pflanzenschutz hat große Nachteile, wie z. B. die Resistenzbildung von Schädlingen und Krankheitserregern gegenüber Pestiziden und die geringe Umweltverträglichkeit. Eine alternative Pflanzenschutzstrategie besteht darin, Nutzpflanzen mit chemischen Verbindungen zu behandeln, die einen Zustand der verstärkten Abwehr hervorrufen. Über die mit der Sauerstofftransferrate (OTR) aufgenommene Atmungsaktivität lassen sich priming-induzierende chemische Komponenten identifizieren. Diese Arbeit zeigt, dass die online Messung des gelöst Sauerstoffdrucks (DOT) in MTPs und die Berechnung des OTR aus dem DOT Rückschlüsse auf die priming-induzierende Aktivität zulässt. Darüber hinaus wurden die Fluoreszenzen der priming-aktiven Referenzverbindung Salicylsäure und von Furanocumarinen in MTPs simultan online überwacht. Die Bestimmung des OTR, der Fluoreszenz der priming-aktiven Salicylsäure und der Furanocumarine in Petersiliensuspensionskulturen in MTPs ermöglicht ein online-Hochdurchsatz Screening nach priming-aktiven Verbindungen.

Funding, publications, and contributions

The data of the first chapter of this work were performed as a part of the project "Selective Production and Analysis of Poly (γ-glutamic acid) (γ-PGA) with Distinct Molecular Weight Distribution and Composition", which was funded by the "Deutsche Forschungsgemeinschaft" (DFG) within the International Research Training Group 1628, "Selectivity in Chemo- and Biocatalysis (SeleCa)".

Parts of this thesis have already been published as scientific journal articles. The publications are inserted in the thesis. Some of the presented data originate from the work of other people contributing to the cooperative publications. This is explicitly stated in the author's contributions to the respective publication or directly at specific parts in the thesis:

- Hoffmann K, Halmschlag B, Briel S, Sieben M, Putri S, Fukusaki E, Blank LM, Büchs J.
  Online measurement of the viscosity in shake flasks enables monitoring of gamma-PGA production in depolymerase knockout mutants of *Bacillus subtilis* with the phosphate-starvation inducible promoter P_{pst}. Biotechnol Prog. doi:10.1002/btpr.3293.

  This journal article is reproduced in Chapter 1

  Authors' contributions: Kyra Hoffmann: Conceptualization (lead); data curation (lead); investigation (lead); methodology (lead); writing – original draft (lead). Birthe Halmschlag: Investigation (supporting); methodology (supporting); resources (supporting); validation (supporting); writing – review and editing (supporting). Simon Briel: Data curation (supporting); investigation (supporting); writing – original draft (supporting); writing – review and editing (supporting). Michaela Sieben: Methodology (supporting); resources (supporting); writing – review and editing (supporting). Sastia Putri: Writing – review and editing (supporting). Eiichiro Fukusaki: Writing – review and editing (supporting). Lars M. Blank: Funding acquisition (supporting); supervision (supporting); writing – review and editing (supporting). Jochen Büchs: Conceptualization (supporting); funding acquisition (lead); methodology (supporting);

project administration (supporting); resources (supporting); supervision (supporting); writing – review and editing (supporting)

- Hoffmann K, Schilling JV, Wandrey G, Welters T, Mahr S, Conrath U, Büchs J. Spotting priming-active compounds using parsley cell cultures in microtiter plates. BMC Plant Biology. 2023; doi:10.1186/s12870-023-04043-y.

  This journal article is reproduced in Chapter 2

  Authors' contributions: Kyra Hoffmann analyzed data, prepared the final form of the figures, and drafted the manuscript. Jana Schilling designed experiments, performed experiments, analyzed data, and prepared figures. Tim Welters performed the experiments shown in Fig. 3e and f and Additional files 1e, f, g, and h. Simon Mahr performed the experiments shown in 3c and d. Georg Wandrey built the BioLector device and supported the experiments performed with the BioLector. Uwe Conrath assisted with the data analysis and revised the manuscript. Jochen Büchs initiated the study and assisted with data analysis and manuscript preparation. The authors read and approved the final manuscript.

Data from the second publication "Spotting priming-active compounds using parsley cell cultures in microtiter plates " are taken from and based on parts of the dissertation of Jana Viola Schilling: "A Biochemical Engineering Approach to Identify Priming-Inducing Compounds in Parsley Cells", who is also one of the authors of the journal article:

- A Biochemical Engineering Approach to Identify Priming-Inducing Compounds in Parsley Cells. *PhD thesis.* RWTH Aachen University.

The author supervised the student thesis of Simon Briel. The thesis was developed as a cooperation between the author and the student. The valuable work of Simon Briel is strongly acknowledged as he assisted in generating data and performing exploratory work that supported the research presented in this dissertation. Some of the work described in Chapter 1 of this thesis is in parts based on the following student thesis:

- Simon Briel (2018): Screening and Characterization of the Poly(γ-glutamic acid) Production under the Control of different Promoter Systems in *Bacillus subtilis* 168 Derivatives with an Online Viscosity Measurement System. *Master's thesis.* RWTH Aachen University.

Contents

1 Poly-γ-glutamic acid production with *Bacillus licheniformis* and *Bacillus subtilis*..... 1

1.1 Introduction..... 1

1.1.1 Inserted promoter systems enable γ-PGA production in *B. subtilis* 168 2

1.1.2 Depolymerase knockouts may prevent degradation of γ-PGA..... 3

1.1.3 By-product knockouts can increase the precursor supply for γ-PGA production 5

1.1.4 Online measuring techniques for γ-PGA fermentation..... 6

1.2 Materials and methods..... 9

1.2.1 Medium composition 9

1.2.2 Bacterial strains and strain development 9

1.2.3 Shake flask cultivation..... 12

1.2.4 Oxygen transfer rate (OTR) 12

1.2.5 Online measured viscosity 12

1.2.6 Offline measured viscosity..... 13

1.2.7 Cetyltrimethylammonium bromide assay 13

1.2.8 Gel permeation chromatography..... 13

1.2.9 HPLC analysis..... 14

1.2.10 Determination of phosphate concentration 15

1.2.11 Osmolality..... 15

1.2.12 Evaporation..... 15

1.3 Results and discussion 16

1.3.1 *B. licheniformis* ATCC 9945 as γ-PGA production host..... 16

1.3.2 *B. subtilis* P_{pst} as γ-PGA production host..... 19

1.3.3 *B. subtilis* P_{xyl} as γ-PGA production host..... 40

1.3.4 Comparison of the γ-PGA produced by the different *Bacillus* strains presented in this study..... 48

1.4 Conclusion and outlook 51

2 Spotting priming-active compounds using parsley cell cultures in microtiter plates... 54

2.1 Introduction 54
2.1.1 Defense priming of plants 54
2.1.2 Methods to detect defense priming 55
2.1.3 High-throughput screening with online DOT and furanocoumarin fluorescence measurements 56
2.2 Materials and methods 58
2.2.1 Media and solutions 58
2.2.2 Shake flask and MTP cultivation 58
2.2.3 Hydrodynamics in a well 59
2.2.4 Standard priming procedure 60
2.2.5 Determination of the DOT and OTR 60
2.2.6 Normalization of DOT and OTR data 62
2.2.7 Fluorescence measurements of SA and furanocoumarins 62
2.2.8 Calculation of errors 63
2.2.9 Statistical analysis 63
2.3 Results and discussion 65
2.3.1 Establishing parsley cell cultivation in MTPs 65
2.3.2 Determining a suitable shaking frequency 65
2.3.3 Volumetric mass transfer coefficient and OTR calculations 66
2.3.4 Identification of priming compounds in MTPs with DOT measurements 69
2.3.5 Reduced oxygen supply 72
2.3.6 Online furanocoumarin and SA fluorescence measurements in MTPs 74
2.3.7 Varying SA concentrations for cell pretreatment 76
2.3.8 Varying the times of SA and Pep13 addition. 78
2.3.9 Comparison of effects caused by two known priming-active and two priming-inactive compounds 82
2.4 Conclusion and outlook 85

3 Bibliography 86

4 Appendix 102

Nomenclature

Abbreviation	Description
3-HBA	3-hydroxybenzoic acid
4-CSA	4-chlorosalicylic acid
4-HBA	4-hydroxybenzoic acid
CTAB	cetyltrimethylammonium bromide
DOT	dissolved oxygen tension
GPC	Gel permeation chromatography
HPLC	High-performance liquid chromatography
MTP	Microtiter plate
OTR	Oxygen transfer rate
pgs	Polyglutamate synthase
P_{pst}	phosphate starvation promoter
P_{xyl}	xylose inducible promoter
RAMOS	Respiration activity monitoring system
SA	Salicylic acid,
SAR	Systemic acquired resistance
ViMOS	Viscosity Monitoring Online System
γ-PGA	Poly-γ-glutamic acid

Symbol	Description	Unit
d_0	Shaking diameter	[mm]
D_w	Inner well diameter	[mm]
f	Fluorescence intensity	[-]
f_0	Fluorescence intensity in the absence of oxygen	[-]
$f_{w/o\ additives}$	The total furanocoumarin fluorescence signal of the untreated culture without additives	[-]
f_{x_c}	Corrected furanocoumarin fluorescence signals	[-]
$f_{x_{rel}}$	Calculated relative furanocoumarin fluorescence	[%]
k_La	Volumetric mass transfer coefficient	[1/h]
k_{sv}	Stern-Volmer constant	[1/%]
L_{O2}	Oxygen solubility	[mol/L/bar]
n	Shaking frequency	[rpm]
n_{crit}	Critical shaking frequency	[rpm]
Osmol	Osmolality	[osmol/kg]
OTR_{calc}	Calculated oxygen transfer rate	[mmol/L/h]
OTR_{max}	Maximal oxygen transfer capacity	[mmol/L/h]
p_{O2}	Oxygen partial pressure	[bar]
p_{O2}^{cal}	Oxygen partial pressure during the calibration of the DOT	[bar]
p_{O2}^{gas}	Oxygen partial pressure of oxygen in the gaseous phase	[bar]
Q_{O2}	Content of the quencher oxygen	[%]
V_L	Filling volume	[mL]
ρL	Liquid density	[kg/m^3]
σ	Surface tension	[N/m]
λ_{em}	Emission wavelength	[nm]
λ_{ex}	Excitation wavelength	[nm]

List of figures and tables

Figures

Figure 1.1 Metabolic engineering targets to improve microbial γ-PGA production. 5

Figure 1.2 Cultivation of γ-PGA producing *B. licheniformis* ATCC 9945 in standard mineral medium E 17

Figure 1.3 Phosphate limitation during shake flask cultivations of *B. subtilis* P_{pst} Δspo. 20

Figure 1.4 Phosphate limitation during shake flask cultivations of *B. subtilis* P_{pst} Δspo under oxygen limited conditions. 21

Figure 1.5 Enhanced γ-PGA production with increasing glucose concentrations 25

Figure 1.6 Detailed investigation of the phosphate depletion-dependent de-repression of the promoter P_{pst}, controlling the poly-γ-glutamic acid (γ-PGA) production in shake flask cultivations of *B. subtilis* P_{pst} Δspo. 27

Figure 1.7 Impact of different depolymerase gene knockouts on γ-PGA production and depolymerization 30

Figure 1.8 Impact of by-product knock outs on growth and viscosity of *B. subtilis* P_{pst} Δspo ΔBP 36

Figure 1.9 Impact of by-product knock outs on γ-PGA production and molecular weight 38

Figure 1.10 Impact of by-product knock outs on by-product formation 39

Figure 1.11 Impact of increased glucose concentrations on OTR and viscosity of *B. subtilis* P_{xyl} Δspo 41

Figure 1.12 Influence of the phosphate concentration on growth and viscosity of *B. subtilis* P_{xyl} Δspo 43

Figure 1.13 Impact of increased glucose concentrations on γ-PGA production of *B. subtilis* P_{xyl} Δspo with adapted phosphate concentration 45

Figure 1.14 Intense foam production of the viscous fermentation medium 47

Figure 1.15 Comparison of the concentration and γ-PGA product yield coefficients of *B. licheniformis* ATCC 9945, *B. subtilis* Δspo, *B. subtilis* P_{pst} Δspo and *B. subtilis* P_{xyl} Δspo 49

Figure 2.1 Suspension behavior of a parsley cell culture in a 48-deep-round-well MTP at different shaking frequency. 66

Figure 2.2 Respiration activity of parsley cell cultures, determined in a shake flask and a 48-deep-round-well MTP. 68

Figure 2.3 OTR of parsley cell cultures in shake flasks and MTPs with two different sensor systems. Measurements from shake flasks (a) and from MTPs (c, e) are shown. 70

Figure 2.4 OTR and online determination of furanocoumarin fluorescence of parsley cell cultures in an MTP. 75

Figure 2.5 Online fluorescence intensities upon treatment with various SA concentrations in a MTP. 77

Figure 2.6 Online fluorescence of parsley cell cultures treated with SA and Pep13 at various cultivation times. 79

Figure 2.7 Online fluorescence intensities of parsley cell cultures treated with salicylic acid (SA) and its derivatives. 83

Figure A 1 Determination of the limiting phosphate concentration during shake flask cultivations of *B. subtilis* P_{pst} Δspo. Duplicates of experiment shown in Figure 1.3 104

Figure A 2 Determination of the limiting phosphate concentration during shake flask cultivations of *B. subtilis* P_{pst} Δspo at oxygen limited conditions by reduced shaking frequency and enlarged filling volume. Duplicates of experiment shown in Figure 1.4 105

Figure A 3 Enhanced γ-PGA production with increasing glucose concentrations. Duplicates of experiment shown in Figure 1.5 106

Figure A 4 Duplicates of the oxygen transfer rate (OTR) from Figure 1.7a and the associated optical densities of the cultivations are shown 107

Figure A 5 Comparison of the specific γ-PGA product yield of four different *B. subtilis* γ-PGA depolymerase gene deletion mutants. 108

Figure A 6 Impact of by-product knock outs on OTR. Original progression of the OTR over time of experiment shown in Figure 1.8 111

Figure A 7 DOT and calculated OTR of parsley cell cultures measured with two different sensor spot systems. 112

Figure A 8 DOT and OTR of parsley cell cultures in a MTP aerated with an air/nitrogen mixture. 114

Figure A 9 DOT of parsley cell cultures before (a and b) and after (c and d) normalization. 115

Tables

Table 1.1 Plasmids used in this study 9

Table 1.2 Strains used in this study..... 10

Table 1.3 Molar amount of carbon of the γ-PGA cultivation media..... 48

Table A 1 Primer used to create the modified *B. subtilis* strains 102

Chapter 1

Poly-γ-glutamic acid production with *Bacillus licheniformis* and *Bacillus subtilis*

1.1 Introduction

Poly-γ-glutamic acid (γ-PGA) is an anionic, natural biopolymer made from D- and L-glutamic acid units linked between the α-amino and γ-carboxylic acid groups [1-3]. γ-PGA is water-soluble, biodegradable, edible, non-toxic and environmentally friendly. The polymer has different lengths depending on the strain and production conditions used, resulting in a broad spectrum of molecular weights ranging from 10 to more than 2,000 kDa [3, 4]. These properties make γ-PGA a suitable substance for a variety of applications in multiple fields. For instance, there are reports about γ-PGA use in the food industry, water treatment, agriculture, and medical industry [1-7]. γ-PGA can be produced through chemical synthesis, peptide synthesis, and microbial fermentation [8]. The properties of γ-PGA strongly depend on its variable molecular size, molecular weight distribution, and enantiomeric composition [9, 10].

The pathogenic *B. anthracis* was the first organism found to produce γ-PGA [11]. It is the only organism known to produce pure D-γ-PGA. The γ-PGA of *B. anthracis* forms a capsule surrounding the organism. This γ-PGA capsule protects *B. anthracis* from the human immune system [12]. Until now PGA was found to be naturally produced by archaea, bacteria, and eukaryotes [11, 13, 14]. The secreted γ-PGA of *Bacillus* species is most commonly used for industrial γ-PGA production [15, 16].

γ-PGA-producing *Bacillus* strains can be divided into two groups. The first group consists of glutamate-dependent strains that produce γ-PGA if glutamate is supplemented as substrate. This group usually produces γ-PGA in high concentrations but has the significant disadvantage of high production costs due to glutamate as substrate [2, 7]. One of these glutamate-dependent strains also discussed shortly in this thesis is *B. licheniformis* ATCC 9945 which is described well in literature as γ-PGA producer with Medium E [16, 17]. The second group comprises glutamate-independent γ-PGA producers [1, 18]. Since the γ-PGA concentration is lower with these strains, improving γ-PGA production in this group is essential. In the first chapter of this thesis modified *B. subtilis* 168 were used as γ-PGA production strains. *B. subtilis* 168 does not produce γ-PGA naturally [1, 19]. However, it is well described in literature and enables metabolic engineering. Therefore, *B. subtilis* 168 was used as the initial strain for this study and modified to produce γ-PGA. The strains used in this study are sporulation-negative derivatives of *B. subtilis* 168, which increases the culture reproducibility [20].

1.1.1 Inserted promoter systems enable γ-PGA production in *B. subtilis* 168

Although *B. subtilis* 168 possesses the genes that encode the polyglutamate synthase (pgs) required for γ-PGA formation, it does not naturally produce γ-PGA, as it lacks a functional promoter [1, 19]. In this study, two promoter systems were introduced to activate the expression of the *pgs* genes. Firstly the phosphate-starvation inducible promoter P_{pst} and secondly the xylose inducible promoter P_{xyl} [21, 22]. The P_{pst} promoter enables the decoupling of growth and production but is rather weak. The P_{xyl} promoter is compared to the P_{pst} a rather strong promoter.

Through the characteristics of the P_{pst} promoter, the separation of the growth phase from the product formation phase is possible. In the growth phase, *B. subtilis* is cultivated as a biocatalyst. One essential element for the cell growth of *B. subtilis* is phosphate. Without phosphate, cell growth and proliferation stop. In this study, the phosphate-starvation inducible promoter P_{pst} is used for γ-PGA synthesis. The P_{pst} promoter becomes active, as soon as phosphate is exhausted. Therefore, γ-PGA is synthesized, when phosphate is depleted and cell proliferation stops. The phosphate-dependent induction of the promoter allows the automatic decoupling of growth and γ-PGA production [22]. This prevents the flow of substrate into cell growth after sufficient biomass as a biocatalyst for γ-PGA synthesis has been generated. This

two-stage process strategy is well established e.g. for IPTG-induced *E. coli* production processes [23].

While P_{pst} is a promoter activated by phosphate limitation the promoter P_{xyl} becomes inducted by xylose [21]. Usually, P_{xyl} controls the *xylAB* operon in *B. subtilis*. This offers the possibility to regulate promoter expression and product synthesis through the inductor concentration. The *xylAB* operon was deleted to ensure that xylose only induces the pgs operon for γ-PGA production [24].

1.1.2 Depolymerase knockouts may prevent degradation of γ-PGA

Naturally, γ-PGA is formed by *Bacillus* strains as an extracellular secondary product and serves as a nutrient store for periods of starvation or as a protective molecule in harsh environments. Therefore, γ-PGA producers usually co-synthesize specific depolymerases to degrade γ-PGA again to make the polymer available as carbon and nitrogen sources. The monomers and peptides thus made available can then be metabolized [25, 26]. This is an undesirable side effect for industrial production of γ-PGA, as it reduces the γ-PGA yield and results in a broad distribution of the molecular weight and thus the polydispersity. Three known specific γ-PGA depolymerases CwlO, Ggt, and PgdS that exhibit γ-PGA depolymerase activity have been reported [27-29]. These enzymes have already been investigated in many studies to achieve high-level γ-PGA production and low molecular weight dispersity [27, 30]. PgdS and Ggt are enzymes specific for γ-PGA, whereas CwlO is a peptidoglycan hydrolase located in the cell wall, which also can cleave γ-PGA. The following Figure 1.1 depicts schematically the γ-PGA production pathway and the depolymerase knockouts CwlO, Ggt, and PgdS on the right side. PgdS is an endo-γ-D-L-glutamyl hydrolase [31], and Ggt is a γ-glutamyl transpeptidase [32, 33]. Combined and single knockouts of the depolymerase genes have already been described in previous studies [30, 34-37]. These studies refer to different γ-PGA-producing *Bacillus* strains such as *B. amyloliquefaciens* [30, 35], *B. licheniformis* [36], and *B. subtilis* [34, 37]. Depending on the strain, different results are obtained regarding the effect of knockouts on γ-PGA production. For *B. amyloliquefaciens,* it could be shown that a double knockout of *pgdS* and *cwlO* leads to a higher γ-PGA yield than a triple knockout [30]. However, for *B. subtilis*, only a double knockout of *pgdS* and *ggt* has been investigated and ascribed to a higher γ-PGA

production [34, 37]. Since knockouts have different effects depending on the *Bacillus* strain and no triple knockout has been investigated for *B. subtilis* 168, a detailed investigation regarding the effect of the knockout of the three depolymerases is of interest. In this study, *B. subtilis* 168 with knockout of *ggt, pgdS*, and *cwlO* are analyzed as single knockouts and as a triple knockout [22].

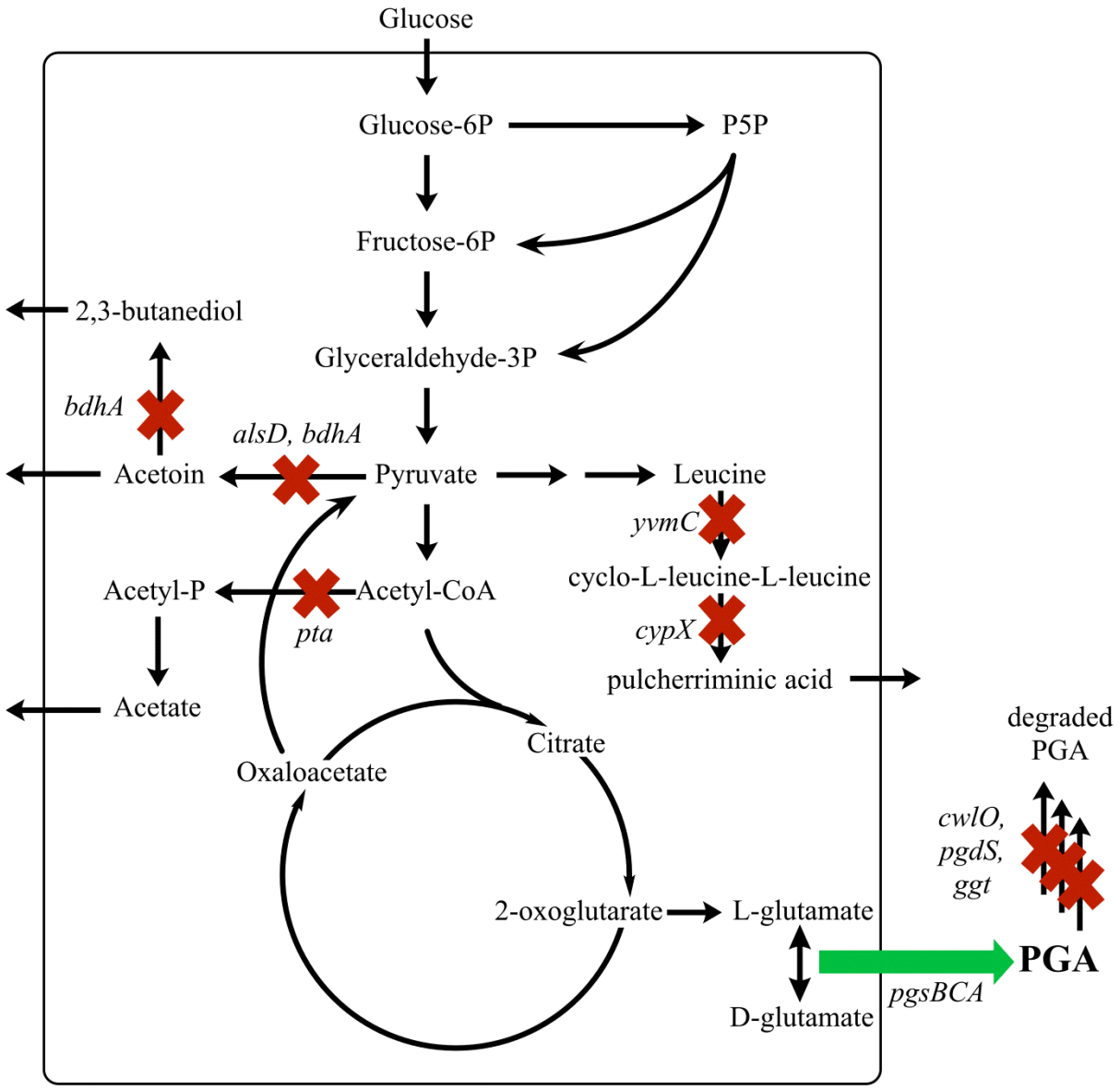

Figure 1.1 Metabolic engineering targets to improve microbial γ-PGA production.
To prevent the synthesized γ-PGA from enzymatic depolymerization the genes *cwlO, pgdS* and *ggt* were deleted (Right site). Additionally, several genes were deleted to prevent by-product formation and to direct the metabolic flux toward γ-PGA synthesis. *alsD* and *bdhA* to prevent acetoin and butanediol formation, *pta* to prevent acetate formation and *yvmC* and *cypX* to prevent pulcherriminic acid production. (Figure from the PhD thesis of Birthe Halmschlag [24])

1.1.3 By-product knockouts can increase the precursor supply for γ-PGA production

One of the drawbacks of γ-PGA production with glutamic acid dependent producers is the high substrate costs for glutamate. That makes the production of γ-PGA with glucose as the sole

carbon source attractive. Nevertheless, γ-PGA production rates with glucose-based media are often low. One reason is low synthesis of glutamate precursors like citrate and 2-oxogluterate (Figure 1.1). To increase the carbon flux towards glutamate and its precursors knocking out by-product pathways is possible. Typical side products of *B. subtilis* by growth on glucose, shown in Figure 1.1, are acetate, acetoin, 2,3-butanediol and pulcherriminic acid [35, 38, 39]. Figure 1.1 shows the side product knockouts tested in this study. *Pta* which is part of the acetate pathway, *alsD* and *bdhA* as part of the acetoin and 2,3-butanediol pathway as well as *yvmC* and *cypX* which are enzymes of the pulcherriminic acid pathway were knocked out to prevent the production of the mentioned by-products. The effect of the by-product knockouts was analyzed in the strain with the P_{pst} promoter.

1.1.4 Online measuring techniques for γ-PGA fermentation

Previous research on γ-PGA production has been based on time-consuming experiments with sampling and offline determination of γ-PGA concentration [40, 41]. In the field of small-scale culture research, the online analysis of cultivation parameters, in particular, has achieved resounding success. Online measurements of the oxygen transfer rate (OTR) with the Respiration Activity MOnitoring System (RAMOS) lead to new insights in shaken cultures [42, 43]. For faster and more detailed strain and process development, non-invasive online techniques to monitor γ-PGA formation combined with OTR measurements are necessary to complement laborious manual sampling. Because γ-PGA is a biopolymer, its synthesis during fermentation increases the culture broth viscosity [41]. This parameter is influenced by γ-PGA concentration as well as molecular weight. Measuring the culture broth viscosity offers the possibility to draw qualitative conclusions about the course of product formation. Hence, online measurement of the viscosity during cultivation is a promising approach to investigate γ-PGA synthesis in combination with offline analysis.

For online γ-PGA analysis via culture broth's viscosity, two methods have been reported so far. One uses the power input measurement during the cultivation, which allows the calculation of the viscosity [44]. The other one is the recently published Viscosity Monitoring Online System (ViMOS), which optically measures the cultivation broth viscosity [45] and has already been used to analyze γ-PGA production [46]. The power input measurement method is based on the

effect of viscosity changes on the power input in unbaffled shake flasks [47, 48]. An increase in fermentation broth viscosity results in an increase in the power input. Thus, the detection of the power input by a torque sensor inserted into the drive of a shaker allows for calculating the broth viscosity [47]. A disadvantage of the reported method is its limited throughput, as only one single parameter set can be performed at a time. However, the optical online viscosity measurement system (ViMOS) used in this study allows the parallel, non-invasive viscosity measurement in eight shake flasks on one device. This device provides a contact-free optical measurement and is also suitable for non-Newtonian liquids like microbial culture broths [45]. The measuring principle is based on the defined rotating liquid position in shake flasks relative to the direction of the centrifugal acceleration, which depends on the viscosity. The bulk of the fluid moves along the hydrophilic shake flask wall. With increasing viscosity, the liquid friction and the friction between the liquid and the shake flask wall increase, which results in a shift of the angular position of the fluid relative to the direction of the centrifugal acceleration. That change in the angular position of the liquid´s leading edge can be optically detected with a method based on transmitted light with an infrared sensor. Each angular position can be assigned to an apparent shear rate-dependent viscosity through previous calibration with viscous model fluids [45]. For calibration, model fluids with various viscosities are measured with a reference cone plate rheometer and the ViMOS in shake flasks. An essential aspect of the calibration is the shear rate. The shear rate in shake flasks depends on shaking parameters e.g. shaking frequency, filling volume, and shake flask diameter, and on the properties of the fluid, the consistency factor K, and the flow behavior index m [49]. The shear rate can be calculated by the correlation of Giese et al. and was shown to be applicable for the calibration of the online viscosity measurement system [45].

The first chapter of the thesis focuses on analyzing the newly generated *B. subtilis* 168 derivatives including strains with the phosphate-starvation inducible promoter P_{pst}, with a knockout of the single genes *ggt, pgdS*, and *cwlO* and triple knockout, by-product deletion mutants and the xylose inducible promoter P_{xyl}. First, the *B. subtilis* 168 P_{pst} Δspo is analyzed in detail to understand and control the promoter system and to test the ViMOS with this new γ-PGA production strain. Subsequently, the knockout strains are analyzed with the aim to reduce enzymatic γ-PGA hydrolysis and thus improve γ-PGA production. For further improvement of γ-PGA production, the ability to increase the precursor supply with the by-product knockout

mutant is tested. As the P_{pst} promoter is rather weak the xylose inducible promoter is introduced as well to achieve higher γ-PGA concentrations. For the online monitoring of γ-PGA production and degradation during the fermentation process the ViMOS is used. Additionally, the OTR is measured by the RAMOS technique, and several offline analytics for the determination of side products, substrate amount in the medium, and γ-PGA concentration and molecular weight are applied. The combination of these online and offline techniques demonstrates the possibilities of online measurements for the analysis and control of the microbial synthesis of viscous products throughout the fermentation process. The ViMOS technology is introduced as a new analytical tool for process development of γ-PGA production. The feasibility of the ViMOS for viscous fermentation processes is shown by analyzing the potential of the phosphate-starvation promoter P_{pst}, the depolymerase deletion strains, the by-product knockout strain, and the P_{xyl} promoter strain.

1.2 Materials and methods

1.2.1 Medium composition

Cultivations to prepare cryogenic stocks and the first preculture of the experiments were performed in lysogeny broth (LB) consisting of 10 g/L peptone, 5 g/L yeast extract, and 5 g/L NaCl. There are two commonly used NaCl concentrations for the LB medium. One with 10 g/L NaCl and one with 5 g/L NaCl. In this study, the variant with 5 g/L NaCl was used. For the second preculture and the main cultivations, a modified glucose-based V3 3-(Morpholin-4-yl) propane-1-sulfonic acid (MOPS) minimal medium [41] was used. The initially used mineral medium contained 20 g/L glucose, 1.01 g/L $MgSO_4 \cdot 7H_2O$, 0.05 g/L $MnCl_2 \cdot 4H_2O$, 0.026 g/L $CaCl_2 \cdot 4H_2O$, 15 g/L $(NH_4)_2SO_4$, 0.53 mg/L $CoCl_2 \cdot 6H_2O$, 0.26 mg/L $ZnCl_2$, 0.01 mg/L H_3BO_3, 0.66 mg/L $NiSO_4 \cdot 6H_2O$, 0.31 mg/L $CuSO_4 \cdot 5H_2O$, 0.65 mg/L $Na_2MoO_4 \cdot 2H_2O$, 0.05 g/L $FeSO_4 \cdot 7H_2O$, and 41.85 g/L MOPS. 3.4 g/L K_2HPO_4 was added as a phosphate source and defined as 100%. In the experiments with lower phosphate concentrations, K_2HPO_4 was substituted in equimolar amounts by KCl. Every component was added separately from sterile stock solutions in the sequence mentioned above to avoid precipitation of medium components. The initial pH value was set to 8.1 using 5 M NaOH. In experiments with higher glucose concentrations, the glucose concentration was increased to 40 g/L, 60 g/L, or 80 g/L. All chemicals and solutions were of analytical grade and purchased from Carl Roth GmbH + Co. KG (Karlsruhe, Germany), Sigma-Aldrich Chemie GmbH (Munich, Germany), and Merck Chemicals GmbH (Darmstadt, Germany).

1.2.2 Bacterial strains and strain development

All steps of the strain development were performed by Birthe Halmschlag at the iAMB. The plasmids used are listed in Table 1.1, and primers are listed in the appendix in Table A 1.

Table 1.1 Plasmids used in this study

Plasmid	Characteristics	Reference
pJOE-8739	Spc^R, *manP*, vector backbone for the use of the mannose-based counter selection system	[50]

Plasmid	Characteristics	Reference
pBs-8	deletion of sporulation-related genes *spoGA, sigG, sigE,* and protease gene *bpr*; integrative vector for *B. subtilis*, Spc^R, *manP*	[24]
pBs-3	Deletion of *pgdS*; integrative vector for *B. subtilis*, Spc^R, *manP*	[24]
pBs-4	P(pst) promoter integration upstream of *pgs*; integrative vector, Spc^R, *manP*	[24]
pBs-5	Deletion of *ggt*; integrative vector for *B. subtilis*, Spc^R, *manP*	[24]
pBs-12	Deletion of *cwlO*; integrative vector for *B. subtilis*, Spc^R, *manP*	[24]
pBs-6	P(xyl_ccpA) promoter integration upstream of *pgs*; integrative vector, Spc^R, *manP*	[24]
pBs-10	Deletion of *bdhA*; integrative vector for *B. subtilis*, Spc^R, *manP*	[24]
pBs-11	Deletion of *pta*; integrative vector for *B. subtilis*, Spc^R, *manP*	[24]
pBs-14	Deletion of *cupX*; integrative vector for *B. subtilis*, Spc^R, *manP*	[24]
pBs-9	Deletion of *alsD*; integrative vector for *B. subtilis*, Spc^R, *manP*	[24]

All cloning steps were carried out in *Escherichia coli* DH5α. The recombinase-positive *E. coli* strain JM101 was used to obtain plasmids for the transformation of *B. subtilis*. For plasmid construction and counter selection, all strains were cultivated at 37 °C in LB medium containing 100 µg/mL spectinomycin or 0.5% (w/v) mannose as needed [50]. All developed strains were stored as cryogenic cultures at -80 °C.

The developed *Bacillus* strains presented in this study and the *E. coli* strains used for plasmid construction and cloning are listed in Table 1.2.

Table 1.2 Strains used in this study

Strain	Genotype/Properties	Reference
Escherichia coli DH5α	*fhuA*2 Δ(*argF-lacZ*)U169 *phoA glnV*44 Φ80 Δ(*lacZ*)M15 *gyrA*96 *recA*1 *relA*1 *endA*1 thi-1 hsdR17	[51]

Strain	Genotype/Properties	Reference
Escherichia coli JM101	*glnV*44 thi-1 Δ(*lac-proAB*) F'[*lacIqZΔM15 traD*36 *proAB*+]	[52]
B. subtilis IIG-Bs2	Derivative of laboratory strain *B. subtilis* 168; Δ*manPA::erm* ΔSPβ Δ*skin* ΔPBSX ΔproΦ1 Δ*pks::CmR*, ΔproΦ3 trp+	[50]
B. subtilis Δspo	*B. subtilis* IIG-Bs2 derivative; Δ*bpr* Δ*spoGA* Δ*sigG* Δ*sigE*	[24]
B. subtilis P_{pst} Δspo	*B. subtilis* Δspo derivative; P(pst)-pgs	[24]
B. subtilis P_{pst} Δspo Δ*pgdS*	*B. subtilis* Δ*pgdS, P(pst)-pgs*	[24]
B. subtilis P_{pst} Δspo Δ*ggt*	*B. subtilis* Δ*ggt*, P(pst)-*pgs*	[24]
B. subtilis P_{pst} Δspo Δ*cwlO*	*B. subtilis* Δ*cwlO*, P(pst)-*pgs*	[24]
B. subtilis P_{pst} Δspo Δ*pgdS* Δ*ggt* Δ*cwlO*	*B. subtilis* ΔTriple, P(pst)-*pgs*	[24]
B. subtilis P_{pst} Δspo ΔBP	*B. subtilis* ΔBP derivative, P(pst)-*pgs*	[24]
B. subtilis P_{xyl} Δspo	*B. subtilis ΔxylAB* derivative; P(xyl)-*pgs*	[24]

B. subtilis IIG-Bs2 was used as a platform for genetic modification. For further strain development, sporulation-related genes were knocked out in *B. subtilis* Δspo with plasmid pBs-8 to allow for reproducible growth [20]. The γ-PGA production with the native *B. subtilis* pgs operon was enabled by integrating the promoter P_{pst} in *B. subtilis* Δspo with plasmid pBs-4. To investigate the influence of depolymerases on γ-PGA production and degradation, the three genes *ggt*, *pgdS,* and *cwlO*, encoding for depolymerases, were knocked out using plasmids pBs-5, pBs-3, and pBs-12, respectively. Additionally, the performance of a triple depolymerase knockout mutant *B. subtilis* P_{pst} Δspo Δ*pgdS* Δ*ggt* Δ*cwlO* was investigated. All genome editing steps were performed by Birthe Halmschlag at the iAMB using the previously published markerless gene deletion system [50].

For maintenance, strains were plated on LB-agar plates and incubated for 16 h. Next, an LB liquid culture was started with a single colony from an agar plate and grown until the late exponential phase. Then, a glycerol stock with 30% (w/v) glycerol was prepared and stored at -80 °C. The glycerol stocks were used as starting cultures for the performed cultivation experiments.

1.2.3 Shake flask cultivation

For each experimental culture, a cryogenic culture was thawed and used as inoculum of a culture in 250 mL unbaffled shake flasks. The cultivation parameters were a filling volume (V_L) of 10 mL or 30 mL, a shaking frequency (n) of 250 rpm or 350 rpm, a shaking diameter (d_0) of 50 mm, a temperature (T) of 37 °C and a starting OD at 600 nm (OD_{start}) of 0.1 in modified glucose-based V3 MOPS mineral medium. A two-stage preculture was performed under the same cultivation conditions, as all the following experimental cultures. The first preculture was grown on LB medium, and the second preculture was grown on a glucose-minimal medium. For the main culture, a master mix of the modified V3 MOPS medium and cells from the second preculture was prepared and equally distributed between all shake flasks. The shake flasks for offline sampling and online analysis were cultivated under identical conditions, to ensure comparable growth conditions.

1.2.4 Oxygen transfer rate (OTR)

The oxygen transfer rate (OTR) of the cultivations was online monitored using an in-house manufactured Respiration Activity MOnitoring System (RAMOS) device [42, 43]. RAMOS enables the quasi-continuous measurement of the oxygen partial pressure in the gas phase from which the OTR can be calculated. Commercial RAMOS versions are available from Kuhner AG, Birsfelden, Switzerland, or HiTech Zang, Herzogenrath, Germany.

1.2.5 Online measured viscosity

The viscosity was online measured with the new Viscosity Monitoring Online System (ViMOS) device previously published [45]. The ViMOS enables the online viscosity measurement in eight parallel shake flasks. The system is based on a transmitted light measurement at 950 nm and evaluates the shift in the angular position of the bulk liquid relative to the direction of the centrifugal acceleration. With increasing viscosity, this shift increases. A detailed description of the VIMOS and calculation methods for the viscosity are reported elsewhere [45]. Using calibration, calculating the corresponding viscosities from the different shifts during the cultivation is possible.

1.2.6 Offline measured viscosity

In addition to online viscosity measurement, the viscosity was offline measured, to validate the online system for viscosity measurements with γ-PGA cultivations. Viscosity was measured offline with a Physica MCR 301 rheometer (Anton Paar Germany GmbH, Ostfildern-Scharnhausen, Germany) in a range of shear rates between 100 s^{-1} and 5,000 s^{-1} with a cone-plate measuring system from Anton Paar (cone CP50-0.5/TG with a cone diameter of 49.945 mm, a cone angle of 0.467 ° and a cone truncation of 54 µm; plate P-PTD200/TG+H-PTD200). The software RheoPlus/32 V3.40 (Anton Paar) was used to analyze the data. 480 µL of fermentation broth was used for viscosity measurements at 37 °C. The effective viscosity in shake flasks depends on the specific shear rate present at the time point of sampling, as γ-PGA solutions exhibit pseudoplastic properties. Thus, shear rates were calculated, as published before, to determine the effective viscosity in shake flasks with the offline measured viscosity data [49].

1.2.7 Cetyltrimethylammonium bromide assay

The γ-PGA concentration was determined with the photometric cetyltrimethylammonium bromide (CTAB) assay [53]. The positively charged CTAB reagent binds to the negatively charged γ-PGA and forms a water-insoluble complex that increases the suspension's turbidity. Samples of 1 mL from the cultivations were centrifuged for 10 min at 17,968 g. The supernatant was diluted to fit the linear measuring range between 0.01 g/L and 0.1 g/L of γ-PGA. 100 µL sample and 100 µL of the CTAB solution consisting of 0.07 M CTAB in 2% (w/w) NaOH were mixed in a 96-well plate and incubated for 3 min at 30 °C. For each sample, triplicates were measured. The turbidity was measured at 400 nm with a Synergy 4 plate reader (BioTek Instruments, Winooski, USA). A calibration curve with standard γ-PGA solutions was newly measured with every experiment.

1.2.8 Gel permeation chromatography

To determine the mass average molecular weight (Mw) and the concentration of γ-PGA, gel permeation chromatography (GPC) was performed [3]. To prepare samples for GPC analysis,

culture broth was centrifuged for 5 min at 17,968 g. Subsequently, the supernatant was diluted with deionized water and sterile-filtered with 0.2 µm filters (Rotilabo Mini-Tip syringe filters, cellulose acetate membrane, N° PP52.1, Carl Roth GmbH + Co. KG, Karlsruhe, Germany). Then, 30 µL of the filtered samples were injected into the GPC system upon the columns at a rate of 40 µL/min. A TSKgel PWxl guard column (40 x 6 mm, Tosoh Bioscience GmbH, Griesheim, Germany) and for separation a TSKgel GMPWxl column (300 x 7.8 mm, Tosoh Bioscience GmbH, Griesheim, Germany) were used. As elution buffer, a 30 mM KNO_3 solution at 40 °C (pump oven also at 40 °C) was used at a flow rate of 1.0 mL/min. The software WinGPC UniChrom (PSS Polymers Standards Service, Mainz, Germany) was used for data analysis. Poly(styrene sulfonate) sodium salt (PSS) standards with a peak molecular weight in the range of 4.21–976 kDa (PSS Polymer Standards Service GmbH, Mainz, Germany) were used to create a calibration curve for molecular weight. γ-PGA sodium salt of cosmetic grade A (kindly provided by Henkel AG & Co. KGaA, Düsseldorf, Germany) was used to create a calibration curve to determine γ-PGA concentrations. Offline samples from the six cultivated *B. subtilis* strains shown in Figure 5 were analyzed by the GPC. The molecular weight is shown in Figure 5H.

For comparison of the achieved product amounts, the γ-PGA yield ($Y_{\gamma\text{-PGA/Glucose}}$) was calculated and depicted in Supplementary Figure 5. The maximal achieved γ-PGA concentration (g/L), measured with the GPC, was set in relation to the consumed glucose concentration (g/L), measured with the HPLC. As a result, the γ-PGA yield in $g_{\gamma\text{-PGA}}$ per $g_{Glucose}$ is presented.

1.2.9 HPLC analysis

High-performance liquid chromatography (HPLC) was used to determine the concentration of glucose, acetate, lactate, 2,3-butanediol, glycerol, succinate, and pulcherriminic acid. Samples were centrifuged for 5 min at 17,968 g. The supernatant was diluted and subsequently sterile-filtered using 0.2 µm filters (Rotilabo Mini-Tip syringe filters, cellulose acetate membrane, N° PP52.1, Carl Roth GmbH + Co. KG, Karlsruhe, Germany). The HPLC (Ultimate 3000, Dionex, USA) was equipped with an Organic Acid-Resin-Column (250 x 8 mm, CS-Chromatographie Service GmbH, Langerwehe, Germany) and an Organic Acid-Resin-Precolumn (40 x 8 mm,

CS-Chromatographie Service GmbH, Langerwehe, Germany) [44]. An elution buffer of 5 mM H_2SO_4 at 60 °C at a flow rate of 0.8 mL/min was used. Detection was performed with a Shodex R1-101 refractometer (Showa Denko Europe), and data were analyzed with the software Chromeleon 6.2 (Dionex, Germany).

1.2.10 Determination of phosphate concentration

The concentration of phosphate ions in the supernatant was photometrically determined. The culture broth was centrifuged for 5 min at 17,968 g using the commercially available Spectroquant® test kits (Merck KGaA, Darmstadt, Germany) (Phosphate: 0.05-5.0 mg/L PO_4-P / 0.2-15.3 mg/L PO_4^{3-}, N°1.14543.0001). The assay was conducted according to the manufacturer's manual. Samples were appropriately diluted after centrifugation with distilled water to be in the measuring range of the assays.

1.2.11 Osmolality

The osmolality, required to calculate the maximum oxygen transfer capacity (OTR_{max}), was determined with a freezing point osmometer (Osmomat 3000, Gonotec, Berlin, Germany).

1.2.12 Evaporation

The evaporation of water from the culture broth during the cultivation was quantified with two offline shake flasks, by measuring the weight loss of the flasks over time. The results of HPLC and GPC analysis as well as of the CTAB and phosphate assay were corrected by the calculated evaporation factor.

1.3 Results and discussion

1.3.1 *B. licheniformis* ATCC 9945 as γ-PGA production host

Glutamic acid-dependent γ-PGA producer strains have generally a better production rate and yield than glutamic acid-independent producers [54-60]. Nevertheless, glutamic acid-dependent producers can have several drawbacks. Figure 1.2 shows some of these disadvantages exemplarily with the glutamic acid dependent γ-PGA wild type producer *B. licheniformis* ATCC 9945a.

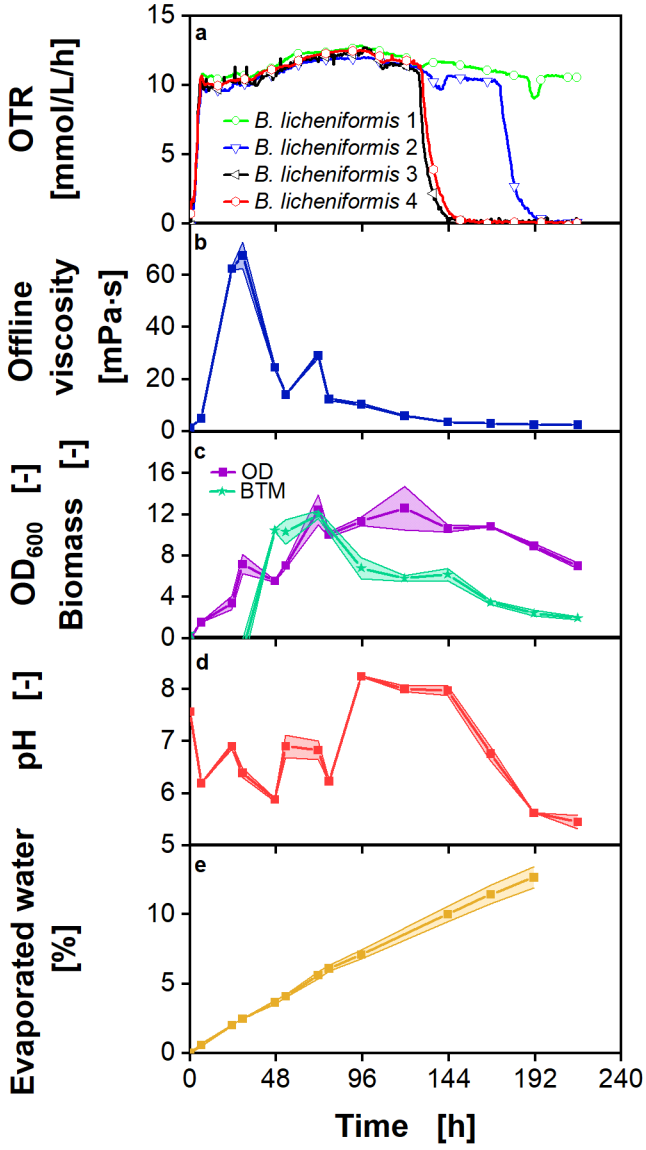

Figure 1.2 Cultivation of γ-PGA producing *B. licheniformis* ATCC 9945 in standard mineral medium E

Oxygen transfer rates (OTR) of 4 simultaneously cultivated RAMOS shake flasks are shown in a. Data in b, c, d, and e were measured from offline shake flasks cultivated parallel to the RAMOS shake flasks. Offline measured viscosity is shown in b. OD_{600}, biomass, and pH are depicted in c and d. e shows the evaporation percentages of water in relation to the start filling volume in the shaking flask during the cultivation. Cultivation conditions: Standard mineral medium E, pH_{start} = 8.4, inoculation from glycerol stock (0.4 % v/v), T = 37 °C, 500 mL shake flask, V_L = 100 mL, n = 250 rpm, d_0 = 50 mm. For clarity, only every tenth measuring point is marked as a symbol (a). For offline data in b, c, d, and e, mean values of 2 replicates are shown. The shadow around the curve indicates highest and lowest value of duplicates.

Figure 1.2a shows the OTR of four identically started *B. licheniformis* ATCC 9945 cultivations. After 10 h the OTR reaches 10.6 mmol/L/h which fits the calculated OTR_{max} of 10.4 mmol/L/h

for 500 mL shake flask with V_L = 100 mL, n = 250 rpm, d_0 = 50 mm after Meier et al [61]. The OTR levels are in a plateau at this time as the cultures grow under oxygen limitation. Just two of the four OTRs run parallel (Figure 1.2 black and red line). The other two cultivations run several days longer which is shown by the later dropping OTR. This phenomenon might be triggered by the sporulation of *B. licheniformis* ATCC 9945.

The viscosity in Figure 1.2b rises steeply after the cultures reach oxygen limitation after 7 h. Microaerophilic conditions often trigger the production of overflow and secondary metabolite products. This might also be the reason for increasing viscosity due to γ-PGA after reaching oxygen limited conditions. The viscosity reaches a maximum of 69 mPa·s after 29 h. Afterward, it drops steeply and shows a second smaller peak at 71 h and then falls slowly but constantly. These changes in viscosity are the effect of another problem of γ-PGA production with wild-type producers. As γ-PGA is presumably produced as a nutrition reservoir wild-type producers possess a broad range of enzymes to degrade γ-PGA and make it available again. The γ-PGA is depolymerized resulting in a huge range of molecular weights. As food and medical applications rely on defined material properties this depolymerization resulting in a high polydispersity is undesirable.

Figure 1.2c shows the pH of the fermentation broth which fluctuates during the cultivation. The reason for this fluctuation is the composition of the used medium E. Medium E has no buffer component and the pH is regulated by the metabolization of the three carbon sources glycerol, citric acid, and glutamic acid. It was shown previously that in some cultivations the pH drops uncontrolled resulting in a pH inhibition [44].

Figure 1.2d depicts the evaporation percentages of water in relation to the start filling volume in the offline shaking flask. As the cultivations run for 7 days and longer evaporation is a significant problem and reaches 10 % by the time the first cultivations stop at 168 h. Cultivations with a smaller cultivation time and thus less evaporation is desirable.

Figure 1.2 is an example of the disadvantages of wild-type γ-PGA producers with the conventionally used medium E. These are high medium costs due to the usage of glutamic acid and citric acid as well as unreproducible growth due to sporulation of *B. licheniformis* ATCC 9945 resulting in unreproducible γ-PGA production. Uncontrolled fluctuation of the pH,

degradation of the product γ-PGA, and long fermentation time leading to high evaporation are additional drawbacks. Due to the variations between cultivations, it is also difficult to relate results from offline samples to online signals. All these factors point out the need for reproducible γ-PGA production strains and alternative media compositions.

1.3.2 *B. subtilis* P_{pst} as γ-PGA production host

The *B. subtilis* P_{pst} Δspo produces γ-PGA under the control of the P_{pst} promoter, hence under phosphate limitation.

1.3.2.1 Influence of various phosphate concentrations on viscosity and OTR

The P_{pst} promoter activity was investigated by cultivations of *B. subtilis* P_{pst} Δspo supplying different phosphate concentrations in the medium. The OTR as an indicator of the metabolic activity of the culture and the viscosity to monitor γ-PGA formation were measured online using the RAMOS and the ViMOS, respectively. The results are shown in Figure 1.3 and Figure 1.4 for two different cultivation experiments. The first cultivation in Figure 1.3 was performed under oxygen-unlimited conditions with 350 rpm and 10 mL filling volume. The second cultivation shown in Figure 1.4 was performed under oxygen limitation with 250 rpm and 30 mL filling volume.

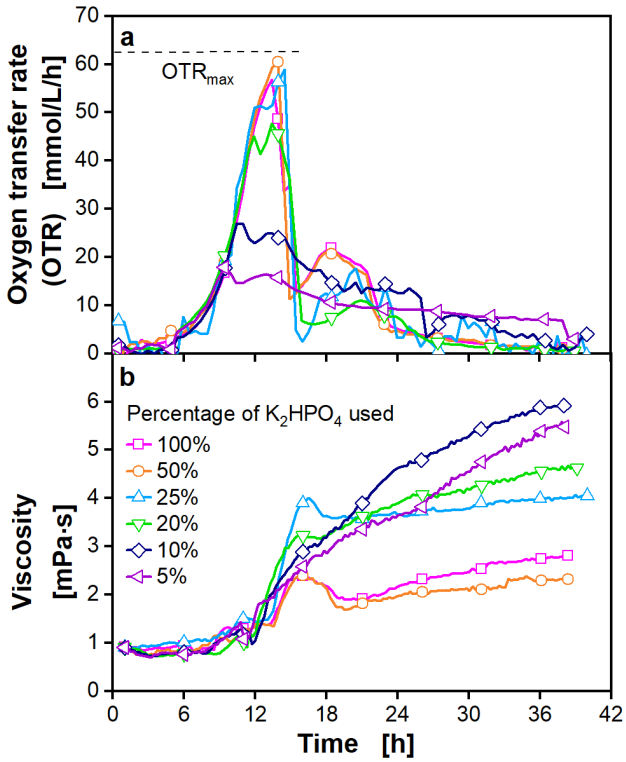

Figure 1.3 Phosphate limitation during shake flask cultivations of *B. subtilis* P_{pst} Δspo.

The oxygen transfer rate (OTR) (a) and the online viscosity measurements (b) of a *B. subtilis* P_{pst} Δspo cultivation in modified V3 glucose minimal medium with varying phosphate concentrations are shown: pH_{start} = 8.1, 20 g/L glucose, phosphate: 100% ≙ 3.4 g/L K_2HPO_4, 0.2 M MOPS; inoculation from pre-culture (OD_{start} = 0.1), T = 37 °C, 250 mL shake flask, V_L = 10 mL, n = 350 rpm, d_0 = 50 mm. Oxygen transfer rates (a) were measured with a RAMOS device. Online viscosity (b) was determined with a new system for parallel online measurement of viscosity in eight shake flasks (ViMOS), described by Sieben et al. 2019. The dashed horizontal line (a) indicates the maximum oxygen transfer capacity (OTR_{max}) at 62.4 mmol/L/h, calculated according to Meier et al. 2016. The cultivations were carried out in duplicates in three experimental runs (run 1: 100%, 50%, run 2: 25%, 10%, run 3: 20%, 10%, 5%). For clarity, only every ninth (a) and twentieth (b) measuring point is marked as a symbol. For clarity, average values are shown. The original complete dataset can be found in the appendix in Figure A 1.

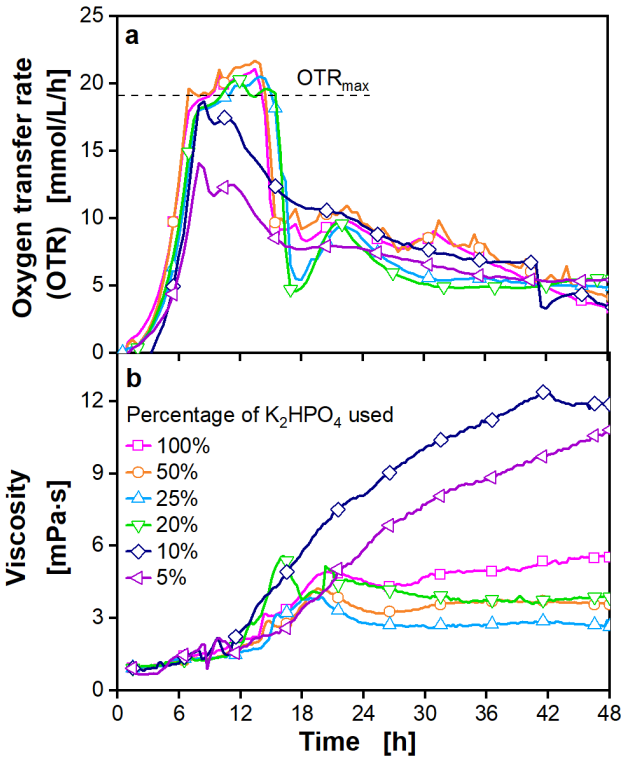

Figure 1.4 Phosphate limitation during shake flask cultivations of *B. subtilis* P_{pst} Δspo under oxygen limited conditions.

The oxygen transfer rate (OTR) (a) and the online viscosity measurements (b) of a *B. subtilis* P_{pst} Δspo cultivation in modified V3 glucose minimal medium with varying phosphate concentrations are shown. In comparison to Figure 1.3, the shaking frequency was reduced and filling volume increased: pH_{start} = 8.1, 20 g/L glucose, phosphate: 100% ≙ 3.4 g/L K_2HPO_4, 0.2 M MOPS; inoculation from pre-culture (OD_{start} = 0.1), T = 37 °C, 250 mL shake flask, V_L = 30 mL, n = 250 rpm, d_0 = 50 mm. Oxygen transfer rates (A) were measured with a RAMOS device. Online viscosity (b) was determined with a new system for parallel online measurement of viscosity in eight shake flasks (ViMOS), described by Sieben et al. 2019. The dashed horizontal line (a) indicates the maximum oxygen transfer capacity (OTR_{max}) at 19.1 mmol/L/h, calculated according to Meier et al. 2016. The cultivations were carried out in duplicates in two different experimental runs (run 1: 100%, 50%, run 2: 25%, 20%, 10%, and 5%). For clarity, only every tenth (a) and twentieth (b) measuring point is marked as a symbol. For clarity, average values are shown. The complete dataset can be found in the appendix in Figure A 2.

Oxygen limitation is of interest as many γ-PGA producing strains change their production behavior under oxygen-limited conditions and produce more γ-PGA [41, 62]. In both experiments, six different phosphate concentrations from 5% - 100% were analyzed. A concentration of 3.4 g/L K_2HPO_4 was defined as 100%. It was already previously used for γ-PGA production in the cultivation medium and was found to be high enough to not be limiting [41]. On this basis, 50%, 25%, 20%, 10%, and 5% of phosphate were investigated. With

350 rpm and 10 mL filling volume, the maximum oxygen transfer rate (OTR_{max}) was calculated to be 62.4 mmol/L/h [61]. As the culture achieved a maximal OTR of approx. 61.7 mmol/L/h (Figure 1.3a), it was grown under oxygen-unlimited conditions.

The curves of the experiments can be divided into three groups with high phosphate concentration (group 1: 100% and 50%), medium phosphate concentration (group 2: 25% and 20%), and low phosphate concentration (group 3: 10% and 5%) with a corresponding pattern. Group 1 comprises 100% and 50% of K_2HPO_4 and shows an identical OTR (Figure 1.3a). After an initial lag phase of approximately 5 h, the OTR increases exponentially until it reaches a maximum of 61.7 mmol/L/h after 15 h. Afterward, the curves drop sharply. The reason for such a drop has been shown several times to be the depletion of the main carbon source glucose [41, 42]. As glucose is depleted, the reason for the following humps in the OTR is the consumption of overflow metabolites. The corresponding online viscosities for 100% and 50% in Figure 1.3b show a similar course. At about 13 h, shortly before the OTR reaches its maximum, a slight increase in viscosity from 1.4 mPa·s to 2.4 mPa·s can be seen. This may be due to changes in the morphology or production of viscous metabolites [7]. In group 2 are the cultivations with phosphate concentrations of 25% and 20%. The OTR does not increase to as elevated values as with 100% and 50% phosphate (Figure 1.3a). This indicates a second substrate limitation [42]. Due to the lower initial phosphate concentration, the cultures grow into a phosphate limitation, and cell growth and breathing activity are becoming restricted. However, the OTR does not show a steep drop until 14 h. The change of the OTR at 13 h, respectively 12 h could be due to a switch in phosphate uptake, which influences the metabolism and breathing activity. This is likely, as P_{pst}, which naturally drives high-affinity uptake of phosphate in *B. subtilis*, becomes active in case of low micromolar environmental phosphate concentrations. This makes the last phosphate reserves available [22]. The viscosities in group 2 show the same course as in group 1 but reach slightly higher values between 3.5 mPa·s and 4.5 mPa·s after 16 h. Although γ-PGA production starts due to phosphate limitation, the viscosity remains low (Figure 1.3b), because there is potentially insufficient glucose left for a significant γ-PGA production. Group 3 includes cultures with 10% and 5% phosphate. The OTR and online viscosities differ from experiments of groups 1 and 2. Maximum OTR values of 25 mmol/L/h and 18 mmol/L/h, respectively, are reached. The OTR of group 3 reaches it's maximum 4 h earlier than groups 1 and 2 and shows no sharp drop afterwards. Instead, the curve progressively decreases until the

end of the cultivation. The online viscosities increase more slowly than for the other experiments but reach higher overall values of 5-7 mPa·s. The decrease in the OTR indicates a second substrate limitation of phosphate and the start of γ-PGA production.

When comparing the groups, three effects can be attributed to the different phosphate concentrations. First, with lower initial phosphate concentrations, the maximum OTR decreases. Cultures start growing identically, but differ from each other after the second substrate limitation of phosphate [42]. Second, with lower phosphate concentrations, higher viscosity values are reached. Phosphate is depleted earlier, and the P_{pst} promoter becomes active. As a result, more glucose is channeled into γ-PGA production than into cell growth. Third, the lower the initial phosphate concentration, the less steep the viscosity increase. Lower phosphate concentrations allow less biomass to be produced. Since the cells are the biocatalysts that produce γ-PGA, the volumetric production rate is lower with less biomass present. This experiment shows the advantage of the combined OTR and online viscosity measurement for generating information on cell growth, product formation, and secondary substrate limitations. With online measurements, it is possible to clearly distinguish between the growth and production phases. This can be used to optimize γ-PGA production.

To get an impression of how oxygen limitation affects γ-PGA production, the shaking frequency was reduced from 350 rpm to 250 rpm. With lower shaking frequency and potentially higher viscosities the risk of out-of-phase conditions increases. Out-of-phase conditions result in undefined liquid movements in the shake flask, leading to unreproducible growth and production behavior and additionally making measurements with the ViMOS impossible [63]. To prevent the out-of-phase phenomenon at elevated viscosities, the filling volume was increased from 10 mL to 30 mL. As calculated after Meier et al. [61] the changes in the shaking frequency and the filling volume reduced the maximum oxygen transfer capacity (OTR_{max}) from 62.4 mmol/L/h to 19.1 mmol/L/h. Figure 1.4a and Figure 1.4b show the OTR and the online-measured viscosity at these conditions, respectively. The curves with 20% - 100% phosphate grow into an oxygen limitation as the OTR shows a plateau after reaching the OTR_{max} of 19.1 mmol/L/h. In the cultures with 10% and 5% phosphate, the glucose is depleted before reaching an oxygen limitation (Figure 1.4a). As in Figure 1.3, the curves can be assigned to three groups. Initially, the OTR and online viscosity curves for 100% and 50% phosphate (group 1) are similar to those in Figure 1.3. After an exponential growth phase until 8 h, the

OTR_{max} of 19.1 mmol/L/h is reached. This is in very good agreement with the calculations according to Meier et al. [61]. The OTR slightly increases for another 6 hours. Afterward, it drops sharply due to glucose depletion [42]. The viscosity, shown in Figure 1.4b, increases only from 2.5 mPa·s to 4.5 mPa·s for the 100% and 50% batches. For group 2 with 25% and 20% phosphate in Figure 1.4a, similar high OTR values are achieved as for group 1. Viscosities increase to 6 mPa·s for the 20% cultivation and are thus slightly higher than for the 100%, 50%, and 25% experiments. For group 3 with 10% and 5% in Figure 1.4, similar courses of the OTR and viscosity as in Figure 1.3 can be seen, as the overall OTR becomes lower and higher end viscosities than with higher phosphate concentrations are achieved. Thus, the cultivations with 10% and 5% phosphate do not reach the OTR_{max}. These cultivations are therefore dominated by phosphate limitation and not by oxygen limitation.

Several effects can be observed when comparing the different phosphate concentrations in Figure 1.3 and Figure 1.4. The decrease in the OTR, associated with phosphate depletion, occurs only at a phosphate concentration of 25% or lower. At higher phosphate concentrations, glucose depletion precedes phosphate limitation. Viscosity in Figure 1.3b and Figure 1.4b increases significantly after the decrease in the OTR signal is detected. With lower phosphate concentrations, more glucose is directed to γ-PGA production instead of cell growth, and therefore, higher viscosity values are reached. Observed viscosities are higher for the oxygen-limited conditions with maximal 12 mPa·s (Figure 1.4) than for the oxygen-unlimited cultivation with a maximum of 7 mPa·s (Figure 1.3). This may be due to an increased γ-PGA production under oxygen-limited cultivation conditions [41]. Possibly, it also may depend on the higher molecular weight of the produced γ-PGA induced by the changed cultivation conditions [1] [41, 64].

It could be shown in this section that γ-PGA is produced in a glucose-minimal medium by *B. subtilis* under the control of the P_{pst} promoter, which can be monitored by online viscosity measurement. As higher viscosities indicate higher γ-PGA formation, the oxygen-limited cultivation conditions were used for further experiments.

1.3.2.2 Influence of increased glucose concentration on OTR and viscosity

To produce more biomass as a biocatalyst and to ensure sufficient carbon supply for γ-PGA production, the glucose concentration was increased. Figure 1.5a shows the OTR for cultivations with 25% phosphate and glucose concentrations of 20 g/L, 40 g/L, 60 g/L, and 80 g/L. Figure 1.5b displays the corresponding online viscosities.

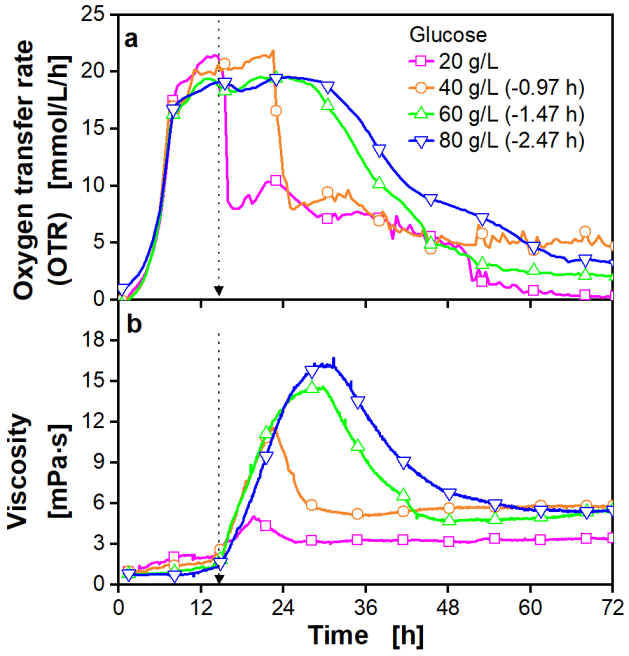

Figure 1.5 Enhanced γ-PGA production with increasing glucose concentrations.

The oxygen transfer rate (OTR) (a) and the online viscosity measurements (b) of a *B. subtilis* P_{pst} Δspo cultivation with varying amounts of glucose from 20 g/L – 80 g/L in the medium are shown. The cultivations were performed in a modified V3 glucose minimal medium: pH_{start} = 8.1, phosphate: 25 % of the original concentration ≙ 0.85 g/L K_2HPO_4, 0.2 M MOPS, inoculation from pre-culture (OD_{start} = 0.1), T = 37 °C, 250 mL shake flask, V_L = 30 mL, n = 250 rpm, d_0 = 50 mm. Oxygen transfer rates (a) were measured with a RAMOS device. Online viscosity (b) was determined with a new system for parallel online measurement of viscosity in eight shake flasks (ViMOS), described by Sieben et al. 2019. The lag phases of cultures with higher glucose concentrations are longer due to increased osmotic pressure. Therefore, the data have been shifted on the X-axis, so that the exponential growth phase of all experiments is superimposed, making the OTR and viscosity data easier to compare. The curves for 40 g/L glucose were shifted by -0.97 h, those for 60 g/L by -1.47 h, and those for 80 g/L by -2.47 h. The dotted vertical lines indicate the assumed time of phosphate depletion and the start of viscosity increase due to γ-PGA production. The cultivations were carried out in duplicates. For clarity, only every fifteenth (a) and eightieth (b) measuring point is marked as a symbol. For clarity, average values are shown. The complete dataset is found in the appendix in Figure A 3.

The maximum oxygen transfer capacity (OTR_{max}) decreases with higher glucose concentrations. This solely is a physicochemical, not a biological effect. With increasing concentrations of glucose, the oxygen solubility and the diffusion coefficient and, thus, the mass transfer coefficient are reduced. The combination of these effects can be correlated to the osmotic pressure, which is easy to measure [61].

After 10 h, due to oxygen limitation under the given fermentation parameters, the OTR is leveling of between 17.5 mmol/L/h and 20 mmol/L/h (Figure 1.5a) [65]. Calculated maximum oxygen transfer capacity [61] with 60 g/L glucose of OTR_{max} = 17.3 mmol/L/h fits the measured maximum OTR at the determined medium osmolality of 1.05 Osmol/kg. With 20 g/L glucose, the OTR sharply drops after 15 h, with 40 g/L after 24 h, while the OTR at 60 g/L and 80 g/L glucose steadily decreases after the plateau. The OTR remains at a plateau for a longer time with higher glucose concentrations, presumably due to higher metabolic activity for γ-PGA production. The presumed phosphate exhaustion at 15 h is marked in Figures 1.5a and b with a vertical dotted arrow. A strong indication for the starting γ-PGA synthesis at 15 h is that the buckling in the OTR associated with the P_{pst} promoter coincides with the increase in viscosity. When phosphate is depleted at 15 h cultivation time, the viscosity steeply increases for all curves in Figure 1.5b. This is because the same phosphate and glucose concentrations were available for cell growth, and thus, the number of microorganisms in all experiments should be the same. However, in the four experiments, the viscosity increases for different lengths, due to the different glucose concentrations. In the cultivations with 20 g/L and 40 g/L, the viscosity increases until the OTR curve drops sharply. At this point, the glucose is presumably metabolized [42]. For 60 g/L and 80 g/L, the viscosity increases until the OTR curve starts to steadily decrease. Phosphate is already depleted, and glucose is still available. Therefore, the slight and steady decrease after the plateau of the OTR for 60 g/L and 80 g/L could indicate that before glucose exhaustion another substrate necessary for γ-PGA synthesis becomes limiting. It is assumed that the highest viscosities reached with 80 g/L glucose indicate the most elevated γ-PGA production. However, due to the higher osmotic pressure at a concentration of 80 g/L glucose and the presumed secondary substrate limitation, further experiments are carried out containing 60 g/L glucose.

1.3.2.3 Promoter sensitivity to phosphate

To support the previous findings and to analyze in detail the P_{pst} promoter, an experiment with offline sampling at a cultivation with 60 g/L glucose in the modified V3 medium is shown in Figure 1.6.

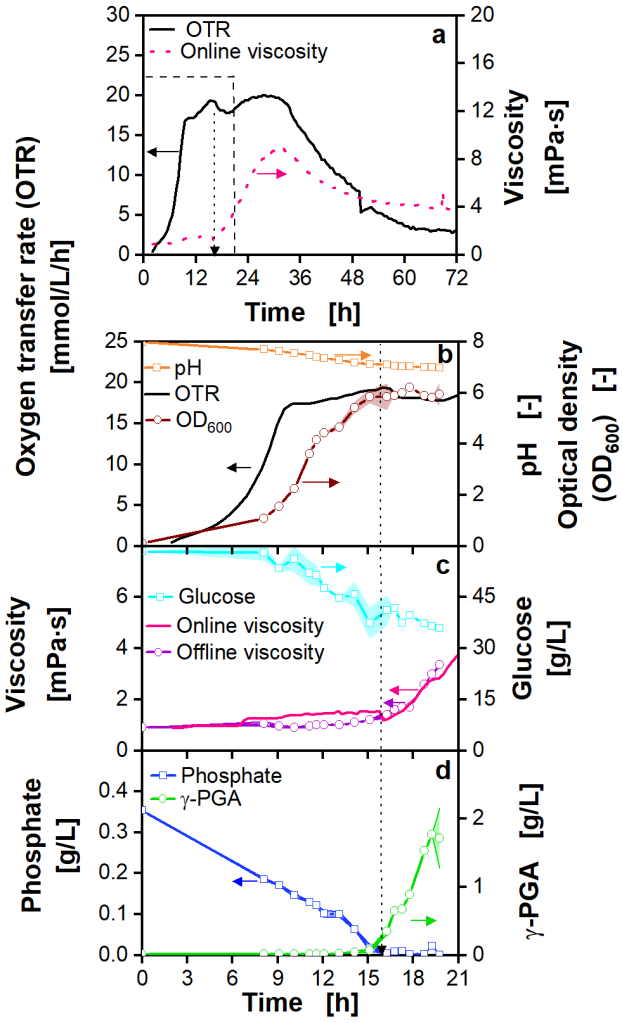

Figure 1.6 Detailed investigation of the phosphate depletion-dependent de-repression of the promoter P_{pst}, controlling the poly-γ-glutamic acid (γ-PGA) production in shake flask cultivations of *B. subtilis* P_{pst} Δspo.

(a) shows the oxygen transfer rate (OTR) and online viscosity during the whole cultivation. (b), (c) and (d) show online and offline data of the first 21 h of the cultivation, illustrated by dashed lines in (a), to analyze the functionality of the promoter. *B. subtilis* P_{pst} Δspo was cultivated in a modified V3 glucose minimal medium: pH_{start} = 8.1, 60 g/L glucose, phosphate: 25% of the original concentration ≙ 0.85 g/L K_2HPO_4, 0.2 M MOPS, inoculation from pre-culture (OD_{start} = 0.1), T = 37 °C, 250 mL shake flask, V_L = 30 mL, n = 250 rpm, d_0 = 50 mm. Oxygen transfer rates (a, b) were measured with a RAMOS device. Online viscosity (a, c) was determined with a new system for

parallel online measurement of viscosity in eight shake flasks (ViMOS), described by Sieben et al. 2019. Glucose measurements, offline and online viscosity measurements are shown in (c), and γ-PGA and phosphate concentration are shown in (d). The dotted vertical lines indicate the time of phosphate depletion and the start of viscosity increase due to γ-PGA production. The means of the offline analyzed values and standard deviation were calculated with biological duplicates and technical triplicates. The standard deviation is indicated by colored shadows.

The P_{pst} promoter naturally regulates the expression of the *pst* operon in *B. subtilis*. Its gene products are required for high-affinity uptake of inorganic phosphate (Pi) from the environment at micromolar concentrations [22]. Phosphate in the medium represses the P_{pst} promoter and inhibits the expression of the γ-PGA synthetase genes. De-repression of P_{pst} should hence occur only at negligible remaining phosphate concentrations in the cultivation medium. The depletion of phosphate was assumed to be the reason for the increase in viscosity due to γ-PGA production in Figure 1.3 and Figure 1.4. To verify this hypothesis, phosphate concentrations in the medium were measured. The extracellular γ-PGA accumulation by *B. subtilis* P_{pst} Δspo was analyzed utilizing the CTAB assay and related to the fermentation broth viscosity (Figure 1.6). Figure 1.6a provides an overview of OTR and online viscosity over the whole cultivation. During the first 21 h, offline sampling was performed. Results for this period are plotted in Figure 1.6b-d.

The OTR in Figure 1.6a rises, as in Figure 1.3a and Figure 1.4a, until it reaches after 11 h the OTR_{max}. Subsequently, the cultivation is oxygen-limited. At a cultivation time of 16 h, a dotted vertical arrow marks the change in metabolism due to phosphate limitation. The OTR in Figure 1.6a at 16 h shows a similar progression over time, already observed in the previous Figure 1.5. Viscosity begins to rise linearly after 16 h of cultivation to a peak value of around 10 mPa·s after 33 h (a) and starts to decrease at the same cultivation time as the OTR. The OTR and medium viscosity strongly hint at carbon source depletion after 33 h. The decrease to ~4 mPa·s until the end of fermentation is potentially due to the digestion of beforehand synthesized γ-PGA by depolymerizing enzymes [25, 30]. Released monomers may have served as a "slow-release" nutritional compound [25, 26], which explains the prolonged respiration activity after 33 h despite glucose depletion.

The optical density (Figure 1.6b) strongly correlates to the OTR and shows exponential growth behavior until 11 h. Cells then multiply linearly in the state of oxygen limitation, and OD_{600} eventually plateau at a value of 6 after 16 h. After 16 h, phosphate is depleted from the medium (Figure 1.6d), causing a secondary substrate limitation, which is further substantiated by the

OTR and the increasing viscosity. As a result, the OD_{600} no longer increases, and cells remain in a state of maintenance. In the following time, γ-PGA is produced. γ-PGA measurement shows 0.05 g/L after 16 h and 2 g/L at 21 h (Figure 1.6d). Qualitatively, the online-determined effective viscosity matches the offline-determined viscosity (Figure 1.6c). These observations solidify the presumption that the online measurement of viscosity gives rise to information on γ-PGA production in liquid shake flask fermentations.

The findings of Figure 1.6 highlight that promoter P_{pst} is tightly regulated and that its repression system is highly affine to P_i, thereby allowing de-repression only at concentrations in a low mg/L range [22]. Furthermore, a correlation between γ-PGA production (Figure 1.6d) and increased effective viscosity (Figure 1.6c) could be demonstrated. Ultimately, the use of phosphate starvation-inducible promoter P_{pst} enables the decoupling of microbial growth and γ-PGA production. This decoupling may be exploited to establish a cultivation with two distinct phases: an initial microbial growth under non-limiting conditions to reach a sufficient cell density and a succeeding phase of product formation.

1.3.2.4 Influence of depolymerase knockouts on γ-PGA synthesis in *B. subtilis* P_{pst}

In the following, the ViMOS is used to investigate the influence of three different depolymerase gene deletions on γ-PGA synthesis and degradation (Figure 1.7).

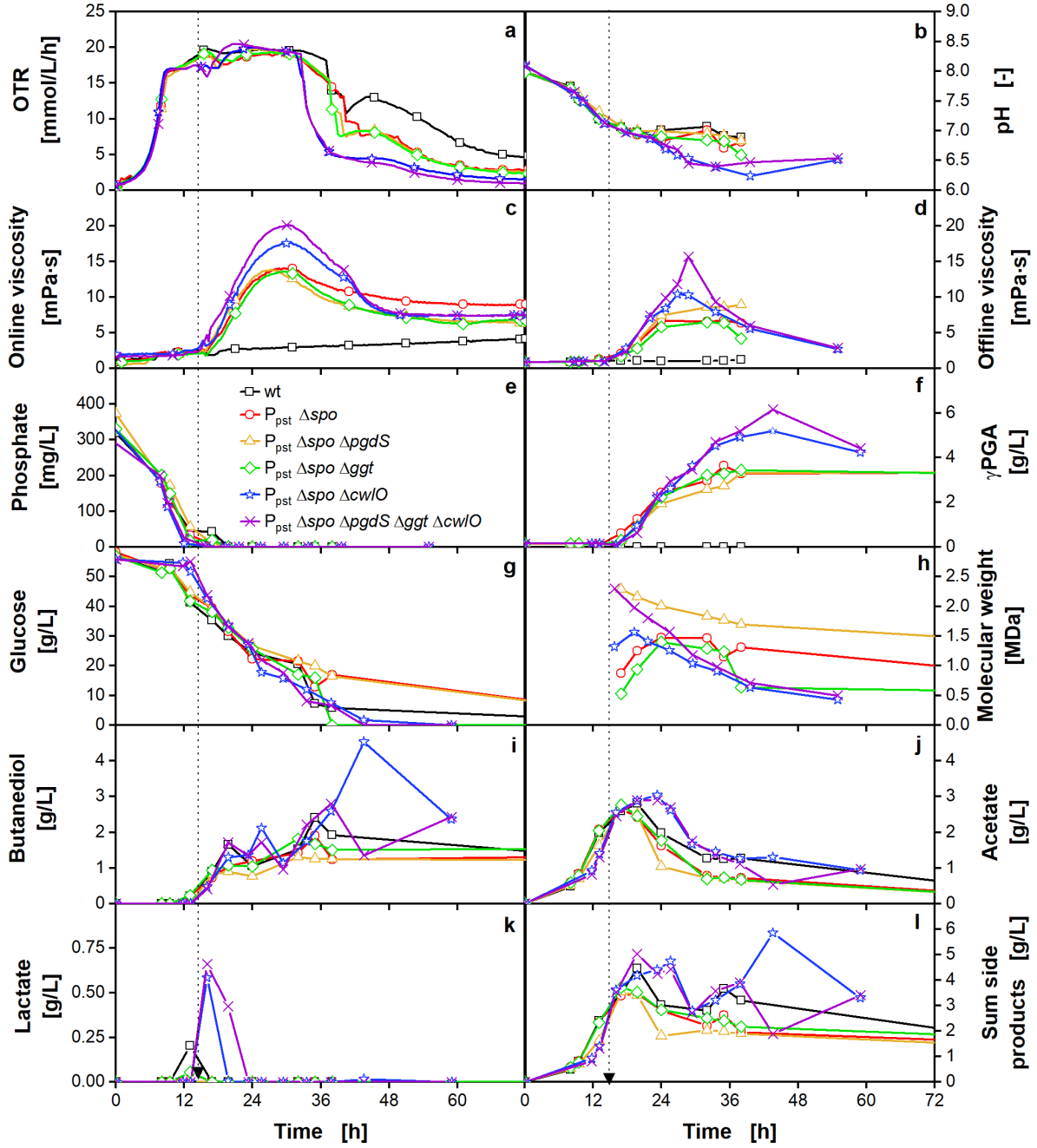

Figure 1.7 Impact of different depolymerase gene knockouts on γ-PGA production and depolymerization.

B. subtilis strains were cultivated in a modified V3 glucose minimal medium: pH_{start} = 8.1, 60 g/L glucose, phosphate: 25% of the original concentration ≙ 0.85 g/L K_2HPO_4, 0.2 MOPS, inoculation from pre-culture (OD_{start} = 0.1), T = 37 °C, 250 mL shake flask, V_L = 30 mL, n = 250 rpm, d_0 = 50 mm. *B. subtilis* wt, lacking a functional promoter, (black) was used as a negative control with no γ-PGA production. The other strains are the *B. subtilis* strains with P_{pst} promoter (red) as well as variants of it, in which the genes for depolymerases were knocked out. The depolymerase genes *pgdS*, *ggt,* and *cwlO* were analyzed both as single knockout (yellow, green, and blue) and as triple knockout (purple). Oxygen transfer rates (OTR) are shown in (a), pH is shown in (b), γ-PGA

concentration in (f), and molecular weight in (h). Effective viscosities were measured online (c) with a new system to measure online and parallel the viscosity in eight shake flasks (ViMOS), as described by Sieben et al. 2019. Offline viscosities measured with a standard rheometer are depicted in (d), phosphate concentration in (e), glucose concentration in (g), and overflow metabolites butanediol in (i), acetate in (j) and lactate in (k). Acetoin could not be quantified due to the equal elution time of the buffering agent MOPS in the liquid medium. The sum of the side products is shown in (l). The dotted vertical lines indicate the time of phosphate depletion and the start of viscosity increase due to γ-PGA production. Oxygen transfer rate (OTR) measurements were carried out in duplicates. For clarity, average values are shown (a). The complete OTR dataset in combination with the associated optical densities of the cultures can be found in the Appendix in Figure A 4. The relation between the microbial growth rate and the OTR is shown in the supplementary data section "Calculation of μ_{max} from OTR data". Data were generated in two experimental runs (run 1: wt, P_{pst} Δspo, P_{pst} Δspo ΔpgdS, P_{pst} Δspo Δggt; run 2: P_{pst} Δspo ΔcwlO, P_{pst} Δspo ΔpgdS Δggt ΔcwlO). In the case of run 2, time data were shifted by -4 h on the x-axis for lag phase adaption. For clarity, only every fifteenth (a) and fortieth (c) measuring point is marked as a symbol.

The three depolymerases PgdS [31], Ggt [32, 33], and CwlO [27-29] are investigated as single gene deletions and in a triple gene deletion mutant (Figure 1.7). As a negative control, *B. subtilis* Δspo deficient in γ-PGA production, and as a reference, the already investigated *B. subtilis* P_{pst} Δspo, are used. In Figure 1.7, the six different *Bacillus* derivatives are compared with each other. The OTR (Figure 1.7a) and the online viscosity (Figure 1.7c) are shown as online signals. These are evaluated in combination with offline data of pH (Figure 1.7b), offline viscosity (Figure 1.7d), phosphate consumption (Figure 1.7e), γ-PGA concentration (Figure 1.7f), glucose consumption (Figure 1.7g), and γ-PGA molecular weight (Figure 1.7h) as an indicator for degradation. In addition, the side products butanediol (Figure 1.7i), acetate (Figure 1.7j), and lactate (Figure 1.7k), as well as their sum (Figure 1.7l), are analyzed for the individual strains. Duplicates of the OTR data are shown in Supplementary Figure 4.

The γ-PGA-producing strains with the P_{pst} promoter (Figure 1.7a) can be divided by their growth and production behavior into two groups. The first group includes the Δ*cwlO* and the triple gene deletion strain. The second group consists of the *B. subtilis* P_{pst} Δspo, the Δ*pgdS,* and the Δ*ggt* strain. The OTRs of group one drop sharply after 34 h cultivation time. The OTRs of the group two strains decrease later only after 40 h – 48 h and show a less pronounced steep decline than the *cwlO* and triple knockout strains. The division of the strains into these two groups can generally also be recognized in the other graphs of Figure 1.7.

The qualitative course of the online and offline viscosity signals are well-matched. In both measurements, the negative control of the *B. subtilis* Δspo shows, as expected, no viscosity increase, due to missing γ-PGA formation. This is confirmed by determining the γ-PGA concentration, which does not show any γ-PGA synthesis for the negative control (Figure 1.7f). The viscosity of the other strains starts to increase after 16 h (Figure 1.7c and d) once phosphate is depleted (Figure 1.7e). These findings are in good agreement with the results shown in Figure 1.6. Like the OTR curves, the viscosity curves can be divided into the before-defined two groups. The viscosity for group one, the Δ*cwlO,* and the triple knockout strain increases faster and reaches higher values than the viscosity of the group two strains (Figure 1.7c). After 34 h *B. subtilis* P_{pst} Δspo *ΔcwlO* reaches a maximum online viscosity of 17.6 mPa·s and the *B. subtilis* triple knockout even slightly higher values with 20.2 mPa·s. The maximum online viscosity of the other strains is lower (with 13.6-14 mPa·s). This observation is supported by the offline viscosity (Figure 1.7d), which shows the same qualitative course, but lower overall values. Online and offline measured viscosity are in good agreement with γ-PGA concentrations' progress (Figure 1.7f). These also show higher γ-PGA concentrations for group one strains, than the group two strains. These γ-PGA concentrations must be regarded as high for glutamate-independent γ-PGA production with glucose as the only relevant carbon source, compared to other glutamate-independent γ-PGA producers described in literature [30, 35, 66, 67]. This increased γ-PGA production with the Δ*cwlO* and the triple knockout mutant fits the deviating OTR curves of these two strains. As shown in other studies, γ-PGA production is likely associated with faster growth rates and substrate uptake rates, demonstrating the driven-by-demand concept [68, 69]. Speculation for enhanced γ-PGA formation of the Δ*cwlO* and triple knockout strains is that the cell morphology changes through the genetic modifications [30]. The deletion of Δ*cwlO* leads to shorter cells that have a higher surface-volume ratio than longer cells. Since γ-PGA is formed by an enzyme complex in the cell membrane, more γ-PGA may be formed due to a relatively larger membrane surface area. Overall, the yield in $g_{\gamma\text{-}PGA}/g_{Glucose}$ increased by 190% in the triple knockout mutant compared to *B. subtilis* P_{pst} Δspo (Appendix Figure A 5). Except for the Δ*cwlO* knockout, neither the Δ*ggt* nor the Δ*pgdS* single knockout shows an effect on maximum γ-PGA concentration or viscosity. The findings concerning Δ*ggt* and the Δ*pgdS* single knockout are in good agreement with comparable studies [27, 30]. The maximum γ-PGA concentrations for P_{pst}, *Δggt,* and *ΔpgdS* are close to 3.4 g/L - 3.6 g/L. With the *ΔcwlO*, the concentration could be increased to 5.2 g/L and in the triple

knockout even to 6.2 g/L. The increase in product formation of the triple knockout is the result of a synergistic effect of knockouts, even though Δ*ggt* and Δ*pgdS* did not show a positive impact on their own. This synergistic effect is also described in other studies [34, 37]. For example, no γ-PGA production increase could be observed for the single knockout of Δ*ggt* and Δ*pgdS* in *B. subtilis* 168. For the double knockout, however, an increase in yield by twice the amount could be determined [34]. Nevertheless, γ-PGA-titers obtained in this study are low, compared to commercial wild-type γ-PGA producers. The *B. subtilis* variants with the P_{pst} promoter used in this study under the applied cultivation parameters are not suitable for commercial production, due to the low γ-PGA yields. Higher product yields can be expected when the cultivation conditions like medium and shaking parameters are optimized. Conventionally, the so-called medium E is used for the production of γ-PGA. However, since medium E does not have a defined pH buffer and is composed of expensive substrates like glutamic acid [16], a modified V3 glucose minimal medium was used instead. It has to be considered that the modified V3 glucose minimal medium with 60 g/L glucose contains just 54.6 % of the carbon provided by medium E. This contributes to lower product titers in this work.

The viscosity of all γ-PGA-producing *B. subtilis* strains decreases after reaching the maximum (Figure 1.7c and d). Proceeding viscosity decreases indicate that γ-PGA is degraded, despite the knockout of the depolymerases. This hypothesis is confirmed by the molecular weight distribution (Figure 1.7h), which shows that γ-PGA is depolymerized in all strains since the molecular weight decreases steadily after 16 h – the start of γ-PGA synthesis. This decrease in the molecular weight may also be due to D/L-endopeptidases other than CwlO and proteases that degrade γ-PGA non-specifically [70]. Mitsui et al. investigated whether the cell wall hydrolases LytE, LytF, and CwlS influence γ-PGA production [27]. Although no effect of knockout mutants on γ-PGA concentration was found, it is still possible that γ-PGA is degraded. In particular, the gene products of *cwlO* and *lytE* share the same activity. Therefore, it is likely that LytE can also cleave γ-PGA. In Figure 1.7h the molecular weight of the single knockout mutant Δ*cwlO* shows a similar drop as the triple knockout mutant, while the knockout of *pgdS* shows just a slight decrease in molecular weight. This drop in the molecular weight seems to be associated with the *cwlO* deletion. Why the *cwlO* deletion results in higher degradation than the other knockouts, is not known yet. However, as CwlO and LytE share the same activity [27, 71, 72], it is possible that *lytE* is stronger expressed and has more influence on γ-PGA

depolymerization, if *cwlO* is deleted. Further studies to investigate the effect of the *cwlO* deletion are necessary.

Furthermore, another γ-PGA specific hydrolase encoded through gene *pghC* was recently identified, which could be responsible for the remaining γ-PGA degradation activity [73, 74], To rule out if this hydrolase is responsible for the ongoing degradation of γ-PGA, knockout derivatives of it remain to be investigated in further studies.

Although the *cwlO* and the triple K knockout strain show the strongest decrease of molecular weight from initially 2 MDa to 0.5 MDa during cultivation, these strains reach the highest γ-PGA production (Figure 1.7f and h). γ-PGA concentration increased from 3.4 g/L with the *B. subtilis* P_{pst} Δspo up to 6.2 g/L with the triple knockout mutant (Figure 1.7f). Despite the depolymerization, γ-PGA concentration remains at the same level in all strains or drops only slightly towards the end of the cultivation. This phenomenon of dropping molecular weight and viscosity, but rising or constant γ-PGA concentrations was also made earlier [44]. The reason for this observation could be that γ-PGA is depolymerized, yet primarily split into smaller chains, but not into monomers [31, 44]. This means that the total concentration of γ-PGA remains constant, while the molecular weight decreases.

The viscosity is not only influenced by the molecular weight but also by the γ-PGA concentration and the pH value [44, 75]. Therefore, there may be deviations between the molecular weight changes and viscosity changes during the cultivation. For example, the viscosity may continue to increase as more γ-PGA is produced. However, the average molecular weight may already decrease, due to depolymerization or the formation of shorter polymers. It can be seen in Figure 1.7c that the viscosity decreases most rapidly for the two *B. subtilis* strains P_{pst} Δspo Δ*pgdS,* Δ*ggt* Δ*cwlO,* and P_{pst} Δspo Δ*cwlO* after 30 h of cultivation. In addition, the molecular weight of these two strains (Figure 1.7h) also decreases most rapidly.

One additional effect that might cause the dropping viscosity in Figures 1.7c and d is a conformational change of the γ-PGA due to a changing pH. It was shown, that γ-PGA in solutions with a pH of ≤ 7 starts to coil, generating smaller particles [75]. Thus, the polymer molecules get a smaller hydrodynamic radius. This would result in a lower viscosity and an apparently smaller molecular weight, as the GPC separates the particles by their size. This

explanation would also fit the results shown in Figures 1.7b, d, and h for the *cwlO* and the triple knockout strains. Figure 1.7b shows a more pronounced drop in the pH for the cultivations of the *cwlO* and the triple deletion strain. The pH even drops below 7. Agreeing with the hypothesis of conformational changes due to a decreasing pH, these two strains show the strongest decrease in viscosity and molecular weight. Further experiments are necessary to clarify, which effects are caused by conformational changes and depolymerization.

Besides γ-PGA production, by-product synthesis and consumption of glucose were analyzed. The Δ*cwlO* and triple knockout strains not only produce the highest amounts of γ-PGA (Figure 1.7f), but also most butanediol (Figure 1.7i), acetate (Figure 1.7j), and lactate (Figure 1.7k). The accumulation of the acidic by-products is reflected in the pH value, which for these two strains decreases more than for the other *B. subtilis* strains (Figure 1.7b).

1.3.2.5 By-product knockouts in *B. subtilis* P_{pst}

In wild-type fermentations, the formation of by-products absorbs a large amount of the available substrates [44]. Preventing by-product formation is one possibility to make substrate available for γ-PGA synthesis. With a strain including deletions of enzymes from the most common by-product pathways, this strategy was investigated.

In Figure 1.1 the by-product pathways of the *B. subtilis* P_{pst} Δspo are shown. Butanediol and acetate are the main by-products during the growth on glucose. As acetoin is a precursor of butanediol it is produced as well. However, this could not be determined by HPLC due to overlapping with the MOPS buffer peak. To analyze if the metabolomic flux can be directed towards the γ-PGA production the pathways for the by-products acetate, butanediol, acetoin, and pulcherriminic acid were knocked out (Figure 1.1). The resulting by-product knockout strain *B. subtilis* P_{pst} Δspo ΔBP was cultivated and analyzed by offline and online analysis. As negative control the *B. subtilis* Δspo with dysfunctional *pgs* operon is cultivated simultaneously. As positive control the *B. subtilis* P_{pst} Δspo is used. The OTR, viscosity, glucose, and phosphate consumption, OD_{600}, and pH of the three cultivated strains are shown in Figure 1.8.

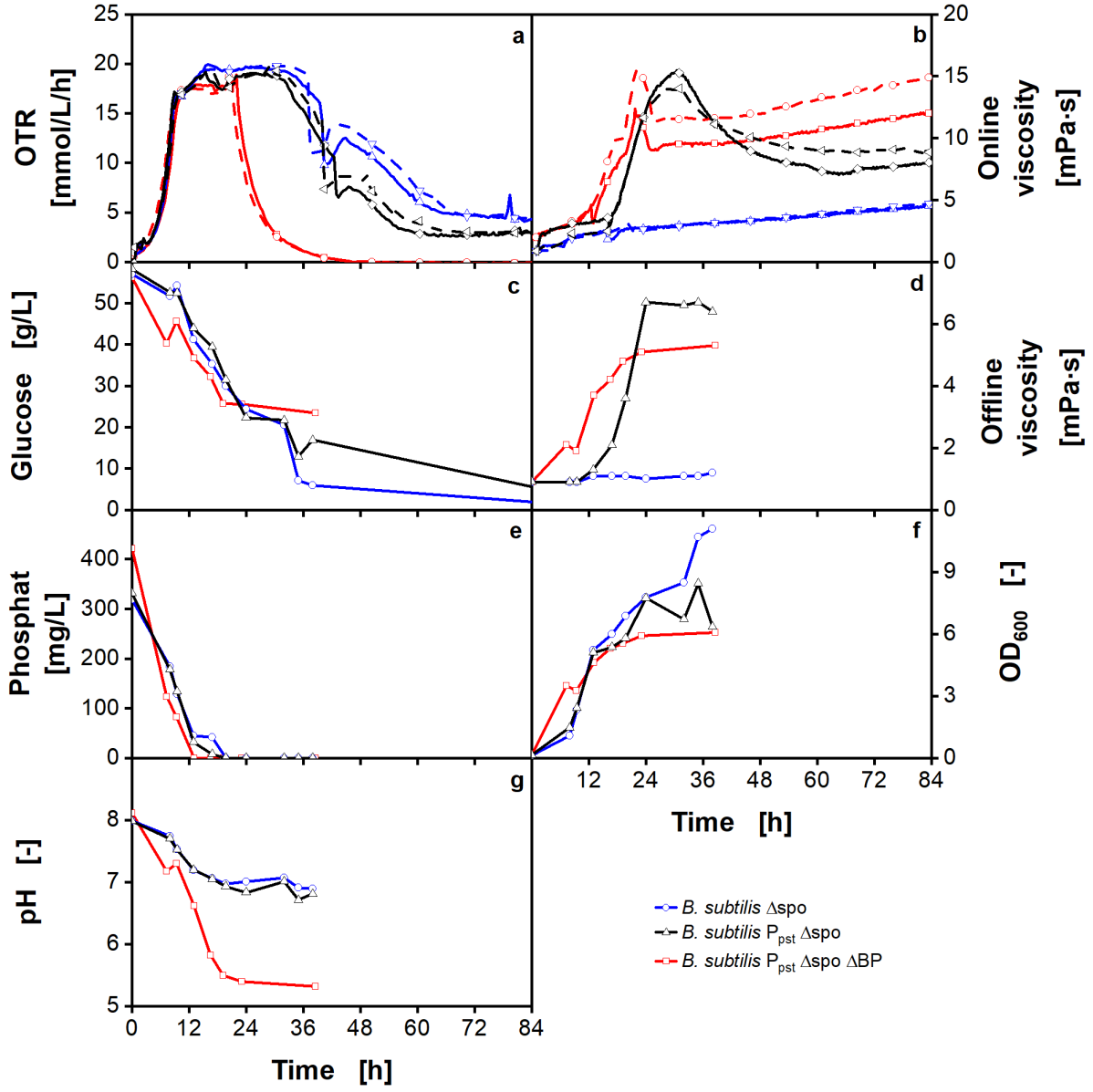

Figure 1.8 Impact of by-product knock outs on growth and viscosity of *B. subtilis* P_{pst} Δspo ΔBP

The OTR (a) and the online viscosity measurements (b) of a *B. subtilis* P_{pst} Δspo ΔBP cultivation (red line) are compared to a *B. subtilis* P_{pst} Δspo (black line) cultivation. The negative control was a *B. subtilis* Δspo culture without γ-PGA production (blue line). Glucose (c), offline viscosity (d), phosphate (e), OD_{600} (f), and pH (g) were analyzed with samples from offline shake flasks. Cultivation conditions: modified V3 glucose minimal medium, pHstart = 8.1, 60 g/L glucose, phosphate: 25% ≙ 0.85 g/L K_2HPO_4, 0.2 M MOPS; inoculation from second pre culture (initial $OD_{600,start}$ = 0.1), T = 37 °C, 250 mL shake flask, V_L = 30 mL, n = 250 rpm, d_0 = 50 mm. Oxygen transfer rates (a) were measured with a RAMOS device. Online viscosity (b) was determined with the ViMOS, described by Sieben et al. 2019. The cultivations were carried out in duplicates in two experimental runs (run 1: *Bacillus subtilis* P_{pst} Δspo and *B. subtilis* Δspo, run 2: *B. subtilis* P_{pst} Δspo ΔBP. The lag phases of *B. subtilis* P_{pst} Δspo ΔBP is longer. Therefore, the data of the *B. subtilis* P_{pst} Δspo ΔBP cultivation have been shifted by -20.46 h on the X-axis, so that the exponential growth

phase of all experiments is superimposed, making the online and offline data easier to compare. The original progressions of the OTR can be found in the appendix in Figure A 6. For clarity, only every 20^{th} (a) and 30^{th} (b) measuring point is marked as a symbol.

The OTR of the negative control *B. subtilis* Δspo and the positive control *B. subtilis* P_{pst} Δspo are similar to each other (Figure 1.8 a). After an exponential growth phase in the beginning from 0-12 h, the OTR levels in a plateau between 12-36 h due to oxygen limitation. The calculated OTR_{max} after Meier et al. is 18.8 mmol/L/h and fits the height of the OTR plateau at 12 h. After the plateau phase, the OTR decreases discontinuously until glucose is nearly consumed (Figure 1.8c) 60 h of cultivation. The OTR of the *B. subtilis* P_{pst} Δspo ΔBP progresses differently from the negative control and positive control strains and shows a very long lag phase of 20.46 h (Appendix, Figure A 6). After this prolonged lag phase, the exponential phase is equivalent to those of the control strains. After reaching the plateau the OTR decreases already after 24 h fast and glucose medium (Figure 1.8c). The pH of *B. subtilis* P_{pst} Δspo ΔBP drops down to 5.4 after 24 h while the pH of the control strains stays around 7 throughout the cultivation (Figure 1.8g). Likely, pH inhibition is also the reason for the dropping OTR of the *B. subtilis* P_{pst} Δspo ΔBP cultivation. Phosphate is consumed in all cultivations after 12 h – 18 h (Figure 1.8e). In the strains with the phosphate starvation promoter $P_{pst,}$ the γ-PGA production should start after phosphate depletion. As glucose is still available at the time of phosphate depletion, the substrate is available for γ-PGA formation (Figure 1.8c). The overall progression of offline and online viscosity is in good agreement with these findings. The viscosities start to rise steeply after phosphate depletion (Figure 1.8b and d). The offline viscosity of the *B. subtilis* P_{pst} Δspo ΔBP shows an increase directly after starting the cultivation. These data fit not well presumably due to the prolonged lag phase of the strain (Appendix Figure A 6). The long lag phase of 20.46 h might lead to deviations between the online and offline cultivations as the lag phase of the online and offline cultivations may be different from each other. The online viscosity of *B. subtilis* P_{pst} Δspo ΔBP starts to rise after phosphate depletion. The viscosity of the *B. subtilis* P_{pst} Δspo ΔBP reaches a lower level than the viscosity of the *B. subtilis* P_{pst} Δspo strain. This indicates lower γ-PGA concentrations or molecular weights of the produced γ-PGA.

Figure 1.9 shows the γ-PGA concentrations and the molecular weight of the three cultivations.

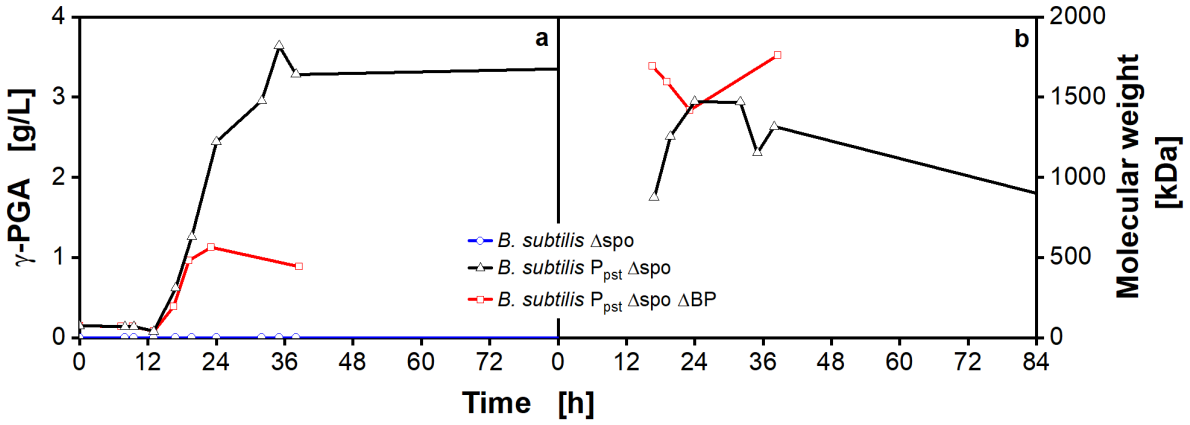

Figure 1.9 Impact of by-product knock outs on γ-PGA production and molecular weight

γ-PGA (a) and molecular weight (b) of *B. subtilis* P_{pst} Δspo and *B. subtilis* P_{pst} Δspo ΔBP are compared. Data were determined with GPC measurements conducted with offline samples of the cultivation shown in Figure 1.8. The cultivations were carried out in duplicates in two experimental runs (run 1: *B. subtilis* Ppst Δspo and *B. subtilis* Δspo, run2: *B. subtilis* P_{pst} Δspo ΔBP. The lag phases of *B. subtilis* P_{pst} Δspo ΔBP is longer. Therefore, the data of the *B. subtilis* P_{pst} Δspo ΔBP cultivation have been shifted by -20.46 h on the X-axis, so that the exponential growth phase of all experiments is superimposed, making the data easier to compare

As the viscosity data in Figure 1.8 already indicated the γ-PGA concentration of the *B. subtilis* P_{pst} Δspo ΔBP and the *B. subtilis* P_{pst} Δspo differ from each other. The *B. subtilis* P_{pst} Δspo ΔBP reaches only 1 g/L γ-PGA while the *B. subtilis* P_{pst} Δspo reaches around 3 g/L γ-PGA. While the achieved γ-PGA concentration of the BP knockout strain is lower than that of the control strain, the molecular weight is higher. Although the by-products are supposed to be deleted the metabolic flux was not directed into γ-PGA synthesis.

To evaluate the effect of the by-product deletions on the by-product formation Figure 1.10 shows the concentration of acetate, lactate, succinate, and 2,3 butanediol.

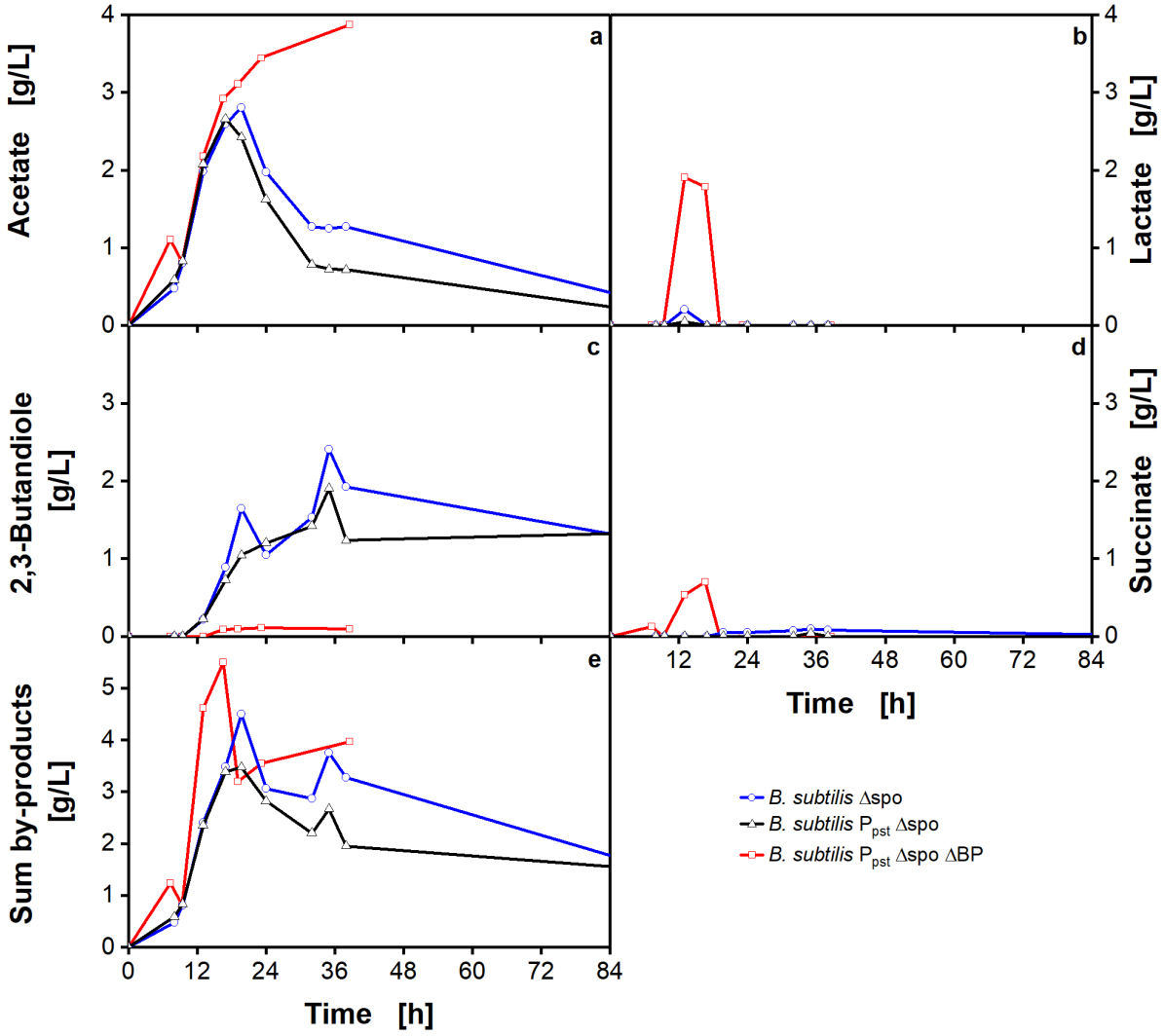

Figure 1.10 Impact of by-product knock outs on by-product formation

Comparison of the by-products acetate (a), lactate (b), 2,3-butandiole (c), and succinate (d) of *B. subtilis* P_{pst} Δspo and *B. subtilis* P_{pst} Δspo ΔBP cultivations. The accumulated by-product concentrations are plotted in e. The by-product concentrations were determined with HPLC measurements conducted with offline samples from the cultivation shown in Figure 1.8. The cultivations were carried out in duplicates in two experimental runs (run 1: *B. subtilis* P_{pst} Δspo and *B. subtilis* Δspo, run2: *B. subtilis* P_{pst} Δspo ΔBP. The lag phases of *B. subtilis* P_{pst} Δspo ΔBP is longer. Therefore, the data of the *B. subtilis* P_{pst} Δspo ΔBP cultivation have been shifted by -20.46 h on the X-axis, so that the exponential growth phase of all experiments is superimposed, making the data easier to compare

In the control strains (Figure 1.10 blue and black curve) the production of by-products is very similar. The by-product formation of the *B. subtilis* P_{pst} Δspo ΔBP differs from the control strains and shows the highest acetate production. Although one enzyme in the pathway for acetate formation was deleted 4 g/L acetate was produced by *B. subtilis* P_{pst} Δspo ΔBP while

the control strains reached only 2.8 g/L. Further, the acetate in the control strains is metabolized again after reaching the peak concentration of 2.8 g/L. In contrast to this, the acetate of the *B. subtilis* P_{pst} Δspo ΔBP is not metabolized. The higher amounts of acetate may be responsible for the dropping pH and the inhibition of further growth (Figure 1.8a, f). Also, the by-products lactate and succinate are produced by the *B. subtilis* P_{pst} Δspo ΔBP in higher amounts than the control strains. Another study with *B. subtilis* P_{pst} Δspo ΔBP showed, that the gene deletions led to an increase of pyruvate and acetyl-coA [24]. These are the main precursors for by-product formation. The accumulation of the precursor is possibly the reason for the increased formation of lactate, acetate, and succinate. Although *pta* was deleted, acetate was produced. It should be analyzed further if other pathways lead to acetate formation as well. The deletion of the butanediol and therefore probably also the acetoin production was successful. Figure 1.10 shows a butanediol production of around 0.1 g/l for the *B. subtilis* P_{pst} Δspo ΔBP while the control strains produce between 1.5 - 2 g/L.

The knockout of by-products was only successful for butanediol but not for acetate. Furthermore, the metabolic flux was not redirected to the production of γ-PGA but rather towards the production of lactate and succinate. Also, further pathways for the production of acetate might need to be knocked out. The decrease of the pH must be stopped to ensure complete metabolization of substrate. The aforementioned study could show a 3.7-fold increase of γ-PGA in a pH-controlled fermentation [24]. Furthermore, an increase of the glutamate synthase might be necessary to ensure that the substrate is directed toward the γ-PGA synthesis. Also, to ensure that the glutamate produced by an increased glutamate synthase activity is used for γ-PGA synthesis a stronger promoter than P_{pst} should be used.

1.3.3 *B. subtilis* P_{xyl} as γ-PGA production host

The previous experiments showed a γ-PGA production of maximal 6.2 g/L. The reasons for this rather low concentration compared to glutamate-dependent producers [15] are a not optimized medium and the weak promoter P_{pst}. To improve this the promoter P_{xyl} was inserted into the *B. subtilis* Δspo. The resulting *B. subtilis* P_{xyl} Δspo should produce γ-PGA upon xylose induction [21].

1.3.3.1 Effect of glucose variations on fermentation broth viscosity of *B. subtilis* P_{xyl} Δspo cultivations

In a first cultivation experiment with *B. subtilis* P_{xyl} Δspo glucose concentrations of 20, 60, 100, and 150 g/L in the modified V3 glucose minimal medium were tested. The results of RAMOS and ViMOS measurements are shown in Figure 1.11.

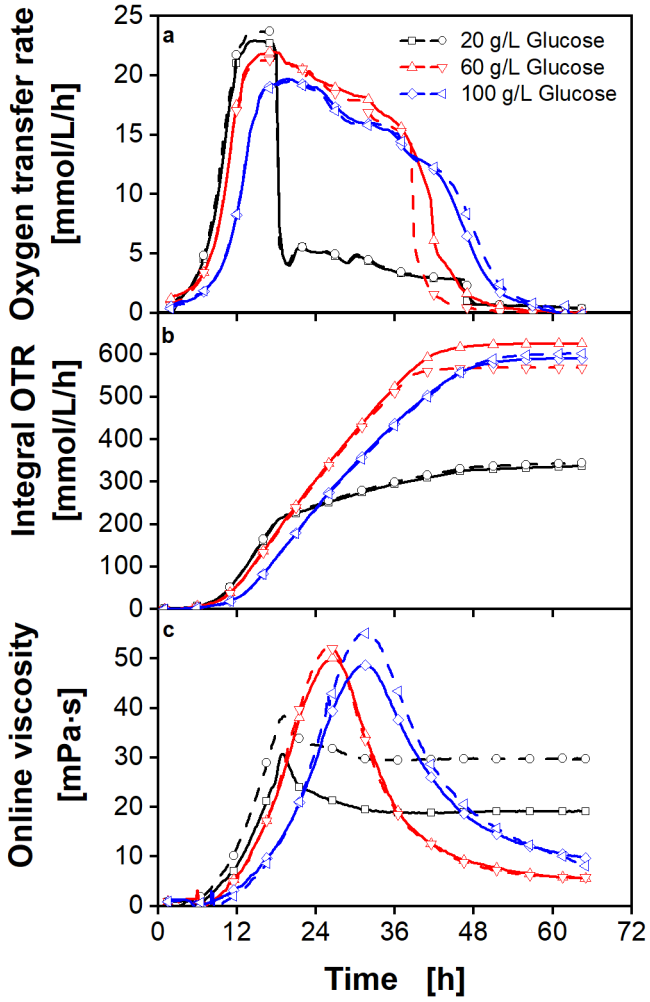

Figure 1.11 Impact of increased glucose concentrations on OTR and viscosity of *B. subtilis* P_{xyl} Δspo

Oxygen transfer rates (OTR) are shown in a. The integral of the OTR over the cultivation time is plotted in b. Online viscosities are presented in c. Cultivation conditions: modified V3 glucose minimal medium, pH_{start} = 8.1, induction with 1 g/L xylose at t = 0 h, varying concentrations of glucose (20, 60, 100 g/L), Phosphate: 25 % ≙ 0.85 g/L K_2HPO_4, 0.02 g/L L-glutamic acid, MOPS: 0.2 M; inoculation from second pre-culture (initial $OD_{600, start}$ = 0.1), T = 37 °C, 250 mL shake flasks, V_L = 30 mL, n = 250 rpm, d_0 = 50 mm. Oxygen transfer rates (a) were measured with a RAMOS device. Online viscosity (b) was determined with the ViMOS, described by Sieben et al.

2019. The cultivations were carried out in duplicates. For clarity, only every tenth (a, and b) and twentieth (c) measuring point is marked as a symbol.

The OTR in Figure 1.11a shows that with higher glucose concentrations the lag phase extends. Furthermore, the maximum of the OTR decreases from 23 mmol/L/h with 20 g/L glucose to 19 mmol/L/h with 100 g/L glucose. As shown before these differences occur through an increased osmotic pressure with higher glucose concentrations, as the oxygen solubility decreases with increasing medium concentration [61]. The data of the cultivations with 150 g/L glucose are not depicted as the *B. subtilis* P_{xyl} Δspo did not grow. The OTR of the cultivation with 20 g/L shows a steep decrease after 20 h due to depletion of the main substrate glucose. The OTR decreases to 5 mmol/L/h followed by a slow decline. For the cultivations with 60 and 100 g/L, the OTR shows a just gentle decline after 20 h. This indicates the limitation through another medium component [42]. This is also confirmed by the integral of the OTR (Figure 1.11b). At 60 h the cultivations are finished. The OTR decreases to 0 mmol/L/h. However, the integral of the OTR does to increase with the same factor as the glucose concentration. This indicates that not all glucose is metabolized and at least one other essential substrate is missing. The missing substrate seems to be also necessary for γ-PGA production. As Figure 1.11c shows the viscosity of the cultivations with 20 g/L and 60 g/L differ clearly. With 20 g/L 30-40 mPa·s are reached and with 60 g/L glucose 55 mPa·s. However, with a further increase in the glucose concentration to 100 g/L, the viscosity does not increase any further than with 60 g/L glucose in the medium.

This first experiment with the P_{xyl} promoter shows already higher viscosity than with the P_{pst} promoter. By increasing the glucose concentration, a secondary substrate limitation becomes visible. This limitation causes cell growth to stop despite the presence of glucose. Furthermore, these substrate limitations also influence the γ-PGA synthesis. This limitation is likely phosphate. Based on the cultivations with the *B. subtilis* P_{pst} Δspo the here used phosphate concentrations were only 0.85 g/L K_2HPO_4. Therefore, in a next step the effect of different phosphate concentration will be analyzed.

1.3.3.2 Influence of phosphate limitation on γ-PGA production with *B. subtilis* Δspo P_{xyl}

For the experiments with the P_{pst} promoter, the phosphate concentration was reduced from 3.5 g/L K_2HPO_4 to 0.85 g/L K_2HPO_4. This was necessary to activate the phosphate starvation promoter P_{pst}. With the P_{xyl} promoter, such phosphate limitation is not necessary and phosphate concentration in the medium can be increased. Therefore phosphate concentrations of 50%, 30%, 20%, and 10% were applied in four cultivations. The results of the phosphate variations are shown in Figure 1.12.

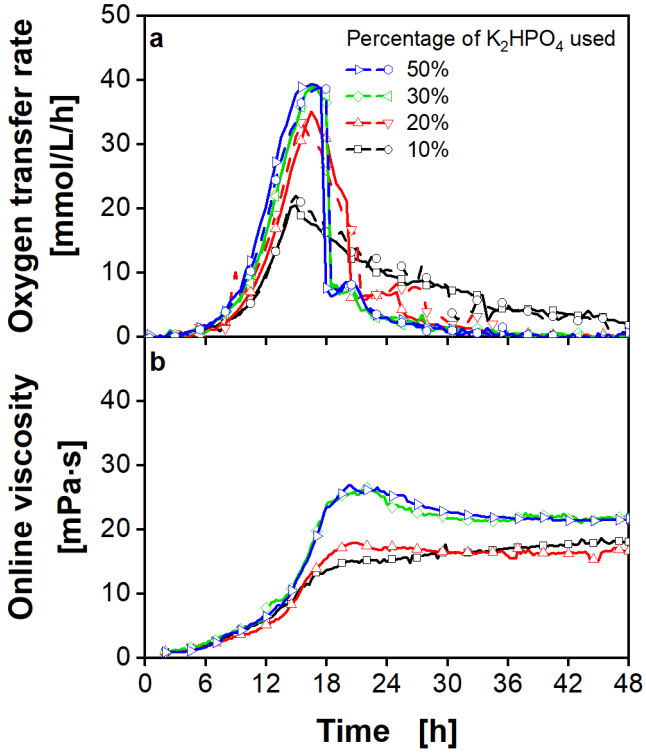

Figure 1.12 Influence of the phosphate concentration on growth and viscosity of *B. subtilis* P_{xyl} Δspo

Oxygen transfer rates (OTR) are shown in a. Online viscosities are presented in b. Cultures are not induced with xylose. Cultivation conditions: modified V3 glucose minimal medium, pH_{start} = 8.1, 20 g/L glucose, varying concentrations of K_2HPO_4 (50 % ≙ 1.7 g/L, 30 % ≙ 1.02 g/L, 20 % ≙ 0.68 g/L, 10 % ≙ 0.34 g/L), 0.02 g/L L-glutamic acid, 0.2 M MOPS; inoculation from second pre-culture (initial $OD_{600, start}$ = 0.1), T = 37 °C, 250 mL shake flasks, V_L = 20 mL, n = 350 rpm, d_0 = 50 mm. Oxygen transfer rates (a) were measured with a RAMOS device. Online viscosity (b) was determined with the ViMOS, described by Sieben et al. 2019. The cultivations were carried out in duplicates. For clarity, only every fifth (a) and tenth (b) measuring point is marked as a symbol.

The cultivations with phosphate concentrations of 50% and 30% (Figure 1.12) show the same OTR and viscosity course as in Figure 1.11 with 20 g/L glucose. Glucose is depleted before phosphate becomes limited. With 20% and 10% phosphate in the medium a gentle decline becomes visible in the OTR and the viscosity does increase less. This shows presumably the negative effects of phosphate limitation on γ-PGA production.

It might be, that phosphate limitation is also the reason for the low γ-PGA concentrations achieved with the P_{pst} promoter. If phosphate is necessary for the γ-PGA production a phosphate depletion promoter should not be used in a batch process. These conflicting demands might be balanced by running a fed-batch process with phosphate. The phosphate concentration should be high enough to enable the production of γ-PGA, but low enough to keep the P_{pst} promoter active.

Another observation of the experiment shown in Figure 1.12 is that the viscosity increases although no xylose was added to the medium or later during the cultivation. This is an indicator of a leaky promoter. Therefore it is necessary to analyze the sensitivity of the P_{xyl} promoter and to create and analyze an induction profile with varying induction times and concentrations.

1.3.3.3 Enhanced γ-PGA production with *B. subtilis* P_{xyl} Δspo

Figure 1.12 shows the negative influence of phosphate limitation on the viscosity increase. The glucose variation experiment in Figure 1.11 was still conducted with a low phosphate concentration of 0.85 g/L K_2HPO_4. Therefore the glucose variation experiment was repeated with glucose concentrations of 20, 40, 60, and 70 g/L and a phosphate concentration of 3.4 g/L K_2HPO_4. The results for cultivations with 20 and 40 g/L glucose are shown in Figure 1.13.

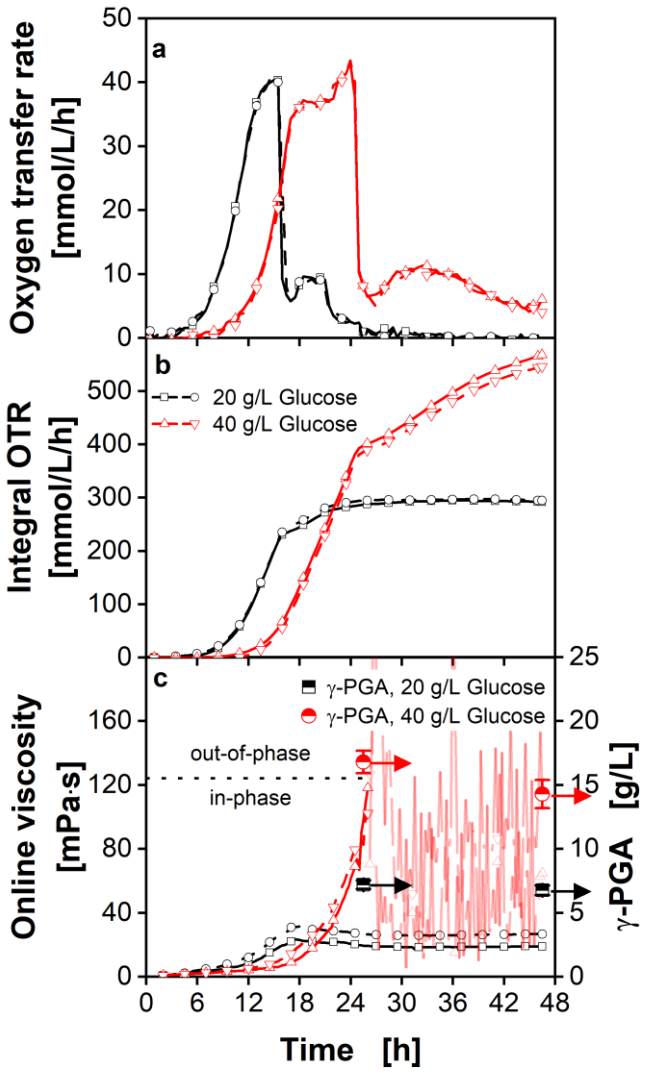

Figure 1.13 Impact of increased glucose concentrations on γ-PGA production of *B. subtilis* P_{xyl} Δspo with adapted phosphate concentration

Oxygen transfer rates (OTR) are shown in a. The integral of the OTR over the cultivation time is plotted in b. Online viscosities and γ-PGA concentration of offline samples are presented in c. Cultivation conditions: modified V3 glucose minimal medium, pH_{start} = 8.1, induction with 1 g/L xylose at t = 0 h, varying concentrations of glucose (20, 40, 60, 70 g/L), 3.4 g/L K_2HPO_4, 0.02 g/L L-glutamic acid, varying concentrations of MOPS (0.2, 0.4, 0.6, 0.7 M); inoculation from second pre-culture (initial $OD_{600, start}$ = 0.1), T = 37 °C, 250 mL shake flasks, V_L = 20 mL, n = 350 rpm, d_0 = 50 mm. Oxygen transfer rates (a) were measured with a RAMOS device. Online viscosity (b) was determined with the ViMOS, described by Sieben et al. 2019. The liquid in the shake flasks was calculated to be out-of-phase at viscosities > 124 mPa·s according to [63]. The dotted horizontal line in c defines the viscosity limit for in-phase conditions with the applied cultivation parameter. Below this limit, the cultivation is in phase, above the limit it gets out of phase. Concentrations of γ-PGA (c) were determined with triplicates with the CTAB assay. The cultivations were carried out in duplicates. For clarity, only every fifth (a, and b) and tenth (c) measuring point is marked as a symbol.

The data with 60 and 70 g/L glucose are not shown as the cultivations did not grow. The OTR of cultivations with 40 g/L glucose features an elongated lag phase and a reduced OTR_{max}, presumably due to osmotic pressure. The OTR of the cultivations with 20 g/L and 40 g/L show a steep decrease after 16 h respectively 26 h usually associated with glucose depletion [42]. But while the OTR for the cultivation with 20 g/L glucose drops to zero finally the OTR of the cultivation with 40 g/L shows a low breathing activity between 5 to 11 mmol/L/h after the steep decrease at 26 h. For the cultivation with 40 g/L, the reason for the steep decrease is not glucose depletion but an out-of-phase condition due to increased viscosity [63]. The explanation of the out-of-phase condition is supported by taking into account the integral OTR and the viscosity. The integral OTR with 20 g/L glucose reaches 295 mmol/L/h when the OTR decreases due to glucose depletion. With the double amount of glucose, the integral OTR should be around double as high at the steep decrease of the OTR in Figure 1.13 at 26 h. However, the integral OTR with 40 g/L is only around 400 mmol/L/h and continues to increase slowly after 26 h. Through the out-of-phase condition with uncontrolled liquid movement and air bubble formation, the oxygen transfer into the liquid becomes unreproducible. The oxygen supply is drastically reduced leading to the steep decrease of the OTR at 26 h. As glucose is still available the organisms grow and show breathing activity resulting in a low OTR. The online viscosity (Figure 1.13c) also shows the disturbance of the cultivation related to the out-of-phase condition. With 20 g/L glucose, the viscosity increases until 18 h and then stays relatively constant. With 40 g/L glucose, the viscosity increases steeply until 26 h. Afterward, the viscosity signal goes up and down wildly. The viscosity measurement did not work any longer. The liquid in the shake flasks was calculated to be out-of-phase at viscosities higher than 124 mPa·s [63] under the applied shaking and cultivation parameters. The out-of-phase condition caused the cultivation liquid to move undefinable and unreproducible in the flasks. Through these liquid movements, the culture broth was not in front of the infrared sensor of the ViMOS in regular movements. Additionally, air bubbles were produced through the swapping liquid. They are detectable in Figure 1.14.

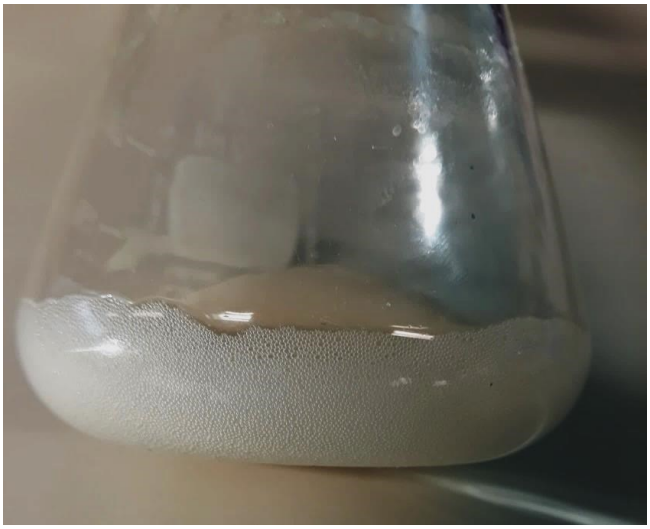

Figure 1.14 Intense foam production of the viscous fermentation medium

Shake flask picture from cultivation with *B. subtilis* P_{xyl} Δspo with 40 g/L glucose. Production of γ-PGA caused increasing medium viscosity resulting in out-of-phase conditions. Shear effects favored foam production which prevented an online measurement of viscosity as trespassing light beams of the LEDs were scattered (Figure 1.13). The picture was taken at 25 h during the cultivation of *B. subtilis* P_{xyl} Δspo described above in Figure 1.13.

Those air bubbles also interfere with the ViMOS measurement. Although the out-of-phase condition though the high viscosity is an unwanted effect, the high viscosity itself indicates a high γ-PGA production.

In Figure 1.13 the γ-PGA concentrations measured with the CTAB assay at two time points are shown. The first measuring point was shortly before the out-of-phase condition occurred. The second sampling is at the end of the cultivation. The γ-PGA concentration of the first sampling of the 20 and 40 g/L glucose cultivations is with 7.2 and 16.8 g/L γ-PGA respectively, slightly higher than at the second sampling with 6.8 and 14.3 g/L γ-PGA. During the out-of-phase period, γ-PGA is not produced anymore but rather consumed or depolymerized. A possible reason for the stopping γ-PGA synthesis is the aforementioned changes in the oxygen supply due to the out-of-phase condition. The γ-PGA synthesis is strongly influenced by oxygen availability and is therefore affected [18, 62]. For further cultivations with the *B. subtilis* P_{xyl} Δspo, the out-of-phase condition should be avoided. This could be achieved by reducing the shaking frequency or increasing the filling volume. As these two parameters strongly influence the oxygen transfer into the liquid, which influences itself the γ-PGA synthesis cultivations should be monitored closely. Another possibility to prevent out-of-phase conditions would be

the reduction of glucose in the medium. With 20 g/L glucose, the out-of-phase condition is avoided as less γ-PGA is produced and viscosity doesn't rise above the critical value.

Despite the out-of-phase condition the produced γ-PGA concentration in the cultivation with 40 g/L glucose is more than twice as high as with the P_{pst} promoter and 60 g/L glucose. The achieved 16.8 g/L γ-PGA without thorough optimization of the cultivation is a very good result for a glutamic independent producer on glucose as the only carbon source. Furthermore, the γ-PGA concentration of 16.8 g/L is already reached after 25 h of cultivation. For a production process, the aspect of a short fermentation time is very favorable. With the additional aspect, that the cultivation was performed with glucose as only carbon source in mineral medium, this makes the *B. subtilis* P_{xyl} Δspo a very promising γ-PGA producer.

1.3.4 Comparison of the γ-PGA produced by the different *Bacillus* strains presented in this study

In the following section, the γ-PGA concentrations produced by the different strain variants of the previous chapters are compared. For the cultivation of the *B. licheniformis* ATCC, 9945 medium E was used which contains glycerol, glutamate, and citrate as carbon sources. The *B. subtilis* 168 cultivations were performed in modified V3 glucose minimal medium. Because of the different carbon sources in the media, the γ-PGA yield coefficient was related to mol carbon. As the substrate left in the media was not determined for all experiments, the whole amount of used carbon source of each cultivation was used for the calculations. The following table shows the molar amount of carbon of the different media used for the γ-PGA cultivations.

Table 1.3 Molar amount of carbon of the γ-PGA cultivation media

Medium	Carbon [mol/L]
Medium E	3.66
Modified V3, 20 g/L glucose	0.67
Modified V3, 40 g/L glucose	1.33
Modified V3, 60 g/L glucose	2

The following Figure 1.15 compares the maximal achieved concentration of γ-PGA and the corresponding yield coefficient of *B. licheniformis* ATCC 9945 (data published in [44]), *B. subtilis* Δspo, *B. subtilis* P_{pst} Δspo and *B. subtilis* P_{xyl} Δspo.

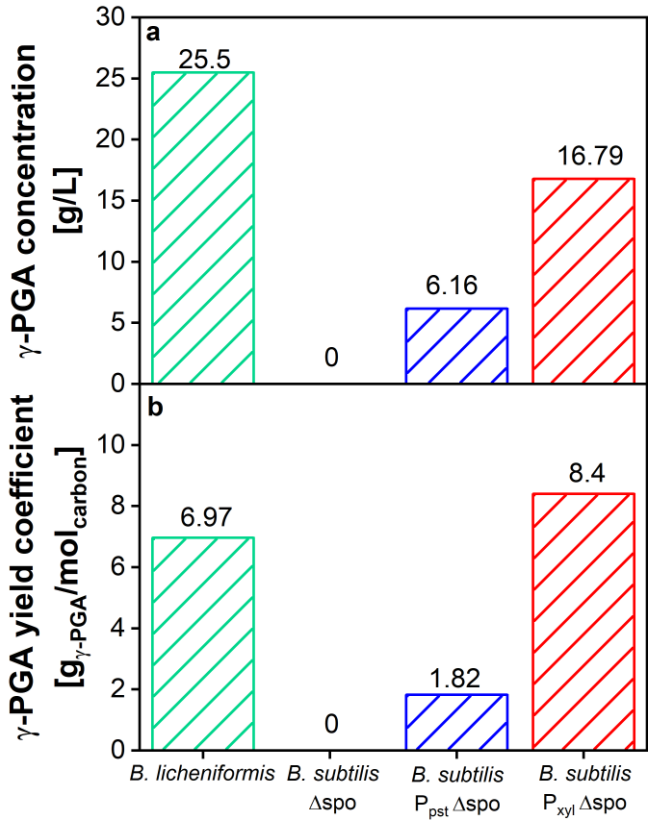

Figure 1.15 Comparison of the concentration and γ-PGA product yield coefficients of *B. licheniformis* ATCC 9945, *B. subtilis* Δspo, *B. subtilis* P_{pst} Δspo and *B. subtilis* P_{xyl} Δspo.

The highest γ-PGA concentrations achieved were set in relation to the carbon concentration contained in the respective carbon source used in the medium. a shows the maximal achieved γ-PGA concentration and b the related yield coefficient. The data for *B. licheniformis* ATCC 9945 were taken from the publication of Meissner et al [44]. *B. licheniformis* ATCC 9945 was cultivated with medium E containing 80 g/L glycerol, 20 g/L glutamic acid, and 12 g/L citric acid. *B. subtilis* Δspo and *B. subtilis* P_{pst} Δspo were cultivated in modified V3 glucose minimal medium with 60 g/L glucose. The cultivation is shown in Figure 1.7. *B. subtilis* P_{xyl} Δspo was cultivated in modified V3 glucose minimal medium with 40 g/L glucose. The cultivation is shown in Figure 1.13. The γ-PGA concentration was determined with GPC measurements for *B. licheniformis* ATCC 9945, *B. subtilis* Δspo, and *B. subtilis* P_{pst} Δspo and with CTAB measurement for *B. subtilis* P_{xyl} Δspo.

Figure 1.15a shows that the highest concentration of 25.5 g/L γ-PGA is synthesized by the wild-type producer *B. licheniformis* ATCC 9945. The *B. subtilis* P_{pst} Δspo and *B. subtilis* P_{xyl} Δspo produce with 6.16 and 16.79 g/L, respectively, less γ-PGA. However, it has to be taken into

account that the medium components differ between the cultivations. While the *B. licheniformis* ATCC 9945 was cultivated with glycerol, glutamic acid, and citric acid the *B. subtilis* P_{pst} Δspo and *B. subtilis* P_{xyl} Δspo use only glucose as carbon source. Therefore, the yield coefficient was presented in Figure 1.15b in relation to the amount of mol carbon used in the respective medium. The yield coefficient shows that by taking the carbon substrate into account the *B. subtilis* P_{xyl} Δspo shows with 8.4 $g_{\gamma\text{-PGA}}/mol_{carbon}$ even a better yield than the *B. licheniformis* ATCC 9945 with 6.97 $g_{\gamma\text{-PGA}}/mol_{carbon}$. Higher concentrations are usually reported for fermentations with glutamic acid and citric acid-based media or complex media [54-60]. But not only are the costs for the medium components' glutamic acid and citric acid significantly higher than for glucose but also the fermentation times extend over several days. With *B. subtilis* P_{xyl} Δspo in only 24 h and glucose as a carbon source, relatively high amounts of γ-PGA were achieved even without thorough process optimization. This shows the potential of *B. subtilis* P_{xyl} Δspo as a γ-PGA producer.

1.4 Conclusion and outlook

In the first chapter of this thesis the applicability of a recently developed optical online viscosity measurement system, ViMOS, to determine γ-PGA production, using multiple *B. subtilis* strains equipped with the P_{pst} or P_{xyl} promoter was demonstrated [45]. The ViMOS offers the possibility for parallel online viscosity measurements and, therefore, higher throughput in microbial cultivation-based polymer research. The promoter P_{pst} was demonstrated to be de-repressed upon phosphate depletion from the cultivation medium. After identifying suitable cultivation parameters using the ViMOS and RAMOS, depolymerase knockout strains were investigated. Cleavage of γ-PGA by enzymes PgdS, Ggt, and CwlO were investigated by analyzing knockout mutants Δ*pgdS*, Δ*ggt*, Δ*cwlO,* and the respective triple knockout. γ-PGA degradation was observed in all derivatives, despite the knockout of the depolymerases. To investigate, which enzymes are responsible for the ongoing depolymerization of γ-PGA, strains with additional knockouts could be engineered.

Overall, only small γ-PGA titers are obtained under the influence of the P_{pst} promoter compared to other production strains like *B. licheniformis* ATCC 9945 [44]. However, considering the use of the P_{pst} promoter and glucose as the only C-source, the γ-PGA concentrations achieved can be compared with other glutamate-independent γ-PGA producers. These reach γ-PGA concentrations between 4 g/L and 9 g/L γ-PGA [30, 35]. One possibility to further increase the titer would be to perform a phosphate-limited fed-batch experiment at low phosphate concentrations. It may be possible to enhance the metabolism of the microorganisms through the maintenance of a low phosphate concentration, allowing the investigation of the influence of the phosphate concentration on the γ-PGA synthesis. This approach would aim to increase product formation. It was shown that by using the P_{pst} promoter, γ-PGA production can be controlled by phosphate concentration. The control over the promoter activity makes it attractive for further studies, as growth and production can be separated. For further and direct evidence of the promoter sensitivity to phosphate, quantitative RT-PCR should be applied in future studies. Furthermore, it should be investigated, whether nitrogen is present in sufficient quantities as the findings of Figure 1.6 indicate another substrate limitation, resulting in limited γ-PGA production. Only the triple knockout and the Δ*cwlO* knockout strain, deficient in

peptidoglycan hydrolase CwlO, showed an increased γ-PGA production. The γ-PGA yield with the triple knockout strain could be increased by 190% compared to *B. subtilis* P_{pst} Δspo. With 6.2 g/L, the triple knockout strain achieved relatively high values for a glutamate-independent γ-PGA producer with glucose as the only carbon source.

The by-product knockout is a promising concept to increase γ-PGA yield. Nevertheless, the desired effects could not fully be shown in this study. One positive result was the drastic reduction of produced butanediol. This pathway was knocked out with success. Acetate was still produced in high amounts and led together with the lactate and succinate production to a pH drop which inhibited the organisms from growing and producing γ-PGA. The knockout of further acetate pathways and an enhanced glutamate synthase activity should be considered. Furthermore, to prevent pH inhibition it should be considered to do a pH-controlled fermentation or to increase the amount of buffer. It was shown that with a pH control within a fermenter, the amount of γ-PGA was increased significantly compared to the control strain [24]. As the P_{pst} promoter led to only small amounts of γ-PGA it is indicated to repeat the knockout studies under the control of a stronger promoter to make differences easier to detect.

Compared to the P_{pst} promoter P_{xyl} showed a higher γ-PGA production with 16.79 g/L synthesized γ-PGA. It was demonstrated that phosphate limitation affects the γ-PGA production negatively. The medium and the shaking parameter should be further optimized to avoid out-of-phase conditions and to achieve even higher γ-PGA yields. Additionally, a xylose induction profile should be performed. First experiments showed that the P_{xyl} might be a leaky promoter even producing γ-PGA without xylose as an inductor. Although the cultivation of *B. subtilis* P_{xyl} Δspo was not optimized for γ-PGA production it already reached 16.79 g/L γ-PGA. The comparison of the yield coefficients related to the molar concentration of carbon in the medium showed that the *B. subtilis* P_{xyl} Δspo with 8.4 $g_{\gamma\text{-PGA}}/mol_{carbon}$ showed even better results than the *B. licheniformis* ATCC 9945 with 6.97 $g_{\gamma\text{-PGA}}/mol_{carbon.}$

Further analysis of the *B. subtilis* P_{xyl} Δspo and the characterization of the γ-PGA itself should be conducted to evaluate *B. subtilis* P_{xyl} Δspo as an industrial production strain.

Chapter 2

Spotting priming-active compounds using parsley cell cultures in microtiter plates

2.1 Introduction

Intensive agriculture depends on the heavy use of synthetic pesticides. The long-term prognosis for their application is unfavorable, as resistance formation of pests and pathogens and the associated loss of biodiversity is just one consequence [76-78]. Hence, the pressure from consumers and politics on agriculture and pesticide producers to practice sustainable cultivation and plant protection increases.

2.1.1 Defense priming of plants

The natural defense of plants is based on plant defense compounds such as phytoalexins that accumulate in response to pathogen contact. However, from the onset of pathogen infestation and following defense response, high fitness losses often occur on the infected part of the plant. The defense response becomes faster and more efficient when the plant is in an increased state of alert. One type of induced resistance resulting in an increased state of alert is systemic acquired resistance (SAR). SAR can also be induced with non-pathogenic chemical compounds, such as salicylic acid (SA) [79-81]. Defense priming enables plants to resist biotic and abiotic stresses more quickly and with fewer fitness costs [79, 80, 82-84]. Thus, one

approach for sustainable agriculture is using substances that induce defense priming. In 1992, a screening system to detect priming-inducing chemistry in parsley cell cultures was introduced [85]. The system is based on fluorescence measurements of furanocoumarins [86]. Parsley cell cultures were primed with a compound such as salicylic acid (SA) after 3 h - 72 h cultivation time. After 96 h the elicitor Pep13 was added to the cell cultures, to stimulate an immune response. Pep13 is a 13 amino acid peptide of a glycoprotein from the soybean pathogen *phytophthora sojae* [87]. If priming occurred, cell cultures responded with increased production of furanocoumarins, fluorescent phytochemicals that belong to the phytoalexins. Furanocoumarins were qualitatively detected by fluorescence measurement at an excitation wavelength of 335 nm and an emission wavelength of 398 nm [85, 86, 88, 89]. Studies based on this method of investigating priming, are discussed below.

2.1.2 Methods to detect defense priming

One online screening technique reported for parsley cell cultures is based on applying the respiratory activity monitoring system (RAMOS) [42, 43]. RAMOS measures the OTR to identify putative priming compounds in shake flasks [90]. To establish the online screening system, parsley cell cultures were pretreated with compounds that were known to be active, or inactive, at activating defense priming before they were treated with Pep13 [85, 86, 88]. Parsley cell cultures were demonstrated to respond with an increase in the OTR after priming and subsequent stimulation with an elicitor [90]. The increase of the OTR after the addition of the elicitor Pep13 was higher, if the cell cultures were previously primed with SA or e.g. the known priming-active SA derivative 4-chlorosalicylic acid (4-CSA). The treatment with the known priming-inactive compounds 4-hydroxybenzoic acid (4-HBA) and 3-hydroxybenzoic acid (3-HBA) did not lead to an increase in the OTR [90]. From the course of the OTR, it was possible to infer which compound was active at priming of the cell cultures [90]. As the OTR is an unspecific signal, applicable to all plant suspension cultures, this technique bears the potential to be transferred to other plant cell cultures.

Another innovative screening device for response-screening activity in plant cells is based on the online measurement of the defense-associated plant hormone ethylene [91]. In this approach, cultured parsley cells were grown in a RAMOS system equipped with

electrochemical ethylene sensors. The device enables the simultaneous recording of the OTR and ethylene. It thus provides more information on the complex interplay of signaling different signaling compounds in a given plant species.

A recently published study aimed at transferring the RAMOS technique from cell suspension cultures to *Arabidopsis thaliana* seedlings [92]. The seedlings were grown in liquid medium and a 48-well MTP with a simulated day-night cycle. The cell suspension cultures were treated with the priming-active compounds SA and methyl 1-(3,4-dihydroxyphenyl)2-oxocyclopentane-1-carboxylate (Tyr020). Later they were challenged with flg22, a 22-amino acid peptide. The respiration activity was measured with a modified µRAMOS technique [93] to enable OTR measurement in every single well of the 48-well MTP to conclude possible priming activity.

2.1.3 High-throughput screening with online DOT and furanocoumarin fluorescence measurements

The here presented data aimed at developing a high-throughput online screening system to identify priming compounds with plant cell suspension cultures. To do so, the oxygen consumption of parsley suspension cells was measured by monitoring the dissolved oxygen tension (DOT) in each well of an MTP. Monitoring of the DOT was performed using a BioLector device and optical fluorescence spots [94, 95]. The OTR can be calculated from the DOT if the volumetric mass transfer coefficient (k_La) is known and constant [96]. The suitability of this method for the identification of priming compounds has been verified in this work, using the above-described system with SA as a known priming-active compound and the elicitor Pep13 [86, 88]. With this high-throughput method for online measuring the DOT in MTPs, it is possible to identify potential priming compounds. In addition to the OTR measurements, the furanocoumarins were fluorometrically analyzed. The secretion of furanocoumarins can online be monitored via fluorescence measurements on the BioLector platform. Besides furanocoumarins, SA can also be monitored fluorometrically [90]. The measurement of the respiration activity and the fluorescence of SA and furanocoumarins in MTPs were used to monitor the response of parsley cell cultures to treatment with SA and Pep13. With the combination of fluorescence and DOT measurement in MTPs, a noninvasive online high-throughput screening system for priming compounds was developed. In addition,

different concentrations and times of treatment with supposed priming compounds can be analyzed.

2.2 Materials and methods

2.2.1 Media and solutions

Media were prepared as described previously: Parsley cell suspension was cultivated in modified Gamborg's B5 medium. The micro- and macro-elements, including vitamins, were purchased from DUCHEFA BIOCHEMIE B.V, Haarlem, the Netherlands. The medium was supplemented with 20 g/L sucrose, 20 mg/L 2,4-dichlorophenoxyacetic acid, and 250 mg/L magnesium sulfate heptahydrate. 1 M potassium hydroxide was used to adjust the pH value to 5.5 [90]. Priming compounds were purchased at Sigma-Aldrich Co. LLC. Priming-active and priming-inactive compounds SA, 4-CSA, 4-HBA, or 3-HBA were dissolved in distilled water to obtain a stock solution of 10 mM. The pH value of the stock solution was adjusted to 5.5 with a 1 M potassium hydroxide solution. The compounds were aliquoted and stored at −20 °C. Pep13 purchased from Thermo Fisher Scientific GmbH, Germany, was dissolved in water to obtain a 5 nM stock solution aliquoted into 1.5 mL microfuge tubes and stored at -20 °C.

2.2.2 Shake flask and MTP cultivation

The liquid culture was prepared from a callus every 3-4 months in modified Gamborg's B5 medium [97] to obtain parsley (*Petroselinum crispum*) suspension cell cultures. The suspension culture was cultivated in the dark at 90 rpm in 500 mL baffled shake flasks with filling volumes of 30 mL to 40 mL, a shaking diameter d_0 of 5 cm and 25 °C [90, 97]. The described procedure was repeated every seven days, and the parsley cells were used for further experiments.

Shake flask experiments were conducted in an in-house built respiration activity monitoring system (RAMOS) device [42, 43]. Custom-made versions of the RAMOS device can be acquired from Kühner AG (Birsfelden, Switzerland) or HiTec Zang GmbH (Herzogenrath, Germany). RAMOS shake flasks without baffles were used with a filling volume (V_L) of 50 mL. The cultures consisted of one part parsley cell cultures and four parts fresh modified Gamborg's B5 medium. The cultivations were performed in the dark with a shaking frequency (n) of 180 rpm and a shaking diameter (d_0) of 5 cm at 25 °C.

MTP experiments were conducted in sterile 48-deep-round-well MTPs (MTP-R48-BOH, Beckman Coulter GmbH, Baesweiler, Germany) using a custom made BioLector device (Beckman Coulter GmbH, Germany) or an in-house built device with a connected Spectrofluorometer (Fluoromax-4, HORIBA Jobin Yvon GmbH, Unterhaching, Germany) [94, 95]. The MTP cultivations were performed in modified Gamborg's B5 Medium with V_L = 2 mL, n = 600 rpm or 800 rpm, and d_0 = 3 mm at 25 °C in the dark. The oxygen level in the inlet gas was set to p_{O2} = 0.21 bar, if not stated otherwise. For the experiments with reduced oxygen content, a mixture of nitrogen and air was used to adjust the oxygen level to p_{O2} = 0.15 bar. The flow of nitrogen and air to the aeration unit was regulated by two mass flow controllers (Brooks Instruments, Ede, The Netherlands). A constant volume flow of 60 mL/min was adjusted.

2.2.3 Hydrodynamics in a well

A miniature CCD camera (XC-777AP, Sony) was attached to a shaking platform to record the shaking behavior of parsley cell suspension in a single well of a clear 48-deep-round-well MTP. The clear MTP was kindly provided by m2p-labs (now Beckman Coulter GmbH) and had the same geometrics as the 48-deep-round-well plates for DOT and fluorescence measurements. The pictures were taken with a filling volume of 2 mL, an inner well diameter (D_w) of 12.4 mm, and a shaking diameter (d_0) = 3 mm [98, 99]. Images of parsley cell suspension cultures were taken for shaking frequencies (n) from 0 rpm to 700 rpm for evaluation of mixing behavior. The critical shaking frequency (n_{crit}) [rpm] was calculated according to Hermann et al. [98] (see Equation 1), taking into account the shaking diameter (d_0) [m] of 0.003 m, the well diameter (D_w) [m] of 0.00124 m and the filling volume (V_L) of 0.002 L. The surface tension (σ) [N/m] of the modified Gamborg's B5 medium was determined by the Wilhelmy plate method (tensiometer from Fa. Lemke Parter, Kaarst, Germany; platin plate from Krüss GmbH, Hamburg, Germany). The mean surface tension of the modified Gamborg's B5 medium was 69.00±1.03 N/m (n = 3). To estimate the liquid density, the modified Gamborg's B5 medium was assumed to act as an ideal mixture without intermolecular interactions and without solving effects of the medium. The weight of each component in 1 L H_2O was added up and combined with the weight of 1 L H_2O. The liquid density (ρL) was 1023.4 kg/m^3.

Equation 1: $n_{crit} = \sqrt{\frac{\sigma \cdot D_W}{4 \cdot \pi \cdot V_L \cdot \rho_L \cdot d_0}}$

2.2.4 Standard priming procedure

The standard priming procedure applied in this study is based on the method developed by Kauss et al. (1992) [85]. This method was successfully used numerous times, to detect priming-active compounds [86, 88, 89, 100]. The parsley suspension cell culture was treated with 2,6-dichloroisonicotinic acid (DCIA) or SA as a priming-active compound. A fungal elicitor was added after 96 h, followed by the fluorescence measurement of the furanocoumarins 24 h later. Kauss et al. tested varying DCIA addition times and concentrations. They also analyzed several time points for measuring the furanocoumarin fluorescence. In the present study, this priming method was adopted as follows. The adopted standard priming procedure included the addition of 100 µM of a priming-active compound or a priming-inactive compound as (salicylic acid (SA), 4-chlorosalicylic acid (4-CSA)), 4-hydroxybenzoic acid (4-HBA) and 3-hydroxybenzoic acid (3-HBA) after 72 h. The priming-active and priming-inactive properties of SA, 4-CSA, 4-HBA, or 3-HBA were shown before [90, 101]. 24 h after the SA, 4-CSA, 4-HBA, or 3-HBA treatment, 50 pM of the elicitor Pep13 were added to the culture. In experiments with varying concentrations or times of addition, the exact doses are specified in each case's results section and the captions of the corresponding figure. In shake flask experiments, the added volume per addition was 1 mL. In MTP experiments, 40 µL of the respective substance was added. A sample was taken after 120 h to determine the furanocoumarin fluorescence intensity in experiments without an online fluorescence signal.

2.2.5 Determination of the DOT and OTR

RAMOS enables the quasi-continuous measurement of the oxygen partial pressure in the headspace of a shake flask. From this measurement, the OTR can be calculated. For the determination of the OTR in MTPs, the dissolved oxygen tension (DOT) was determined via online fluorescence measurements. For this purpose, each well of the MTP was equipped with an oxygen sensor spot. Two different sensor spots, the PreSens spots, already integrated into the MTP from Beckman Coulter, and spots from PyroScience (OXSP5, PyroScience GmbH,

Aachen, Germany), were used. The wavelength pair for DOT measurement in MTPs with PreSens sensor spots (MTP-R48-BOH, Beckman Coulter GmbH (formerly m2p-labs), Baesweiler, Germany) was λ_{ex} = 520 nm and λ_{em} = 600 nm and the experiments were conducted using a custom made BioLector device from Beckman Coulter. The wavelength pair for DOT measurements in MTPs with PyroScience spots was λ_{ex} = 610 nm and λ_{em} = 760 nm, and the experiments were conducted using the in-house built BioLector. For calibration, wells were filled with 2 mL modified Gamborg's B5 medium. Oxygen partial pressure of p_{O2} = 0 bar and p_{O2} = 0.21 bar, or p_{O2} = 0.15 bar were adjusted. The Stern-Volmer relationship allowed the calculation of the oxygen partial pressure from fluorescence intensities using the following equation:

Equation 2: $\frac{f_0}{f} = 1 + k_{sv} \cdot DOT$

f_0 is the fluorescence intensity in the absence of oxygen, f is the fluorescence intensity for given content of the quencher oxygen DOT [%], and k_{sv} is the Stern-Volmer constant. With the obtained DOT, the OTR can be calculated (OTR_{calc}) using the correlation from Wewetzer et al. [96].

Equation 3: $OTR_{calc} = k_L a \cdot L_{O2} \cdot \left(pO_2^{gas} - \left(\frac{DOT}{100}\right) \cdot pO_2^{cal}\right)$

k_La [1/h] is the volumetric oxygen mass transfer coefficient, L_{O2} [mol/L/bar] is the oxygen solubility, p_{O2}^{gas} [bar] is the partial pressure of oxygen in the gaseous phase, and p_{O2}^{cal} [bar] is the partial pressure during the calibration of the DOT. Oxygen solubility was calculated to be 1.22 mmol/L/bar as described before [102-104]. The k_La in the MTPs with V_L = 2 mL, n = 600 rpm and d_0 = 3 mm at 25 °C was approximated to be 37 1/h by the smallest sum of square errors between OTR and OTR_{calc} vectors from both shake flask and MTP [96, 105]. The calculation of the OTR was performed under the assumption of a constant oxygen partial pressure p_{O2}^{gas} of 0.21 bar. The maximum oxygen transfer capacity (OTR_{max}), used to ensure oxygen-unlimited conditions in MTP cultivations, was calculated with the following equation:

Equation 4: $OTR_{max} = k_L a \cdot L_{O2} \cdot pO_2^{gas}$

2.2.6 Normalization of DOT and OTR data

The parsley cell cultures differ in their respiration activity even before the addition of SA and Pep13. Since differences after priming and the addition of the elicitor are investigated, the DOT and OTR values are normalized on the y-axis before the addition of SA at 72 h cultivation time. Hence, the mean value of all cultures between 68 and 70 h cultivation time was calculated. Subsequently, the difference between the mean values of all cultures and the mean value of the individual cultures in the given time was calculated. This difference was then subtracted from all values of each culture in the entire cultivation period. As a result, curves were aligned on top of each other before SA was added. Figure A 9 in the appendix shows an example of the normalization for the curves shown in Figure 2.3.

2.2.7 Fluorescence measurements of SA and furanocoumarins

In shake flask cultivations, the fluorescence of furanocoumarins was measured offline in cuvettes. The culture broth was harvested after 120 h and centrifuged at 4000 rpm for 10 min at 4 °C. Subsequently, 3 mL of the supernatant were transferred into a quartz cuvette (10x10 mm Suprasil quartz, Hellma GmbH & Co. KG, Müllheim, Germany) and measured with a fluorescence spectrometer (Fluoromax-4, HORIBA Jobin Yvon GmbH, Unterhaching, Germany) with an excitation wavelength of λ_{ex} = 335 nm and an emission wavelength of λ_{em} = 398 nm [86, 88, 90]. The online fluorescence measurements of furanocoumarins and salicylic acid in MTPs were performed at n = 600 rpm using the in-house built BioLector with an attached fluorescence spectrometer. The furanocoumarin fluorescence was measured at λ_{ex} = 335 nm and λ_{em} = 398 nm, and the salicylic acid fluorescence at λ_{ex} = 295 nm and λ_{em} = 405 nm. Two different types of fluorescence data are shown in this paper: On the one hand, the absolute values of fluorescence (raw data) of salicylic acid or furanocoumarin (f_x), and on the other hand, the calculated relative furanocoumarin fluorescence($f_{x_{rel}}$). To calculate the corrected furanocoumarin fluorescence signals (f_{x_c}), the total furanocoumarin fluorescence signal of the SA and Pep13 treated cultures was subtracted by the total furanocoumarin fluorescence signal of the untreated culture without additives ($f_{w/o\ additives}$).

Equation 5: $f_{x_c} = f_x - f_{w/o\ additives}$

To gain the relative furanocoumarin fluorescence ($f_{x_{rel}}$) in %, the sum of the corrected fluorescence intensities of the cultures treated exclusively with SA or Pep13 was set to 100%. The corrected fluorescence intensities of SA and Pep13 treated specimens were put in relation.

Equation 6: $f_{x_{rel}} = \frac{f_{x_c}}{f_{PrimimngCompound_c} + f_{Pep13_c}} \cdot 100$

2.2.8 Calculation of errors

The number of replicates is different, depending on the experiment. Each experiment was conducted with at least three replicates and with a maximum of ten replicates. The only exceptions are the OTR curves from the shake flask experiments in Figure 2.2 and Figure 2.3a. Here, no further replicates were carried out, as these experimental conditions had already been investigated several times and published in a preceding paper [90]. The OTRs of this shake flask experiments in Figure 2.2 and Figure 2.3a are in agreement with the published data, which ensures the reliability of the results. The number of relevant replicates for error calculation for each experiment is specified in the figure captions. The following equation was used to calculate the standard deviation:

Equation 7: $s(x) = \sqrt{\frac{1}{N-1}\sum_{i=1}^{N}(x_i - x)^2}$

The standard error propagation for calculating the standard deviation of the relative fluorescence intensities was calculated by equation 8.

Equation 8: $s_f = \sqrt{\left(\frac{\partial_f}{\partial_x}\right)^2 \cdot s_x^2 + \left(\frac{\partial_f}{\partial_y}\right)^2 \cdot s_y^2 + \left(\frac{\partial_f}{\partial_z}\right)^2 \cdot s_z^2 + \cdots}$

2.2.9 Statistical analysis

To determine whether or not the OTR of the Pep13-treated cultures and the SA- and Pep13-treated experiments analyzed by PyroScience and PreSens sensor spots differ significantly, a

student´s t-test was performed [106]. The difference in OTR values was validated by a 5% significance level.

2.3 Results and discussion

2.3.1 Establishing parsley cell cultivation in MTPs

For higher throughput at the identification of putative priming compounds, parsley cell culture aliquots were transferred from shake flasks to MTPs. To allow for the comparison with data from previous studies [90] and the scalability between the different cultivation systems, the conditions of cultivation in MTPs should be as similar as possible to those in shake flasks. Shaking frequency was used as the parameter for downscaling. When determining the suited shaking frequency for cell cultivation, three factors need to be considered. First, the shaking frequency needs to be high enough to obtain a homogeneously suspended cell culture [107, 108]. Therefore, the critical shaking frequency (n_{crit}) should be calculated [98]. This parameter is derived from the balance of the centrifugal force and the interfacial tension of the liquid and the walls of the wells. Below the $n_{crit,}$ the centrifugal force is insufficient to overcome the interfacial tension. This then results in a horizontal liquid surface with heterogeneously mixed fluid. Above the n_{crit}, the fluid slides up the wall of the well thus increasing mixing and the mass transfer area. Second, an oxygen limitation must be avoided, to ensure oxygen-unlimited cultivation conditions like those in shake flasks [109-111]. Third, the resolution of the DOT signal needs to be high enough to enable the calculation of OTR values from DOT measurement. The resolution of the DOT signal increases with low but by no way limiting oxygen content in the liquid at maximum breathing activity. As parsley cell cultures have a generally low oxygen uptake rate [90], the shaking frequency must be sufficiently low to allow for a reasonable resolution of the DOT signal. The three requirements described above are partially conflicting as increasing the shaking frequency needed for sufficient mixing and oxygen-unlimited conditions also increases the DOT resulting in lower DOT signal resolutions.

2.3.2 Determining a suitable shaking frequency

Figure 2.1 displays the suspension behavior of parsley cell cultures in a 48-deep-round-well MTP at varying shaking frequency between 0 and 700 rpm.

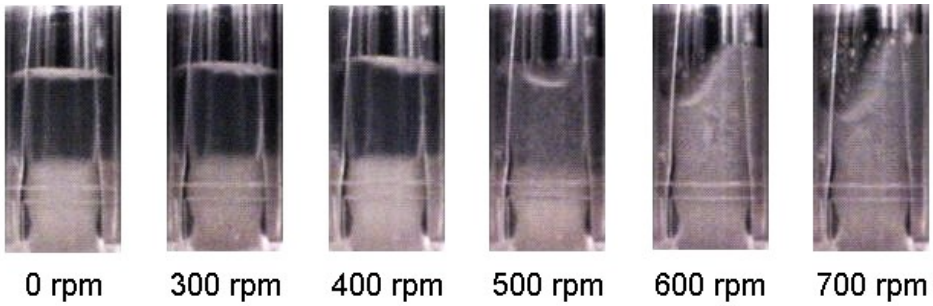

Figure 2.1 Suspension behavior of a parsley cell culture in a 48-deep-round-well MTP at different shaking frequency.

Photos were taken with a CCD camera installed on the shaker platform. An aliquot of a parsley cell culture in a shake flask was transferred, after 120 h of cultivation, to the well of an MTP. Shaking parameters: 48-deep-round-well MTP, shaking diameter d_0 = 3 mm, filling volume V_L = 2 mL, surface tension σ = 0.068 N/m, well diameter D_w = 12.4 mm, liquid density ρ_L = 1.0 kg/L. The contrast and brightness of the photo were edited to distinguish better between the phases with cells in suspension and the unmixed cell broth.

From 0 rpm to 400 rpm, the parsley cells are not suspended at all. They rather accumulate at the bottom of the well. At 500 rpm, the boundary layer is blurred, and the cells are partially suspended (Figure 2.1). At 600 rpm and more, the cells are extensively dispersed in the cultivation liquid. The liquid slides up the wall of the well with a crescent shape. Hence, shaking at 600 rpm and more seems to be needed for the cultivation of parsley culture cells in the MTPs. However, according to calculations with Equation 1 (see, "Materials and Methods"), the theoretical n_{crit} for this experimental setup is 188 rpm [98]. One reason for the inconsistency between theoretical and practically determined critical shaking frequency might be the formation of parsley cell aggregates [107, 108]. A similar effect was observed when mixing water with cellulose fibers [28]. The authors reported that cellulose particles also were suspended at a shaking frequency that was far above the theoretical n_{crit} [99]. Thus, one can assume that the presence of cell aggregates could increase the shaking frequency needed for homogeneous dispersion of cells. Together, we found that a shaking frequency of 600 rpm and more is needed to achieve sufficient homogenization of the parsley cells in suspension in MTPs.

2.3.3 Volumetric mass transfer coefficient and OTR calculations

To assess whether the parsley cell cultures in MTPs are limited in oxygen, the maximum oxygen transfer capacity (OTR_{max}) given in a fixed set of cultivation conditions is required. According

to the data of m2p-labs (now Beckman Coulter GmbH) and the literature [110, 112], the OTR_{max} is 6.1 mmol/L/h at the chosen cultivation conditions (48-deep-round-well MTPs, V_L = 2 mL, n = 600 rpm, d_0 = 3 mm and 25 °C). This value was determined with a 0.5 M sulfite oxidation system [110] by m2p-labs (now Beckman Coulter GmbH) and is shown in the technical data sheet for MTP-R48 plates. The oxygen solubility of the sulfite system differs from the modified Gamborg's B5 medium used for cultivating the parsley cells. The oxygen solubility of the sulfite system is 0.84 mmol/L/bar, whereas the oxygen solubility of the modified Gamborg's B5 medium is 1.22 mmol/L/bar (See Materials and methods: Determination of the DOT and OTR) [102-104]. The OTR_{max} increases with increasing oxygen solubility (Equation 4, see Materials and Methods). Consequently, the OTR_{max} for the Gamborg's B5 medium is expected to be above 6.1 mmol/L/h. Parsley cell cultures in previous shake flask experiments reached an OTR of 3 - 4 mmol/L/h [90]. Consequently, no oxygen limitation seems to occur in MTPs at the chosen cultivation conditions.

For comparison of results with shake flasks and MTPs, the OTR in the MTP was calculated from the measured DOT. To do so, the volumetric mass transfer coefficient (k_La) had to be determined (see, Materials and Methods). The k_La depends on the well geometry, plate material, and cultivation conditions, which include the shaking frequency, filling volume, and shaking diameter [113]. It is possible to determine the k_La in MTPs by simultaneous measurement of the OTR in shake flasks and the DOT in MTPs at oxygen-unlimited conditions. This method has been published for microbial cultures [96, 105]. Equation 3 shows the relationship between OTR and DOT and enables the estimation of the k_La value in the MTP to be 37 1/h (see, Materials and Methods). When knowing the k_La value in the MTP, the OTR (OTR_{calc}) in the MTP can be concluded from the DOT (see, Equation 3). Figure 2.2 shows the DOT and OTR of parsley cells cultivated in MTPs (red and blue curves) and the OTR obtained in shake flasks (green curve) cultivated simultaneously.

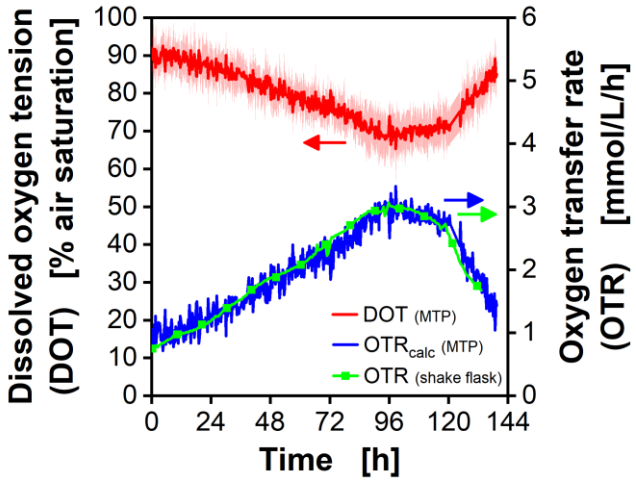

Figure 2.2 Respiration activity of parsley cell cultures, determined in a shake flask and a 48-deep-round-well MTP.

Air-supplied (p_{O2} = 0.21 bar) parsley cell cultures were simultaneously cultivated in 250-mL shake flasks using a RAMOS device (green curve) and in 48-deep-round-well MTP using a custom-made BioLector device from m2p-labs (now Beckman Coulter GmbH). Mean values for the DOT (red) were calculated from 10 wells. The standard deviation (SD) is indicated by blue and red shadows. OTR_{calc} in the MTP is calculated from the measured DOT according to Equation 3. Parameters: k_La = 37 1/h, L_{O2} = 1.22 mmol/L/bar, partial pressure of oxygen in air p_{O2} = 0.21 bar. Shake flasks cultivation conditions: V_L = 50 mL, n = 180 rpm, d_0 = 50 mm, and 25 °C in modified Gamborg's B5 medium. For clarity, only every twentieth measuring point of the OTR RAMOS curve is marked as a square symbol. MTP cultivation conditions: V_L = 2 mL, n = 600 rpm, d_0 = 3 mm, and 25 °C in modified Gamborg's B5 medium. PreSens sensor spots were used for measuring the DOT in MTPs.

The DOT in the MTPs decreased from 90% to almost 70% at 96 h and increased afterward. The OTR during shake flask cultivation shows an inverse course with a maximum of 3 mmol/L/h after 96 h before it decreased again. To compare the calculated data with the measured ones, the OTR_{calc} that we calculated from the DOT values of the MTP is shown in blue in Figure 2.2. The similarity in OTR progression in shake flasks and MTPs discloses similar culture behavior and a seemingly correct estimation of the k_La value in the MTP. Consequently, the scale-down of parsley cell cultures from shake flask to MTPs has been successful. The selected cultivation conditions (V_L = 2 mL, n = 600 rpm, d_0 = 3 mm) are suitable for cultivating parsley cells in 48-well MTPs. In addition, we demonstrated that the signal of the DOT optode in chosen cultivation conditions was suited to follow the culture progression with sufficient resolution.

2.3.4 Identification of priming compounds in MTPs with DOT measurements

After finding suitable conditions for parsley cell cultivation, we investigated whether the online data obtained from cultivation in MTPs would allow for a conclusion as to whether a chemical compound in question would possibly be a defense priming-activating compound in plants. As shown before [90], the treatment of parsley cell cultures with priming-activating compounds and subsequent elicitation lead to more robust OTR. Because the measurements in the MTPs do not detect the OTR but rather the DOT, two different sensor spots were tested for their suitability for detecting the DOT. One of the sensors was obtained from PreSens (m2p-labs (now Beckman Coulter GmbH), Baesweiler, Germany) and the second one from PyroScience (OXSP5, PyroScience GmbH, Aachen, Germany). For evaluation, the DOT measurements of the two sensor-spots systems were compared to the OTR curves obtained with shake-flask cultivations of parsley cells. The optical sensor spot from PreSens measures the DOT at an excitation wavelength (λ_{ex}) of 520 nm and an emission wavelength (λ_{em}) of 600 nm. The sensor spot of PyroScience rather uses λ_{ex} of 610 nm and λ_{em} of 760 nm. All experiments were done in oxygen-unlimited conditions. The OTR_{max} in the RAMOS-using experiment (Figure 2.3a) was calculated as 7.7 mmol/L/h with a k_La of 43 h^{-1} [61].

Figure 2.3 shows the online-recorded OTR and fluorescence of SA-treated parsley cell cultures in shake flasks (Figure 2.3a, b) and MTPs (Figure 2.3c, d, e, f).

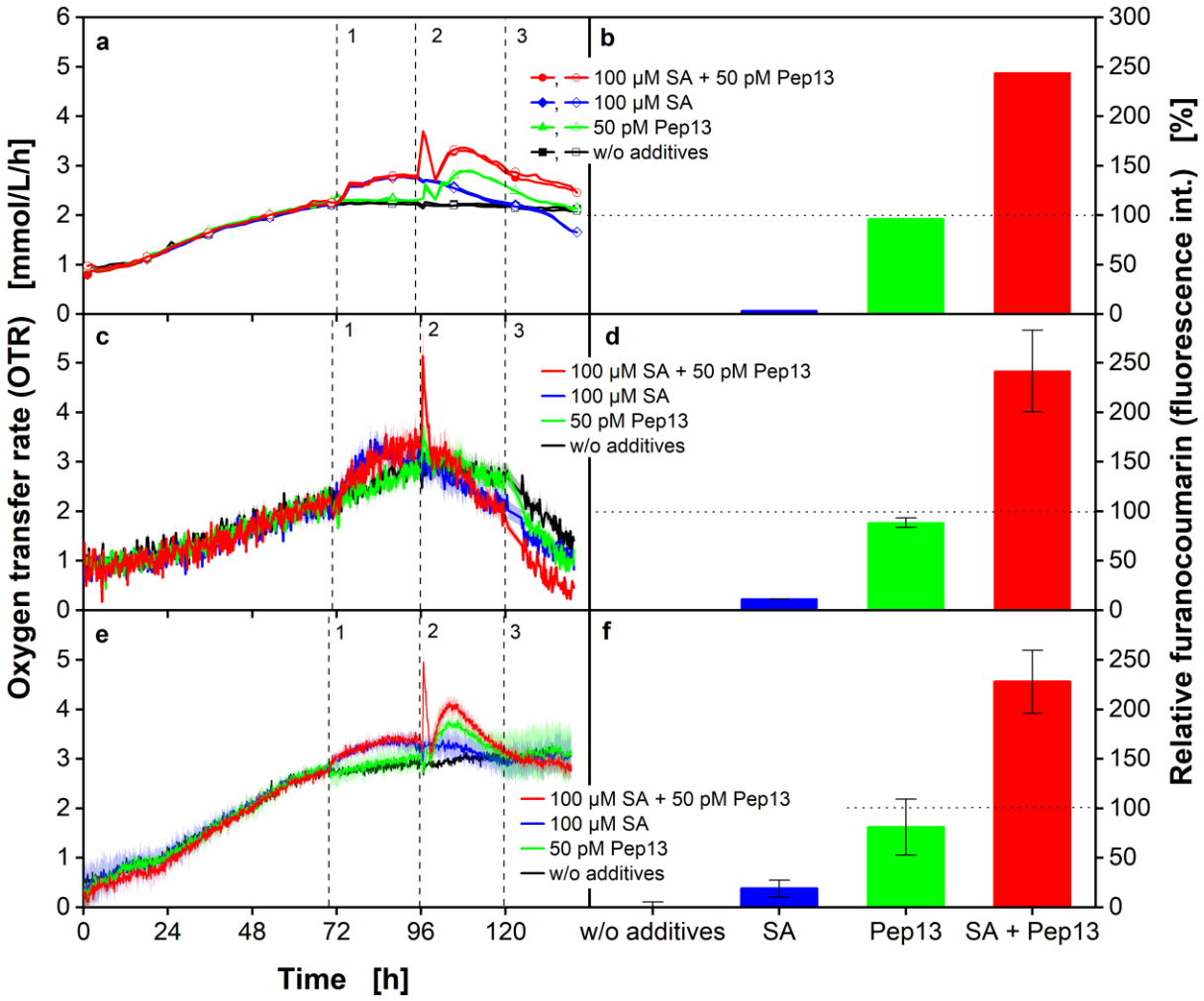

Figure 2.3 OTR of parsley cell cultures in shake flasks and MTPs with two different sensor systems. Measurements from shake flasks (a) and from MTPs (c, e) are shown.

Corresponding relative furanocoumarin fluorescence intensities at 120 h of cultivation in cultures primed with SA and elicited with Pep13 (b, d, f). Parsley cell cultures were cultivated in 250 mL shake flasks using the RAMOS device (a, data from Schilling et al. 2015), in 48-deep-round-well MTPs with PreSens sensor spots using a custom-made industrial BioLector device (c) and with PyroScience sensor spots using an in-house built BioLector (e) for measuring the DOT. Dashed vertical lines (a, c, e) indicate the addition of 100 µM SA (1), 50 pM Pep13 (2), and offline fluorescence measurement of furanocoumarins (3). Shake flask cultivation conditions: 250 mL RAMOS flasks, V_L = 50 mL, n = 180 rpm, d_0 = 50 mm, 25 °C in modified Gamborg's B5 medium. For the OTR (a) two replicates are shown. Every tenth measuring point of the OTR curve is marked as symbol (a). MTP cultivation conditions: V_L = 2 mL, n = 600 rpm, d_0 = 3 mm, and 25 °C in modified Gamborg's B5 medium. Mean values were calculated from 10 wells (c) and three wells (e), respectively. Data were normalized (see 2.2.6 Normalization of DOT and OTR data) and the SD is indicated by colored shadows and (c, e). The OTR in (c, e) is calculated from the DOT according to Equation 3. Parameters for MTP fluorescence measurements in the in-house built BioLector: n = 600 rpm, d_0 = 3 mm and 25 °C. Relative furanocoumarin fluorescence (b, d, f) was calculated according to Equation 6. The dotted horizontal lines represent the 100% threshold. Since the red curves in (c, e) cover partly the green curves, the graphs are shown without the red curves in the Additional files 1c and **g**.

Figures 2.3a and b show data from Schilling et al. (2015) as a reference, to evaluate the novel results obtained with cell cultures in MTPs as shown in Figures 2.3c, d, e, and f. The OTR values in Figure 2.3c and e were calculated with Equation 3 and are based on the measured DOT. The raw DOT data with their inverse course are shown in Figure A 7 in the appendix.

Since the course of the red curves in Figure 2.3c and e match those of the green and blue curves, the same graph is plotted also with the omitted red curve in Figure A 7 in the appendix. For Figure 2.3c, the DOT was measured with PreSens sensor spots, while the DOT for Figure 2.3e was determined with PyroScience spots. In Figure 2.3b, d, and f, the relative furanocoumarin fluorescence after 120 h was calculated using Equation 6. The fluorescence measurements are used as a reference to assess whether suspension cells were in an alert state of defense in the MTP. Relative furanocoumarin fluorescence intensities over 100% for cultures subsequently treated with the priming compound first and elicitor second indicate a successful priming experiment. That is because primed cells secreted much more furanocoumarins than non-primed ones [86, 90]. For reference, the furanocoumarin fluorescence of naïve cell cultures (e.g. with no addition of SA and Pep13; Figure 2.3a, c, e, black curve) and cultures treated with either SA (Figure 2.3a, c, e, blue curve) or Pep13 (Figure 2.3a, c, e, green curve) are shown.

In experiments with both shake flask and MTPs, treatment with SA followed by elicitation with Pep13 led to about 2.5-fold enhancement of furanocoumarin fluorescence (Figure 2.3b, d, f). As the relative furanocoumarin fluorescence in Figure 2.3b, d and f are similar, the treatment of parsley cell cultures with SA and Pep13 in MTPs and shake flasks seems to mobilize similar physiological responses, independent of the cultivation container.

Comparing the OTR in Figure 2.3a, c, and e, the addition of SA at 72 h post-cultivation lead to an OTR increase (blue curve). In the cultures experiencing Pep13 addition at 96 h, the OTR shows a short peak and a prolonged rise in the OTR (green curve). The peak and the following increase of the breathing activity after Pep13 addition is much higher in the cultures that were treated with SA before Pep13 elicitation (red curve).

The calculated OTR values obtained in MTP using PreSens spots (Figure 2.3c) have a higher scatter than the OTR curves shown in Figure 2.3a (shake flask). This is most likely caused by a technical problem but was not analyzed in detail as the signals from PyroScience spots show

good resolution. The different standard deviations and resolutions of the OTR curves in Figure 2.3c and e, as measured with the different sensor spots, are also remarkable. The DOT signals from the PreSens spots (Figure 2.3c) are noisy, which prevents a distinct differentiation of the primed and unprimed parsley cell cultures.

The calculated OTR curves from the MTP with PyroScience spots (Figure 2.3e) show better resolution, less background noise, and lower standard deviations, compared to the calculated OTR curves from the MTP with PreSens spots (Figure 2.3c). The data generated with the PyroScience spots show the same qualitative characteristics as the OTRs in Figure 2.3a, obtained in shake flasks. The PyroScience sensor spots (Figure 2.3e) deliver a signal with lower scattering than the sensor spots from PreSens (Figure 2.3c), although the depicted mean values were calculated from 3 versus 10 parallel wells respectively. The OTRs calculated from the DOT using PyroScience spots (Figure 2.3e) reach slightly higher overall values, compared to shake flasks (Figure 2.3a). The reference cultures without any treatment in Figure 2.3a reached an OTR of approximately 2.2 mmol/L/h, whereas the reference cultures without any treatment in Figure 2.3e reached around 3.0 mmol/L/h. This difference can be attributed to independent experimental setups and inoculums. The significance in DOT values was validated by a 5% significance level students' t-test and is shown in Figure A 7d and h in the appendix. It was demonstrated that differences in the OTR were successfully determined from DOT measurements in MTPs, using sensor spots from PyroScience. The experiments in MTPs resulted in similar results to previous experiments with parsley cell cultures in shake flasks.

2.3.5 Reduced oxygen supply

Although the resolution of the signals from the MTP experiment with PyroScience spots is already significant in the decisive cultivation period after Pep13 addition (Figure A 7h in the appendix), a further improvement of the signal quality is desirable for the application with other putative but possible weaker priming-activating compounds. This would increase the detection of priming-active compounds with an even lower effect on defense priming than SA. The overall signal quality should increase if lower DOT values are reached during the cultivation. A better resolution at lower DOT values is obtained, as the relationship between the DOT and the fluorescence signal intensity is not linear. Because of the Stern-Volmer relationship, the

sensor spot displays a low signal resolution at high oxygen concentrations. Therefore, experiments at reduced DOT levels were performed. The oxygen content of the supply air was adjusted to p_{O2} = 15% by mixing air and nitrogen. The DOT values and calculated OTR curves are shown in Figure A 8 in the appendix.

Compared to the OTR from shake flask cultures aerated with air (p_{O2} = 21%) (Figure A 8b, black curve in the appendix), the calculated OTR from MTPs shows lower overall values. The DOT at a p_{O2} = 15% (Figure A 8a in the appendix) is only slightly reduced when compared to the experiment with air aeration (p_{O2} = 21%) (Figure A 7e in the appendix). The lower OTR indicates an impaired oxygen uptake. A possible reason for this observation may lie in sensitivity against oxygen level changes of the parsley cell cultures. The plant cells might sense the reduced oxygen content in the gas phase and change their metabolism. The changed metabolism may lead to reduced breathing activity. This kind of response is documented for whole plants and should be considered in further experiments [114-116]. Since no signal improvement could be achieved at reduced oxygen concentration in the gas supply, this approach was not pursued further in this study.

Another technique for measuring the OTR in MTPs is the µRAMOS approach [93, 117, 118]. µRAMOS enables OTR measurements in any individual well of a 48-well MTP applying oxygen-sensitive fluorescence sensor spots. The µRAMOS technique is also suitable to investigate the defense priming of parsley suspension cell cultures. In contrast to the DOT measurements via the fluorescence sensor spots with a spectrofluorometer, no mathematical conversions of DOT values to OTR are necessary. µRAMOS measurements showed good resolution in measurements with parsley suspension cell cultures [93]. However, measuring the DOT using the fluorescence sensor spots provides additional information. It reports whether the cultures are well supplied with oxygen and whether they are approaching oxygen limitation. This is important information, especially for work with plant suspension cell cultures, which seem to be very prone to varying oxygen levels (Figure A 8 in the appendix). In addition, with a spectrometer for DOT measurements, it is possible to online monitor additional fluorescence signals (2.3.6 Online furanocoumarin and SA fluorescence measurements in MTPs).

2.3.6 Online furanocoumarin and SA fluorescence measurements in MTPs

As shown above, defense priming can be analyzed in MTPs by measuring the DOT signal. In addition, the cultivation of cells in the BioLector device enables the measurement of fluorescence signals, including those of SA at λ_{ex} = 295 nm and λ_{em} = 405 nm and secreted furanocoumarins of the parsley cells upon priming, at λ_{ex} = 335 nm and λ_{em} = 398 nm [119]. The concentration of SA and furanocoumarins can be measured online, simultaneously with the breathing activity, providing additional insights into the culture behavior.

In Figure 2.4a, the course of the calculated OTR from Figure 2.3e is depicted and compared to the online fluorescence signals of SA (Figure 2.4b) and furanocoumarins (Figure 2.4c) during cultivation.

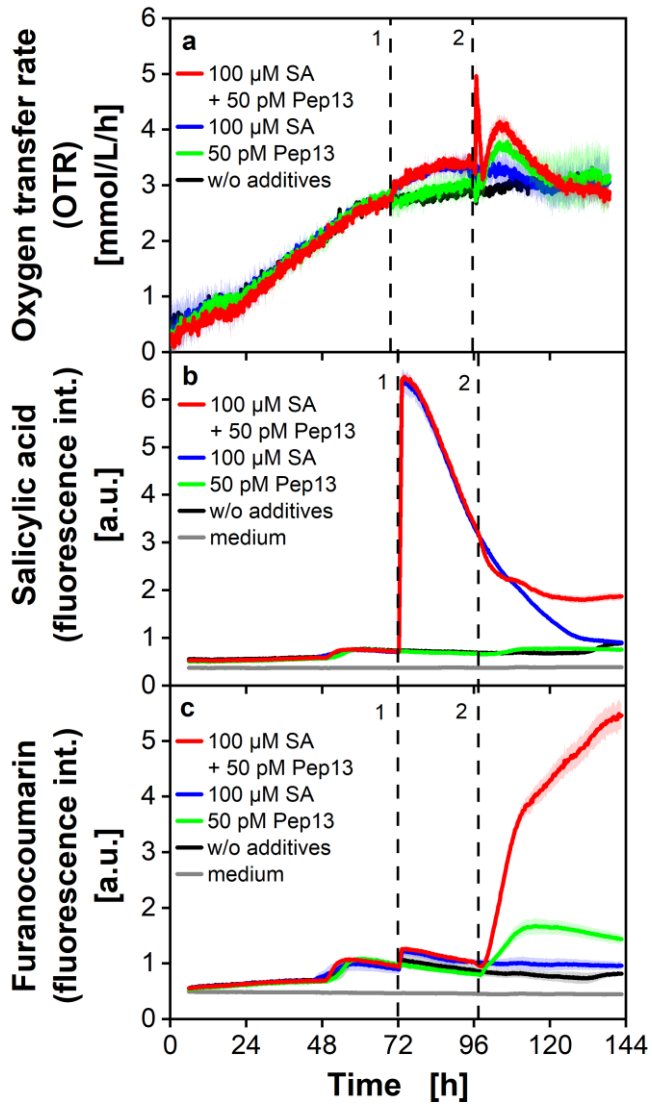

Figure 2.4 OTR and online determination of furanocoumarin fluorescence of parsley cell cultures in an MTP.

Parsley cells were cultivated in a 48-deep-round-well MTP with PyroScience sensor spots, aerated with air (p_{O2} = 0.21 bar) in an in-house built BioLector device. The OTR was calculated from the DOT according to equation 3 and plotted in Figure 2.4**a**. In a different experiment, SA (**b**) and furanocoumarin fluorescence (**c**) were measured by an in-house built BioLector in a 48-deep-round-well MTP. Wavelength combination for SA fluorescence measurement: λ_{ex} = 295 nm and λ_{em} = 405 nm (**b**) and furanocoumarin fluorescence: λ_{ex} = 335 nm and λ_{em} = 398 nm (**c**). Mean values were calculated from 3 wells in **a** and from 5 wells in **b** and **c**. Colored shadows indicate SD. Dashed vertical lines indicate the times of addition of SA (1) and/or Pep13 (2). Cultivation conditions: V_L = 2 mL, n = 600 rpm, d_0 = 3 mm and 25 °C in modified Gamborg's B5 medium.

In general, the reproducibility of the fluorescence data was excellent. The standard deviations as calculated from 5 wells are depicted as colored shadows and are very small. In most cases, the standard deviation is hardly visible. The OTR (Figure 2.4a) increases after SA addition at

72 h (red and blue curve) and again after the Pep13 addition at 96 h (red and green curve). The SA fluorescence intensity (Figure 2.4b all curves) increases slightly for the first time after 48 h, although no addition took place at this time. A change in metabolism could cause this increase, due to substrate limitation in the medium of the cell cultures [120, 121]. After the addition of SA at 72 h (Figure 2.4b, red and blue curve), the SA fluorescence increases rapidly [119]. Afterward, the fluorescence signal in those cultures within 58 h dropped to their initial value (blue curve). The decrease in SA fluorescence might be due to the conversion of SA to its presumed storage form SA-glucoside, as reported for parsley, soybean, and tobacco [122-126]. SA fluorescence intensity is influenced by Pep13 addition, resulting in a lower decrease after 108 h (Figure 2.4b, red curve). The elicitor Pep13 triggers the defense mechanisms of parsley cell cultures [87]. The slower decrease of the SA fluorescence in cultures treated with SA and Pep13 might point towards a priming effect, as SA remains longer in primed cells.

In Figure 2.4c, the signal of secreted furanocoumarins slightly increases, if SA was added to the cells after 72 h (red and blue curve). This increase might be due to the overlapping spectra of SA and furanocoumarins [119]. With previous priming, the Pep13 addition leads to a substantial increase in the furanocoumarin fluorescence (Figure 2.4c, red curve). But also, without priming by SA, the furanocoumarin fluorescence increases (Figure 2.4c, green curve), as it is triggered by the addition of Pep13. Compared with the OTR, SA fluorescence and furanocoumarin fluorescence data match very well and confirm the success of the cell pretreatment.

2.3.7 Varying SA concentrations for cell pretreatment

The possibility to online monitor the fluorescence signals of SA and furanocoumarins in MTPs enables a detailed investigation of the effect on defense priming of different priming compounds, concentrations, and combinations for priming compound and elicitor addition times. In the following section, different concentrations of the model priming compound SA are analyzed.

Figure 2.5 shows the fluorescence signals for cell cultures treated with SA concentrations ranging from 1 µM to 200 µM at constant Pep13 concentration (50 pM).

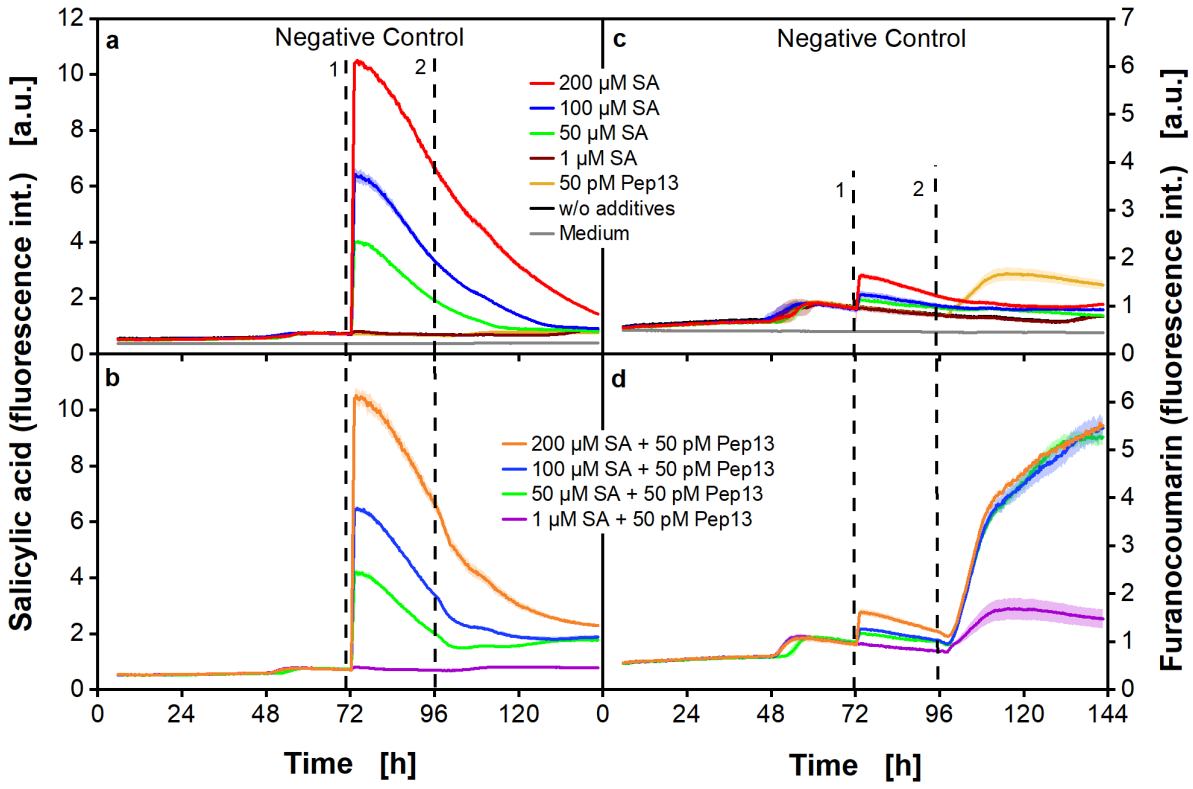

Figure 2.5 Online fluorescence intensities upon treatment with various SA concentrations in a MTP.

Parsley cells were cultivated in 48-deep-round-well MTPs aerated with air (p_{O2} = 0.21 bar) in an in-house built BioLector. SA fluorescence was measured at λ_{ex} = 295 nm and λ_{em} = 405 nm (**a**, **b**) whereas furanocoumarin fluorescence was determined at λ_{ex} = 335 nm and λ_{em} = 398 nm (**c**, **d**). Mean values were calculated from three wells. SD is indicated as colored shadows. Dashed vertical lines indicate the addition of SA (1) and 50 pM Pep13 (2). Cultivation conditions: V_L = 2 mL, n = 800 rpm, d_0 = 3 mm and 25 °C in modified Gamborg's B5 medium.

Addition times of 72 h for SA and 96 h for Pep13 are used. In Figures 2.5a and c, the negative controls with either SA or Pep13 addition are depicted. The SA fluorescence signal (Figure 2.5a) shows a dose-dependent increasing fluorescence intensity with increasing SA concentration. After SA addition at 72 h (Figure 2.5a, dashed black line marked with 1), the fluorescence signal decreases for 48 h – 72 h. Only the SA concentration of 1 µM (Figure 2.5a, brown curve) is not distinguishable from the culture without SA addition (Figure 2.5a, black curve) and neither increases nor decreases.

In Figure 2.5c, the furanocoumarin signal shows a slight increase after SA addition at 72 h (Figure 2.5c, dashed black line). The increase is more substantial with higher SA concentrations. As mentioned before, this might be caused by overlapping fluorescence spectra

of SA and furanocoumarins [119]. The treatment with Pep13 after 96 h (Figure 2.5c, yellow curve) also increases the furanocoumarin fluorescence, as it triggers the defense mechanisms of the plant cells to a limited extent. The fluorescence signals of the cultures treated with SA after 72 hours and Pep13 after 96 hours are shown in Figures 2.5b and d. In Figure 2.5b a dose-dependent increase of SA fluorescence, except for 1 µM SA is demonstrated. For the subsequent addition of 50 µM SA and Pep13 (Figure 2.5b, green curve), the SA fluorescence signal even increases slowly after 100 h of cultivation. For this increase a combination of a slower degradation and an overlap with the increasing furanocoumarin fluorescence signal may be responsible [119]. In Figure 2.5d, the furanocoumarin fluorescence signals do not show dependence on dose. The addition of 1 µM SA (Figure 2.5d, violet curve) seems to be a too-low concentration for measuring defense priming with the here-used fluorescence technique. With 50 µM (Figure 2.5d, green curve), 100 µM (Figure 2.5d, blue curve), and 200 µM (Figure 2.5d, yellow curve) SA priming results in the same furanocoumarin production over time. It is possible, though, that dose-dependent differences may become visible at a later stage of cultivation. The results show that it is generally possible to use lower SA concentrations for effective priming of parsley cell cultures, as the furanocoumarin synthesis for the cultures primed with 50 µM, 100 µM or 200 µM SA was identical until 144 h cultivation time. In the future, concentrations of SA between 1 µM and 50 µM could be investigated to identify the lowest concentration necessary for successful priming. Our results disclose the need for continuous online monitoring and the relevance of fluorescence-based analyses in MTPs to thoroughly understand plant defense priming.

2.3.8 Varying the times of SA and Pep13 addition.

In the above experiments, SA was applied to parsley cell cultures at 72 h and Pep13 at 96 h of cell cultivation. Figure 2.6 shows the fluorescence signal of SA and furanocoumarins after the combined addition of SA and Pep13 at varying times.

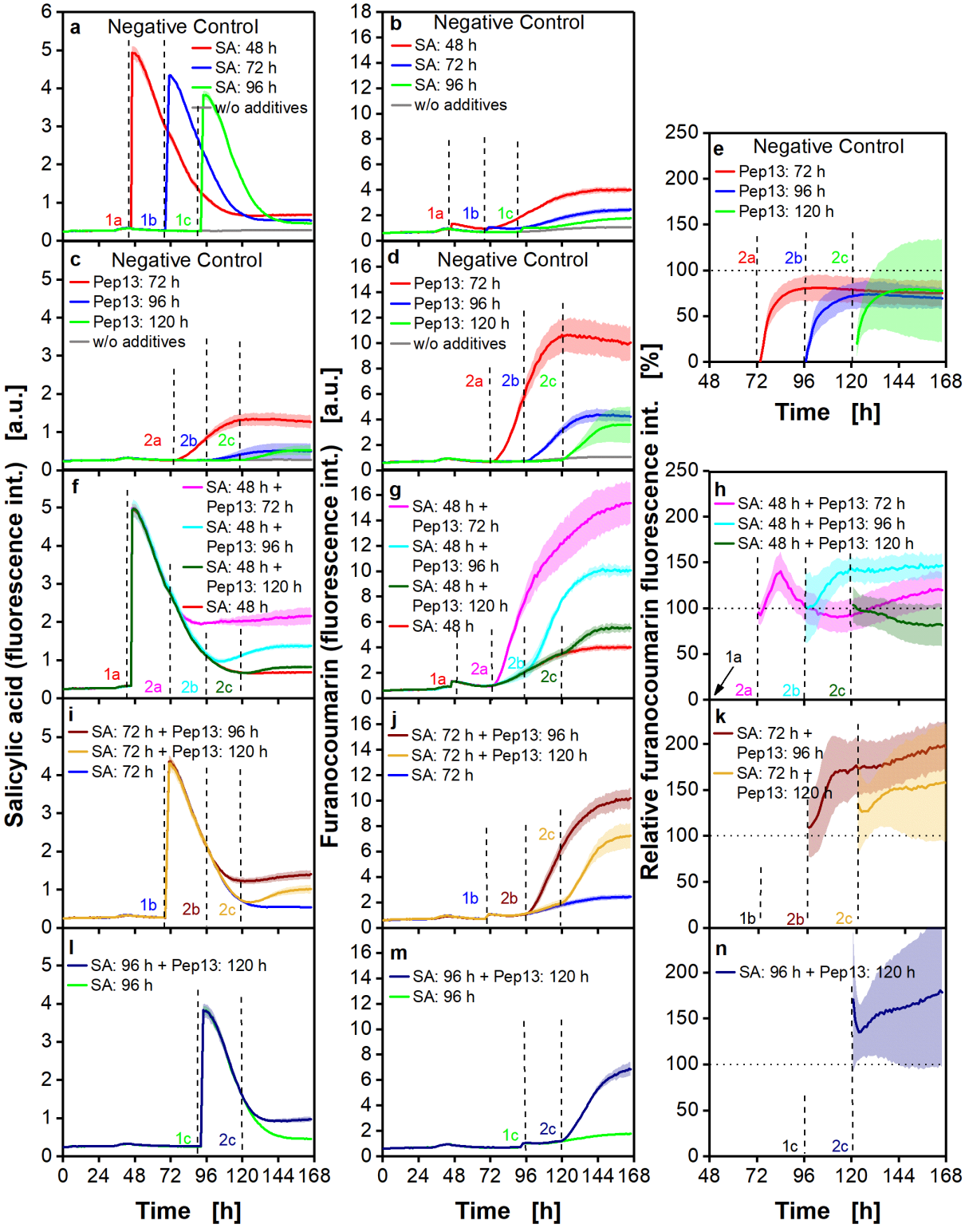

Figure 2.6 Online fluorescence of parsley cell cultures treated with SA and Pep13 at various cultivation times.

Parsley cells were cultivated in 48-deep-round-well MTPs aerated with air (p_{O2} = 0.21 bar) in an in-house built BioLector. Measurement of SA fluorescence at λ_{ex} = 295 nm and λ_{em} = 405 nm (**a**, **c**, **f**,

i, **l**) and of furanocoumarin fluorescence at λ_{ex} = 335 nm and λ_{em} = 398 nm (**b**, **d**, **g**, **j**, **m**). The negative controls were treated with either 100 µM SA at 48 h, 72 h, and 96 h (**a** and **b**) or with 50 pM Pep13 at 72 h, 96 h and 120 h (**c** and **d**). The calculated relative furanocoumarin fluorescence intensity is shown in **e**, **h**, **k,** and **n** and was calculated according to Equation 6. Dotted horizontal lines in Figure 2.6**e**, **h**, **k,** and **n** represent the 100% threshold value which is the sum of the corrected fluorescence intensities of the cultures treated exclusively with SA or Pep13 (Materials and Methods: Fluorescence measurements of SA and furanocoumarins). Relative furanocoumarin fluorescence intensities over 100% for cultures treated with both, priming compounds and elicitor, indicate successful priming. Mean values were calculated from three wells. SD is indicated by colored shadows. The SD for the relative furanocoumarin fluorescence intensity (**e**, **h**, **k**, **n**) was calculated by error propagation as described in "Materials and Methods". Dashed vertical lines indicate the addition of 100 µM SA (1a: ~48 h, 1b: ~72 h, 1c: ~96 h) and 50 pM Pep13 (2a: ~72 h, 2b: ~96 h, 2c: ~120 h) at varying time points. Cultivation conditions: V_L = 2 mL, n = 800 rpm, d_0 = 3 mm and 25 °C in modified Gamborg's B5 medium.

The columns displayed in Figure 2.6 give the values of SA fluorescence, furanocoumarin fluorescence, and relative furanocoumarin fluorescence. The latter allows a direct conclusion as to the time combinations that lead to the strongest defense priming seen in the parsley cell cultures, without the necessity to compare the fluorescence data for any single experiment with the negative controls. In the first two rows of Figure 2.6 (a, b, c, d, and e), the control treatment of either SA or Pep13 is shown. In rows 3 to 5 of Figure 2.6 (f, g, h, i, j, k, l, m, and n), the fluorescence intensities of SA and Pep13-treated cultures are displayed. SA was added at 48 h, 72 h or 96 h. We added Pep13 after 72 h, 96 h or 120 h. Dashed vertical lines indicate the addition time points and are specifically numbered. Rows 3 to 5 show the different addition time points of SA combined with various Pep13 addition time points. All graphs of Figure 2.6 indicate that SA and furanocoumarin fluorescence increase to higher levels if SA or Pep13 are added earlier. One explanation for the higher fluorescence signals of younger cultures may be a higher cell density at later cultivation times, which interferes with the fluorescence signal. Another assumption is that with the same concentrations of SA and Pep13 but higher cell densities, the concentration of the priming compound per cell and the resulting furanocoumarin fluorescence is lower. The SA fluorescence signals strongly increase in response to SA, followed by a decrease during several days (Figure 2.6a, c, f, i, l). The period of decreasing SA fluorescence is shorter, if SA is added later. These observations are possible because of the faster metabolization of SA by the cells in higher density in aged cultures. Figure 2.6d depicts that also the Pep13-elicited increase in furanocoumarin fluorescence was faster and higher when cells were elicited at early rather than late times of cultivation. Different treatment times with Pep13 result in the synthesis of different amounts of furanocoumarin (Figure 2.6d,

g, j, m). A possible explanation for the varying response of the cells after Pep13 treatment is a growth state-dependent reaction of parsley cell cultures [127, 128].

To correctly evaluate the priming effect at different addition times of SA and Pep13, it is helpful to consider the relative furanocoumarin fluorescence intensity. Applying the relative fluorescence, priming at different addition times was compared. Consequently, the relative furanocoumarin fluorescence was calculated by equation 6, as described in Material and Methods. The relative furanocoumarin fluorescence is shown in the third column (Figure 2.6e, h, k, and n). To calculate the relative furanocoumarin fluorescence, the furanocoumarin fluorescence intensity of the negative controls with either SA or Pep13 and the intensity of an SA and Pep13 treated culture are set into relation. The furanocoumarin fluorescence increases after the addition of SA or Pep13. The sum of the negative controls with SA and Pep13 is set to 100%. It is defined that up to this level, no priming is existent. Relative furanocoumarin fluorescence above the horizontal dotted line at the 100% threshold indicates increased furanocoumarin production due to previous successful priming. Figure 2.6e shows only negative controls with either SA or Pep13-treated cultures. Defense priming should not be measurable in the negative controls. The relative furanocoumarin fluorescence should stay below 100% for these negative controls. The relative fluorescence below 100% fits the expectations and shows that no priming effect was measured.

For the addition of SA at 48 h followed by different addition times of Pep13, the relative fluorescence is plotted in Figure 2.6h. As can be seen, the relative fluorescence for the addition time of Pep13 of 72 h (Figure 2.6h, magenta curve) and 96 h (Figure 2.6h, turquoise curve) reaches approximately the same maximum value of 150% and shows successful priming. However, the course of the two curves is different. While for an addition time of Pep13 of 48 h (Figure 2.6h, magenta curve) the curve rises at first and reaches a maximum of 150% after 12 h. Afterward, it decreases and even falls below the 100% limit. In contrast, the curve for the addition time of Pep13 of 96 h (Figure 2.6h, turquoise curve) rises to 150% within 20 h after Pep13 addition and remains stable on this plateau. For the addition time of Pep13 of 120 h (Figure 2.6h, dark green curve), the relative fluorescence remains below the 100% threshold. This indicates that a time shift of 72 h between SA addition and Pep13 treatment is too long to reliably detect priming.

The combination of SA addition at 72 h and Pep13 treatment at 96 h (Figure 2.6k, dark brown curve) results in the most potent immune response of the experiment, with a relative fluorescence of around 200%. This confirms the suitability of the previously used standard test system as described in the literature [85, 86, 88]. The light brown curve in Figure 2.6k also demonstrates priming with the combination of SA addition at 72 h and Pep13 treatment at 120 h, however, to a weaker extent, than if Pep13 is added after 96 h.

The graphs in Figure 2.6l, m, and n (dark blue curve) show the combination of SA addition at 96 h and Pep13 treatment at 120 h. Regardless of the lower SA and furanocoumarin fluorescence values (Figure 2.6l and m), compared to earlier addition times, the relative furanocoumarin fluorescence shows a potent immune response upon Pep13 treatment. The relative fluorescence (Figure 2.6n) is permanently above 100% after exposure to Pep13 and increases to 180% at the end of the cultivation.

The fluorescence data in Figure 2.6 illustrate that the time of addition of SA or Pep13 has a decisive influence on the development of the SA, furanocoumarin, and relative furanocoumarin fluorescence signals. This experiment shows the value of the relative furanocoumarin fluorescence. By only considering the absolute fluorescence signals, the optimal conditions for priming seem to be the addition of SA at 48 h and following elicitation with Pep13 at 72 h. However, the relative furanocoumarin fluorescence, considering the negative controls, proves that the best conditions for priming are the addition of SA at 72 h and Pep13 at 96 h.

2.3.9 Comparison of effects caused by two known priming-active and two priming-inactive compounds

After examining the priming procedure with SA and Pep13 in MTPs in more detail, the effect on defense priming of another priming compound and two non-priming compounds is analyzed. The aim is to show that online fluorescence measurements of furanocoumarins are suitable for identifying further priming compounds. SA and 4-CSA are used as priming-active compounds whereas 4-hydroxybenzoic acid (4-HBA) and 3-hydroxybenzoic acid (3-HBA) are as priming-inactive compounds [101]. The SA and furanocoumarin fluorescence data are presented in Figure 2.7.

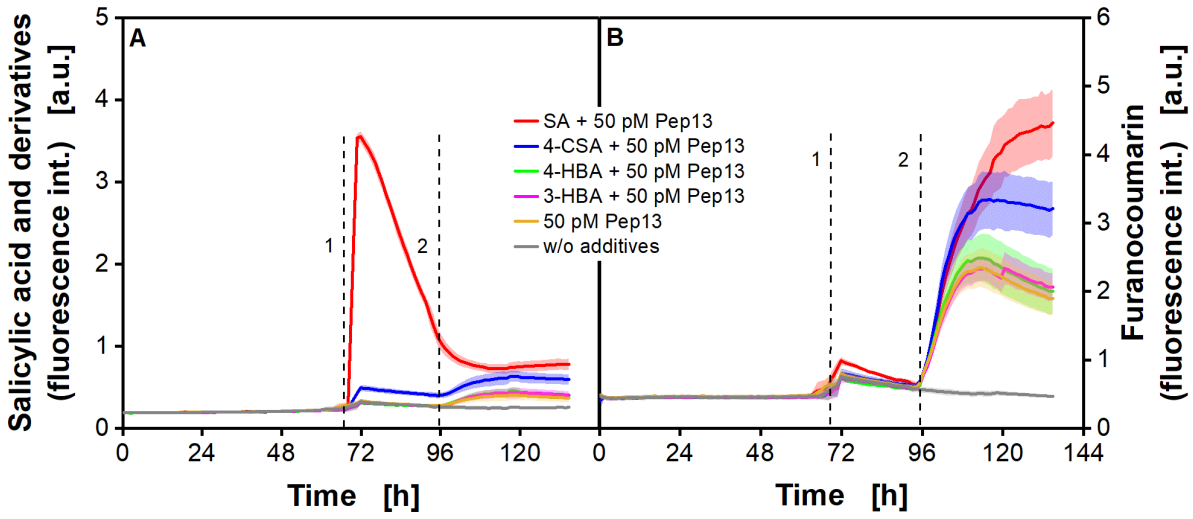

Figure 2.7 Online fluorescence intensities of parsley cell cultures treated with salicylic acid (SA) and its derivatives.

Parsley cells were cultivated in 48-deep-round-well MTPs aerated with air (p_{O2} = 0.21 bar) in an in-house built BioLector. 100 µM of the priming-active compounds SA and 4-chlorosalicylic acid (4-CSA) and 100 µM of the priming-inactive compounds 4-hydroxybenzoic acid (4-HBA) and 3-hydroxybenzoic acid (3-HBA) were added after 72 h. Measurement of SA fluorescence at λ_{ex} = 295 nm and λ_{em} = 405 nm (**a**) and of furanocoumarin fluorescence at λ_{ex} = 335 nm and λ_{em} = 398 nm (**b**). Mean values were calculated from six wells. SD is indicated by colored shadows. Dashed vertical lines indicate the addition of SA or derivatives (1) and Pep13 (2). Cultivation conditions: V_L = 2 mL, n = 800 rpm, d_0 = 3 mm and 25 °C in modified Gamborg's B5 medium.

The results for the cultures treated with SA and Pep13 are similar to the results shown in Figure 2.4, Figure 2.5, and Figure 2.6 and demonstrate very good reproducibility. The fluorescence properties of the three SA derivatives strongly differ from SA. The signal of SA reaches significantly higher levels (Figure 2.7a, red curve) than the other compounds (Figure 2.7a, blue, green, and magenta curve). In Figure 2.7b, an apparent increase in furanocoumarin fluorescence can be seen for SA (Figure 2.7b, red curve) as well as for 4-CSA (Figure 2.7b, blue curve). The online furanocoumarin fluorescence signal of both substances confirms their reported priming properties [101, 126]. The priming with SA leads to a higher production of furanocoumarins than 4-CSA. 4-HBA and 3-HBA lead to a similar furanocoumarin fluorescence increase as the negative control with only Pep13 addition (Figure 2.7b, green, pink, and brown curve, respectively) and confirm the priming-noninducing characteristic of 4-HBA and 3-HBA. The results are consistent with data from the literature and prove the suitability of this method to detect defense priming. In a previous study, the four substances were examined for their priming

properties based on the OTR measured in shake flasks [90]. The results show that online furanocoumarin fluorescence measurements are suited to distinguishing compounds that are active at priming and those inactive at defense priming.

2.4 Conclusion and outlook

The second chapter of this thesis describes the scale-down of defense priming in parsley cell cultures from shake flasks to MTPs. The scale-down was validated by comparison of the OTR in shake flasks and the OTR, as calculated from DOT measurement in MTPs. It was shown that online monitoring of the OTR in MTPs via DOT provides a unique opportunity to spot priming compounds. Furthermore, OTR monitoring was combined with fluorescence measurement of SA and furanocoumarins. The combination provided additional, valuable insight into the dynamics of priming experiments. It was demonstrated that in MTPs, low SA concentration already causes a readily detectable priming response. Additionally, it was shown that multiple combinations and times of treatment with SA and Pep13 induce successful priming. The validity of identifying priming-activating compounds based on furanocoumarin fluorescence was demonstrated with SA, 4-CSA, 4-HBA, and 3-HBA. Thus, two options of high-throughput screening systems, the online DOT measurements, and the online furanocoumarin fluorescence measurements, to identify and analyze the effect of known and candidate priming compounds were presented. The non-specific method for detecting priming compounds via the OTR has the advantage of being applicable for cell suspension cultures and whole plants of species other than parsley.

Bibliography

1. Shih IL, Van YT. The production of poly-(γ-glutamic acid) from microorganisms and its various applications. Bioresour Technol. 2001; doi:10.1016/s0960-8524(01)00074-8.

2. Luo ZT, Guo Y, Liu JD, Qiu H, Zhao MM, Zou W, Li SB. Microbial synthesis of poly-γ-glutamic acid: current progress, challenges, and future perspectives. Biotechnol Biofuels. 2016; doi:10.1186/s13068-016-0537-7.

3. Ogunleye A, Bhat A, Irorere VU, Hill D, Williams C, Radecka I. Poly-γ-glutamic acid: production, properties and applications. Microbiology (London, U K). 2015; doi:10.1099/mic.0.081448-0.

4. Sung MH, Park C, Kim CJ, Poo H, Soda K, Ashiuchi M. Natural and edible biopolymer poly-γ-glutamic acid: synthesis, production, and applications. Chem Rec. 2005; doi:10.1002/tcr.20061.

5. Ashiuchi M. Microbial production and chemical transformation of poly-γ-glutamate. Microb Biotechnol. 2013; doi:10.1111/1751-7915.12072.

6. Richard A, Margaritis A. Poly(glutamic acid) for biomedical applications. Crit Rev Biotechnol. 2001; doi:10.1080/07388550108984171.

7. Buescher JM, Margaritis A. Microbial biosynthesis of polyglutamic acid biopolymer and applications in the biopharmaceutical, biomedical and food industries. Crit Rev Biotechnol. 2007; doi:10.1080/07388550601166458.

8. Sanda F, Fujiyama T, Endo T. Chemical synthesis of poly-γ-glutamic acid by polycondensation of γ-glutamic acid dimer: synthesis and reaction of poly-γ-glutamic acid methyl ester. J Polym Sci, Part A: Polym Chem. 2001; doi:10.1002/1099-0518(20010301)39:5<732::Aid-pola1045>3.0.Co;2-p.

9. Candela T, Fouet A. Poly-gamma-glutamate in bacteria. Mol Microbiol. 2006; doi:10.1111/j.1365-2958.2006.05179.x.

10. Shih IL, Van YT, Sau YY. Antifreeze activities of poly(γ-glutamic acid) produced by *Bacillus licheniformis*. Biotechnol Lett. 2003; doi:10.1023/a:1026042302102.

11. Ivánovics G, Bruckner V. Über die chemische Natur der immunspezifischen Kapselsubstanz der Milzbrandbazillen. Naturwissenschaften. 1937; doi:10.1007/BF01492386.

12. Green BD, Battisti L, Koehler TM, Thorne CB, Ivins BE. Demonstration of a capsule plasmid in *Bacillus anthracis*. Infect Immun. 1985; doi:10.1128/iai.49.2.291-297.1985.

13. Hezayen FF, Rehm BHA, Tindall BJ, Steinbuchel A. Transfer of Natrialba asiatica B1T to Natrialba taiwanensis sp nov and description of Natrialba aegyptiaca sp nov., a novel extremely halophilic, aerobic, non-pigmented member of the Archaea from Egypt that produces extracellular poly(glutamic acid). Int J Syst Evol Microbiol. 2001; doi:10.1099/00207713-51-3-1133.

14. Weber J. Poly-(gamma-glutamic acid)s are the major constituents in hydra (hydrozoa, cnidaria). J Biol Chem. 1990.

15. Parati M, Khalil I, Tchuenbou-Magaia F, Adamus G, Mendrek B, Hill R, Radecka I. Building a circular economy around poly(D/L-gamma-glutamic acid)- a smart microbial biopolymer. Biotechnol Adv. 2022; doi:10.1016/j.biotechadv.2022.108049.

16. Leonard CG, Housewright RD, Thorne CB. Effects of some metallic ions on glutamyl polypeptide synthesis by *Bacillus subtilis.* . J Bacteriol. 1958; doi:10.1128/jb.76.5.499-503.1958.

17. Thorne CB, Gomez CG, Noyes HE, Housewright RD. Production of glutamyl polypeptide by *Bacillus subtilis*. J Bacteriol. 1954; doi:10.1128/jb.68.3.307-315.1954.

18. Bajaj I, Singhal R. Poly (glutamic acid) - An emerging biopolymer of commercial interest. Bioresour Technol. 2011; doi:10.1016/j.biortech.2011.02.047.

19. Ashiuchi M, Soda K, Misono H. A Poly-γ-glutamate Synthetic System of *Bacillus subtilis* IFO 3336: Gene Cloning and Biochemical Analysis of Poly-γ-glutamate Produced by *Escherichia coli* Clone Cells. Biochem Biophys Res Commun. 1999; doi:10.1006/bbrc.1999.1298.

20. Halmschlag B, Steurer X, Putri SP, Fukusaki E, Blank LM. Tailor-made poly-γ-glutamic acid production. Metab Eng. 2019; doi:10.1016/j.ymben.2019.07.009.

21. Gärtner D, Geissendorfer M, Hillen W. Expression of the *Bacillus subtilis* xyl operon is repressed at the level of transcription and is induced by xylose. J Bacteriol. 1988.

22. Qi Y, Kobayashi Y, Hulett FM. The *pst* operon of *Bacillus subtilis* has a phosphate-regulated promoter and is involved in phosphate transport but not in regulation of the pho regulon. J Bacteriol. 1997; doi:10.1128/jb.179.8.2534-2539.1997.

23. Stargardt P, Striedner G, Mairhofer J. Tunable expression rate control of a growth-decoupled T7 expression system by L-arabinose only. Microb Cell Fact. 2021; doi:10.1186/s12934-021-01512-7.

24. Halmschlag B. Tailored poly-γ-glutamic acid production with *Bacillus subtilis* 168 [PhD Thesis]. Germany: Rheinisch-Westfälische Technische Hochschule Aachen. 2019.

25. Birrer GA, Cromwick AM, Gross RA. γ – Poly(glutamic acid) formation by *Bacillus licheniformis* 9945a: physiological and biochemical studies. Int J Biol Macromol. 1994; doi:10.1016/0141-8130(94)90032-9.

26. Goto A, Kunioka M. Biosynthesis and hydrolysis of Poly(γ-glutamic acid) from *Bacillus subtilis* IFO3335. Biosci Biotechnol Biochem. 1992; doi:10.1271/bbb.56.1031.

27. Mitsui N, Murasawa H, Sekiguchi J. Disruption of the cell wall lytic enzyme CwlO affects the amount and molecular size of poly-γ-glutamic acid produced by *Bacillus subtilis (natto)*. J Gen Appl Microbiol. 2011; doi:10.2323/jgam.57.35.

28. Yamaguchi H, Furuhata K, Fukushima T, Yamamoto H, Sekiguchi J. Characterization of a new *Bacillus subtilis* peptidoglycan hydrolase gene, *yvcE* (named *cwlO*), and the enzymatic properties of its encoded protein. J Biosci Bioeng. 2004; doi:10.1016/s1389-1723(04)00262-2.

29. Qiu YB, Zhu YF, Sha YY, Lei P, Luo ZS, Feng XH, Li S, Xu H. Development of a robust *Bacillus amyloliquefaciens* cell factory for efficient poly(γ-glutamic acid) production from jerusalem artichoke. ACS Sustainable Chem Eng. 2020; doi:10.1021/acssuschemeng.0c02107.

30. Feng J, Gao WX, Gu YY, Zhang W, Cao MF, Song CJ, Zhang P, Sun M, Yang C, Wang SF. Functions of poly-gamma-glutamic acid (γ-PGA) degradation genes in γ-PGA synthesis and cell morphology maintenance. Appl Microbiol Biotechnol. 2014; doi:10.1007/s00253-014-5729-0.

31. Ashiuchi M, Nakamura H, Yamamoto T, Kamei T, Soda K, Park C, Sung MH, Yagi T, Misono H. Poly-γ-glutamate depolymerase of *Bacillus subtilis*: production, simple purification and substrate selectivity. J Mol Catal B: Enzym. 2003; doi:10.1016/s1381-1177(03)00087-0.

32. Abe K, Ito Y, Ohmachi T, Asada Y. Purification and properties of two isozymes of γ-glutamyltranspeptidase from *Bacillus subtilis* TAM-4. Biosci Biotechnol Biochem. 1997; doi:10.1271/bbb.61.1621.

33. Kimura K, Tran LSP, Uchida I, Itoh Y. Characterization of *Bacillus subtilis* γ-glutamyltransferase and its involvement in the degradation of capsule poly-γ-glutamate. Microbiology (London, U K). 2004; doi:10.1099/mic.0.27467-0.

34. Scoffone V, Dondi D, Biino G, Borghese G, Pasini D, Galizzi A, Calvio C. Knockout of *pgdS* and *ggt* genes improves γ-PGA yield in *B. subtilis*. Biotechnol Bioeng. 2013; doi:10.1002/bit.24846.

35. Feng J, Gu YY, Quan YF, Cao MF, Gao WX, Zhang W, Wang SF, Yang C, Song CJ. Improved poly-γ-glutamic acid production in *Bacillus amyloliquefaciens* by modular pathway engineering. Metab Eng. 2015; doi:10.1016/j.ymben.2015.09.011.

36. Ojima Y, Kobayashi J, Doi T, Azuma M. Knockout of *pgdS* and *ggt* gene changes poly-γ-glutamic acid production in *Bacillus licheniformis* RK14-46. J Biotechnol. 2019; doi:10.1016/j.jbiotec.2019.08.003.

37. Wang LY, Wang N, Mi DD, Luo YM, Guo JH. Poly-γ-glutamic acid productivity of *Bacillus subtilis* BsE1 has positive function in motility and biocontrol against *Fusarium graminearum*. J Microbiol. 2017; doi:10.1007/s12275-017-6589-y.

38. Zhu YQ, Romain C, Williams CK. Sustainable polymers from renewable resources. Nature. 2016; doi:10.1038/nature21001.

39. Uffen RL, Canalepa.E. Synthesis of pulcherriminic acid by *Bacillus subtilis*. J Bacteriol. 1972; doi:10.1128/jb.111.1.86-93.1972.

40. Li M, Zhang ZL, Li SW, Tian ZA, Ma X. Study on the mechanism of production of γ-PGA and nattokinase in *Bacillus subtilis* natto based on RNA-seq analysis. Microb Cell Fact. 2021; doi:10.1186/s12934-021-01570-x.

41. Wilming A, Begemann J, Kuhne S, Regestein L, Bongaerts J, Evers S, Maurer KH, Büchs J. Metabolic studies of γ-polyglutamic acid production in *Bacillus licheniformis* by small-scale continuous cultivations. Biochem Eng J. 2013; doi:10.1016/j.bej.2013.01.008.

42. Anderlei T, Büchs J. Device for sterile online measurement of the oxygen transfer rate in shaking flasks. Biochem Eng J. 2001; doi:10.1016/s1369-703x(00)00116-9.

43. Anderlei T, Zang W, Papaspyrou M, Büchs J. Online respiration activity measurement (OTR, CTR, RQ) in shake flasks. Biochem Eng J. 2004; doi:10.1016/s1369-703x(03)00181-5.

44. Meissner LRN, Arndt J, Palmen TG, Jestel T, Mitsunaga H, Fukusaki E, Büchs J. Investigation of poly(γ-glutamic acid) production via online determination of viscosity and oxygen transfer rate in shake flasks. J Biol Eng. 2017; doi:10.1186/s13036-017-0065-4.

45. Sieben M, Hanke R, Büchs J. Contact-free determination of viscosity in multiple parallel samples. Sci Rep. 2019; doi:10.1038/s41598-019-44859-z.

46. Halmschlag B, Hoffmann K, Hanke R, Putri SP, Fukusaki E, Büchs J, Blank LM. Comparison of isomerase and Weimberg pathway for γ-PGA production from xylose by engineered *Bacillus subtilis*. Frontiers in Bioengineering and Biotechnology. 2020; doi:10.3389/fbioe.2019.00476.

47. Büchs J, Maier U, Milbradt C, Zoels B. Power consumption in shaking flasks on rotary shaking machines: I. Power consumption measurement in unbaffled flasks at low liquid viscosity. Biotechnol Bioeng. 2000; doi:10.1002/(sici)1097-0290(20000620)68:6<589::Aid-bit1>3.0.Co;2-j.

48. Büchs J, Maier U, Milbradt C, Zoels B. Power consumption in shaking flasks on rotary shaking machines: II. Nondimensional description of specific power consumption and flow regimes in unbaffled flasks at elevated liquid viscosity. Biotechnol Bioeng. 2000; doi:10.1002/(sici)1097-0290(20000620)68:6<594::Aid-bit2>3.0.Co;2-u.

49. Giese H, Klöckner W, Pena C, Galindo E, Lotter S, Wetzel K, Meissner L, Peter CP, Büchs J. Effective shear rates in shake flasks. Chem Eng Sci. 2014; doi:10.1016/j.ces.2014.07.037.

50. Wenzel M, Altenbuchner J. Development of a markerless gene deletion system for *Bacillus subtilis* based on the mannose phosphoenolpyruvate-dependent

phosphotransferase system. Microbiology (London, U K). 2015; doi:10.1099/mic.0.000150.

51. Meselson M, Yuan R. DNA restriction enzyme from *E. coli*. Nature. 1968; doi:10.1038/2171110a0.

52. Messing J, Crea R, Seeburg PH. A system for shotgun DNA sequencing. Nucleic Acids Res. 1981; doi:10.1093/nar/9.2.309.

53. Ashiuchi M. Analytical approaches to poly-γ-glutamate: Quantification, molecular size determination, and stereochemistry investigation. J Chromatogr B: Anal Technol Biomed Life Sci. 2011; doi:10.1016/j.jchromb.2011.03.029.

54. Shi F, Xu ZN, Cen PL. Optimization of gamma-polyglutamic acid production by *Bacillus subtilis* ZJU-7 using a surface-response methodology. Biotechnology and Bioprocess Engineering. 2006; doi:10.1007/bf02932039.

55. Xu H, Jiang M, Li H, Lu DQ, Ouyang P. Efficient production of poly(gamma-glutamic acid) by newly isolated *Bacillus subtilis* NX-2. Process Biochem. 2005; doi:10.1016/j.procbio.2003.09.025.

56. Huang J, Du YM, Xu GH, Zhang HL, Zhu F, Huang L, Xu ZN. High yield and cost-effective production of poly(gamma-glutamic acid) with *Bacillus subtilis*. Eng Life Sci. 2011; doi:10.1002/elsc.201000133.

57. Chen J, Shi F, Zhang B, Zhu F, Cao WF, Xu ZN, Xu GH, Cen PL. Effects of cultivation conditions on the production of gamma-PGA with *Bacillus subtilis* ZJU-7. Appl Biochem Biotechnol. 2010; doi:10.1007/s12010-008-8307-z.

58. Kongklom N, Shi ZP, Chisti Y, Sirisansaneeyakul S. Enhanced production of poly-gamma-glutamic acid by *Bacillus licheniformis* TISTR 1010 with environmental controls. Appl Biochem Biotechnol. 2017; doi:10.1007/s12010-016-2376-1.

59. Kongklom N, Luo HZ, Shi ZP, Pechyen C, Chisti Y, Sirisansaneeyakul S. Production of poly-gamma-glutamic acid by glutamic acid-independent *Bacillus licheniformis* TISTR 1010 using different feeding strategies. Biochem Eng J. 2015; doi:10.1016/j.bej.2015.04.007.

60. Peng YY, Jiang B, Zhang T, Mu WM, Miao M, Hua YF. High-level production of poly(gamma-glutamic acid) by a newly isolated glutamate-independent strain, *Bacillus methylotrophicus*. Process Biochem. 2015; doi:10.1016/j.procbio.2014.12.024.

61. Meier K, Klöckner W, Bonhage B, Antonov E, Regestein L, Büchs J. Correlation for the maximum oxygen transfer capacity in shake flasks for a wide range of operating conditions and for different culture media. Biochem Eng J. 2016; doi:10.1016/j.bej.2016.01.014.

62. Cromwick AM, Birrer GA, Gross RA. Effects of pH and aeration on γ-poly(glutamic acid) formation by *Bacillus licheniformis* in controlled batch fermenter cultures. Biotechnol Bioeng. 1996.

63. Büchs J, Lotter S, Milbradt C. Out-of-phase operating conditions, a hitherto unknown phenomenon in shaking bioreactors. Biochem Eng J. 2001; doi:10.1016/s1369-703x(00)00113-3.

64. Flores C, Medina-Valdez A, Pena C, Serrano-Carreon L, Galindo E. Oxygen transfer rate determines molecular weight and production of poly(γ-glutamic acid) as well as carbon utilization by *Bacillus velezensis* 83. J Chem Technol Biotechnol. 2020; doi:10.1002/jctb.6420.

65. Giese H, Azizan A, Kümmel A, Liao AP, Peter CP, Fonseca JA, Hermann R, Duarte TM, Büchs J. Liquid films on shake flask walls explain increasing maximum oxygen transfer capacities with elevating viscosity. Biotechnol Bioeng. 2014; doi:10.1002/bit.25015.

66. Cao MF, Geng WT, Liu L, Song CJ, Xie H, Guoa WB, Jin YH, Wang SF. Glutamic acid independent production of poly-γ-glutamic acid by *Bacillus amyloliquefaciens* LL3 and cloning of *pgs*BCA genes. Bioresour Technol. 2011; doi:10.1016/j.biortech.2010.12.065.

67. Zhang HL, Zhu JZ, Zhu XC, Cai J, Zhang AY, Hong YZ, Huang J, Huang L, Xu ZN. High-level exogenous glutamic acid-independent production of poly-(γ-glutamic acid) with organic acid addition in a new isolated *Bacillus subtilis* C10. Bioresour Technol. 2012; doi:10.1016/j.biortech.2011.11.085.

68. Tiso T, Sabelhaus P, Behrens B, Wittgens A, Rosenau F, Hayen H, Blank LM. Creating metabolic demand as an engineering strategy in *Pseudomonas putida* - Rhamnolipid synthesis as an example. Metab Eng Commun. 2016; doi:10.1016/j.meteno.2016.08.002.

69. Koebmann BJ, Westerhoff HV, Snoep JL, Nilsson D, Jensen PR. The glycolytic flux in *Escherichia coli* is controlled by the demand for ATP. J Bacteriol. 2002; doi:10.1128/jb.184.14.3909-3916.2002.

70. Fukushima T, Uchida N, Ide M, Kodama T, Sekiguchi J. DL-endopeptidases function as both cell wall hydrolases and poly-γ-glutamic acid hydrolases. Microbiology (London, U K). 2018; doi:10.1099/mic.0.000609.

71. Smith TJ, Blackman SA, Foster SJ. Autolysins of Bacillus subtilis: multiple enzymes with multiple functions. Microbiology-(UK). 2000; doi:10.1099/00221287-146-2-249.

72. Bisicchia P, Noone D, Lioliou E, Howell A, Quigley S, Jensen T, Jarmer H, Devine KM. The essential YycFG two-component system controls cell wall metabolism in Bacillus subtilis. Mol Microbiol. 2007; doi:10.1111/j.1365-2958.2007.05782.x.

73. Mamberti S, Prati P, Cremaschi P, Seppi C, Morelli CF, Galizzi A, Fabbi M, Calvio C. γ-PGA hydrolases of phage origin in *Bacillus subtilis* and other microbial genomes. PLoS One. 2015; doi:10.1371/journal.pone.0130810.

74. Fujimoto Z, Kimura K. Crystal structure of bacteriophage ΦNIT1 zinc peptidase PghP that hydrolyzes γ-glutamyl linkage of bacterial poly-γ-glutamate. Proteins: Struct, Funct, Bioinf. 2012; doi:10.1002/prot.23229.

75. Wang LL, Chen JT, Wang LF, Wu S, Zhang GZ, Yu HQ, Ye XD, Shi QS. Conformations and molecular interactions of poly-gamma-glutamic acid as a soluble microbial product in aqueous solutions. Sci Rep. 2017; doi:10.1038/s41598-017-13152-2.

76. Oerke EC. Crop losses to pests. J Agric Sci. 2006; doi:10.1017/s0021859605005708.

77. Robinson RA, Sutherland WJ. Post-war changes in arable farming and biodiversity in great britain. J Appl Ecol. 2002; doi:10.1046/j.1365-2664.2002.00695.x.

78. Storkey J, Meyer S, Still KS, Leuschner C. The impact of agricultural intensification and land-use change on the European arable flora. Proc R Soc B-Biol Sci. 2012; doi:10.1098/rspb.2011.1686.

79. Beckers GJ, Conrath U. Priming for stress resistance: from the lab to the field. Curr Opin Plant Biol. 2007; doi:10.1016/j.pbi.2007.06.002.

80. Conrath U, Beckers GJM, Langenbach CJG, Jaskiewicz MR. Priming for enhanced defense. In: VanAlfen NK, editor. Annual Review of Phytopathology. 53. Palo Alto: Annual Reviews; 2015. p. 97-119.

81. Senaratna T, Touchell D, Bunn E, Dixon K. Acetyl salicylic acid (Aspirin) and salicylic acid induce multiple stress tolerance in bean and tomato plants. Plant Growth Regulation. 2000; doi:10.1023/a:1006386800974.

82. Conrath U, Beckers GJM, Flors V, Garcia-Agustin P, Jakab G, Mauch F, Newman MA, Pieterse CMJ, Poinssot B, Pozo MJ, Pugin A, Schaffrath U, Ton J, Wendehenne D, Zimmerli L, Mauch-Mani B, Prime APG. Priming: getting ready for battle. Mol Plant-Microbe Interact. 2006; doi:10.1094/mpmi-19-1062.

83. Conrath U, Pieterse CMJ, Mauch-Mani B. Priming in plant-pathogen interactions. Trends Plant Sci. 2002; doi:10.1016/s1360-1385(02)02244-6.

84. Savvides A, Ali S, Tester M, Fotopoulos V. Chemical priming of plants against multiple abiotic stresses: mission possible? Trends Plant Sci. 2016; doi:10.1016/j.tplants.2015.11.003.

85. Kauss H, Theisingerhinkel E, Mindermann R, Conrath U. Dichloroisonicotinic and salicylic acid, inducers of systemic acquired resistance, enhance fungal elicitor responses in parsley cells. Plant J. 1992; doi:10.1111/j.1365-313X.1992.tb00134.x.

86. Katz VA, Thulke OU, Conrath U. A benzothiadiazole primes parsley cells for augmented elicitation of defense responses. Plant Physiol. 1998; doi:10.1104/pp.117.4.1333.

87. Nürnberger T, Nennstiel D, Jabs T, Sacks WR, Hahlbrock K, Scheel D. High-affinity binding of a fungal oligopeptide elicitor to parsley palsma-membranes triggers multiple defense responses. Cell. 1994; doi:10.1016/0092-8674(94)90423-5.

88. Siegrist J, Mühlenbeck S, Buchenauer H. Cultured parsley cells, a model system for the rapid testing of abiotic and natural substances as inducers of systemic acquired resistance. Physiol Mol Plant Pathol. 1998; doi:10.1006/pmpp.1998.0176.

89. Schillheim B, Jansen I, Baum S, Beesley A, Bolm C, Conrath U. Sulforaphane modifies histone H3, unpacks chromatin, and primes defense. Plant Physiol. 2018; doi:10.1104/pp.17.00124.

90. Schilling JV, Schillheim B, Mahr S, Reufer Y, Sanjoyo S, Conrath U, Büchs J. Oxygen transfer rate identifies priming compounds in parsley cells. BMC Plant Biology. 2015; doi:10.1186/s12870-015-0666-3.

91. Schulte A, Schilling JV, Nolten J, Korona A, Kromke H, Vennekotter JB, Schillheim B, Wessling M, Conrath U, Büchs J. Parallel online determination of ethylene release rate

by shaken parsley cell cultures using a modified RAMOS device. Bmc Plant Biology. 2018; doi:10.1186/s12870-018-1305-6.

92. Loogen J, Müller A, Balzer A, Weber S, Schmitz K, Krug R, Schaffrath U, Pietruszk J, Conrath U, Büchs J. An illuminated respiratory activity monitoring system identifies priming-active compounds in plant seedlings. Bmc Plant Biology. 2021; doi:10.1186/s12870-021-03100-8.

93. Flitsch D, Krabbe S, Ladner T, Beckers M, Schilling J, Mahr S, Conrath U, Schomburg WK, Büchs J. Respiration activity monitoring system for any individual well of a 48-well microtiter plate. J Biol Eng. 2016; doi:10.1186/s13036-016-0034-3.

94. Samorski M, Müller-Newen G, Büchs J. Quasi-continuous combined scattered light and fluorescence measurements: A novel measurement technique for shaken microtiter plates. Biotechnol Bioeng. 2005; doi:10.1002/bit.20573.

95. Kensy F, Zang E, Faulhammer C, Tan RK, Büchs J. Validation of a high-throughput fermentation system based on online monitoring of biomass and fluorescence in continuously shaken microtiter plates. Microb Cell Fact. 2009; doi:10.1186/1475-2859-8-31.

96. Wewetzer SJ, Kunze M, Ladner T, Luchterhand B, Roth S, Rahmen N, Kloss R, Silva ACE, Regestein L, Büchs J. Parallel use of shake flask and microtiter plate online measuring devices (RAMOS and BioLector) reduces the number of experiments in laboratory-scale stirred tank bioreactors. J Biol Eng. 2015; doi:10.1186/s13036-015-0005-0.

97. Gamborg OL, Miller RA, Ojima K. Nutrient requirements of suspension cultures of soybean root cells. Exp Cell Res. 1968; doi:10.1016/0014-4827(68)90403-5.

98. Hermann R, Lehmann M, Büchs J. Characterization of gas-liquid mass transfer phenomena in microtiter plates. Biotechnol Bioeng. 2003; doi:10.1002/bit.10456.

99. Jäger G, Wu ZJ, Garschhammer K, Engel P, Klement T, Rinaldi R, Spiess AC, Büchs J. Practical screening of purified cellobiohydrolases and endoglucanases with alpha-cellulose and specification of hydrodynamics. Biotechnol Biofuels. 2010; doi:10.1186/1754-6834-3-18.

100. Schmitz K, Werner L, Conrath U. High-throughput screening for defense priming-inducing compounds in parsley cell cultures. Bio-protocol. 2021; doi:10.21769/BioProtoc.4200.

101. Conrath U, Chen ZX, Ricigliano JR, Klessig DF. Two inducers of plant defense responses, 2,6-dichloroisonicotinec acid and salicylic acid, inhibit catalase activity in tobacco. Proc Natl Acad Sci U S A. 1995; doi:10.1073/pnas.92.16.7143.

102. Rischbieter E, Schumpe A, Wunder V. Gas solubilities in aqueous solutions of organic substances. J Chem Eng Data. 1996; doi:10.1021/je960039c.

103. Weisenberger S, Schumpe A. Estimation of gas solubilities in salt solutions at temperatures from 273 K to 363 K. AIChE J. 1996; doi:10.1002/aic.690420130.

104. Wilhelm E, Battino R, Wilcock RJ. Low-pressure solubility of gases in liquid water. Chem Rev. 1977; doi:10.1021/cr60306a003.

105. Ladner T, Flitsch D, Schlepütz T, Büchs J. Online monitoring of dissolved oxygen tension in microtiter plates based on infrared fluorescent oxygen-sensitive nanoparticles. Microb Cell Fact. 2015; doi:10.1186/s12934-015-0347-9.

106. Kalpić D, Hlupić N, Lovrić M. Student's t-Tests. In: Lovric M, editor. International Encyclopedia of Statistical Science. Berlin, Heidelberg: Springer Berlin Heidelberg; 2011. p. 1559-63.

107. Doran PM. Design of mixing systems for plant cell suspensions in stirred reactors. Biotechnol Prog. 1999; doi:10.1021/bp990042v.

108. Georgiev MI, Weber J, Maciuk A. Bioprocessing of plant cell cultures for mass production of targeted compounds. Appl Microbiol Biotechnol. 2009; doi:10.1007/s00253-009-2049-x.

109. Freyer SA, Konig M, Kunkel A. Validating shaking flasks as representative screening systems. Biochem Eng J. 2004; doi:10.1016/s1369-703x(03)00175-x.

110. Funke M, Diederichs S, Kensy F, Muller C, Büchs J. The baffled microtiter plate: increased oxygen transfer and improved online monitoring in small scale fermentations. Biotechnol Bioeng. 2009; doi:10.1002/bit.22341.

111. Klöckner W, Diederichs S, Büchs J. Orbitally shaken single-use bioreactors. In: Eibl D, Eibl R, editors. Advances in Biochemical Engineering-Biotechnology. 138. Berlin: Springer-Verlag Berlin; 2014. p. 45-60.

112. Lattermann C, Funke M, Hansen S, Diederichs S, Büchs J. Cross-section perimeter is a suitable parameter to describe the effects of different baffle geometries in shaken microtiter plates. J Biol Eng. 2014; doi:10.1186/1754-1611-8-18.

113. Maier U, Büchs J. Characterisation of the gas-liquid mass transfer in shaking bioreactors. Biochem Eng J. 2001; doi:10.1016/s1369-703x(00)00107-8.

114. van Dongen JT, Gupta KJ, Ramirez-Aguilar SJ, Araujo WL, Nunes-Nesi A, Fernie AR. Regulation of respiration in plants: a role for alternative metabolic pathways. J Plant Physiol. 2011; doi:10.1016/j.jplph.2010.11.004.

115. Bailey-Serres J, Fukao T, Gibbs DJ, Holdsworth MJ, Lee SC, Licausi F, Perata P, Voesenek L, van Dongen JT. Making sense of low oxygen sensing. Trends Plant Sci. 2012; doi:10.1016/j.tplants.2011.12.004.

116. Geigenberger P. Response of plant metabolism to too little oxygen. Curr Opin Plant Biol. 2003; doi:10.1016/s1369-5266(03)00038-4.

117. Müller J, Beckers M, Mussmann N, Bongaerts J, Büchs J. Elucidation of auxotrophic deficiencies of Bacillus pumilus DSM 18097 to develop a defined minimal medium. Microb Cell Fact. 2018; doi:10.1186/s12934-018-0956-1.

118. Ladner T, Held M, Flitsch D, Beckers M, Büchs J. Quasi-continuous parallel online scattered light, fluorescence and dissolved oxygen tension measurement combined with monitoring of the oxygen transfer rate in each well of a shaken microtiter plate. Microb Cell Fact. 2016; doi:10.1186/s12934-016-0608-2.

119. Schilling JV. A biochemical engineering approach to identify priming-inducing compounds in parsley cells. PhD Thesis. Aachen, Germany: Rheinisch-Westfälische Technische Hochschule Aachen. 2016.

120. Ullisch DA, Muller CA, Maibaum S, Kirchhoff J, Schiermeyer A, Schillberg S, Roberts JL, Treffenfeldt W, Büchs J. Comprehensive characterization of two different nicotiana tabacum cell lines leads to doubled GFP and HA protein production by media optimization. J Biosci Bioeng. 2012; doi:10.1016/j.jbiosc.2011.09.022.

121. Raval KN, Hellwig S, Prakash G, Ramos-Plasencia A, Srivastava A, Büchs J. Necessity of a two-stage process for the production of azadirachtin-related limonoids in suspension cultures of Azadirachta indica. J Biosci Bioeng. 2003; doi:10.1263/jbb.96.16.

122. Chen ZX, Malamy J, Henning J, Conrath U, Sanchezcasas P, Silva H, Ricigliano J, Klessig DF. Induction, modification, and transduction of the salicylic acid signal in plant defense responses. Proc Natl Acad Sci U S A. 1995; doi:10.1073/pnas.92.10.4134.

123. Dean JV, Mohammed LA, Fitzpatrick T. The formation, vacuolar localization, and tonoplast transport of salicylic acid glucose conjugates in tobacco cell suspension cultures. Planta. 2005; doi:10.1007/s00425-004-1430-3.

124. Dean JV, Shah RP, Mohammed LA. Formation and vacuolar localization of salicylic acid glucose conjugates in soybean cell suspension cultures. Physiol Plant. 2003; doi:10.1034/j.1399-3054.2003.00117.x.

125. Lee HI, Raskin I. Glucosylation of salicylic acid in nicotiana tabacum cv. xanthi-nc. Phytopathology. 1998; doi:10.1094/phyto.1998.88.7.692.

126. Thulke O, Conrath U. Salicylic acid has a dual role in the activation of defence-related genes in parsley. Plant J. 1998; doi:10.1046/j.1365-313X.1998.00093.x.

127. Kombrink E, Hahlbrock K. Responses of cultured parsley cells to elicitors from phytopathogenic fungi. Plant Physiol. 1986; doi:10.1104/pp.81.1.216.

128. Whitehead IM, Threlfall DR. Production of phytoalexins by plant tissue cultures. J Biotechnol. 1992; doi:10.1016/0168-1656(92)90069-l.

129. Sieben M, Steinhorn G, Müller C, Fuchs S, Chin LA, Regestein L, Büchs J. Testing plasmid stability of *Escherichia coli* using the continuously operated shaken BIOreactor system. Biotechnol Prog. 2016; doi:10.1002/btpr.2341.

130. Wechselberger P, Sagmeister P, Herwig C. Real-time estimation of biomass and specific growth rate in physiologically variable recombinant fed-batch processes. Bioprocess Biosystems Eng. 2013; doi:10.1007/s00449-012-0848-4.

131. Mühlmann MJ, Forsten E, Noack S, Büchs J. Prediction of recombinant protein production by *Escherichia coli* derived online from indicators of metabolic burden. Biotechnol Prog. 2018; doi:10.1002/btpr.2704.

Appendix

Table A 1 Primer used to create the modified *B. subtilis* strains

Primer	Sequence (5'-3')	Description
BS-001	CCAGGGGGATCACCATCCGTCGCCCCATCCCTATGATTTCAGAAGC	Amplification of TS1 for pBs-3
BS-002	CAGCTTCTTTCGGGGCCAGAATGAATATGCTGGGC	Amplification of TS1 for pBs-3
BS-003	CATATTCATTCTGGCCCCGAAAGAAGCTGGT	Amplification of TS2 for pBs-3
BS-004	ACAGAGTGATATTATTGACACGCCCAGCGCTGCTGGATGACTT	Amplification of TS2 for pBs-3
BS-005	CCAGGGGGATCACCATCCGTCGCCCGTTAAGCAAATACTGTTTGACTTC	Amplification of TS1 for pBs-5
BS-006	AAGCGAGTACAGTGTGCATAATGCCGTTTTTC	Amplification of TS1 for pBs-5
BS-007	CGGCATTATGCACACTGTACTCGCTTCAAATGAGTAC	Amplification of TS2 for pBs-5
BS-008	ACAGAGTGATATTATTGACACGCCCCGACCCGAATGAGCAGGC	Amplification of TS2 for pBs-5
BS-015	ATGTGTCCGGGAAAGG	Verification of *pgdS* KO
BS-016	ACCATTTGCACGGGAAG	Verification of *pgdS* KO
BS-019	GAAGGATATCAGGCGAAATCGGCAGGGAAGTAATG	Amplification of P(pst) for pBs-4
BS-020	AGTAACCACATTGCCTGAATTCCCCCTGCGTATAATG	Amplification of P(pst) for pBs-4
BS-025	GGGCGTGTCAATAATATCACTC	Vector backbone linearization
BS-026	GGGCGACGGATGGTGATCCC	Vector backbone linearization
BS-041	GGGATCACCATCCGTCGCCCTCGCAGCCTATTATATCAG	Amplification of TS1 for pBs-12
BS-042	TACCCATATCATCAAGTTTCGTTCCTCATAC	Amplification of TS1 for pBs-12
BS-043	GAAACTTGATGATATGGGTAAGGAATACGTTTG	Amplification of TS2 for pBs-12
BS-044	GTGATATTATTGACACGCCCTCACCGGTTACCGTATCG	Amplification of TS2 for pBs-12
BS-033	GGGATCACCATCCGTCGCCCGCTTTAGGGCTAACATCCAG	Amplification of TS1 for pBs-10
BS-034	ACCCGAGTGCCCGCACCGGTCAATATGAAC	Amplification of TS1 for pBs-10
BS-035	ACCGGTGCGGGCACTCGGGTGCGGATTC	Amplification of TS2 for pBs-10
BS-036	GTGATATTATTGACACGCCCAAACGGGCAGCAGCTGAG	Amplification of TS2 for pBs-10
BS-037	GGGATCACCATCCGTCGCCCACCAGTTGTCGTTGCCAG	Amplification of TS1 for pBs-11
BS-038	CAGAAGCGCATTACTAGCATACTCTTCTTCCAATC	Amplification of TS1 for pBs-11
BS-039	ATGCTAGTAATGCGCTTCTGTATAGCCC	Amplification of TS2 for pBs-11

Primer	Sequence (5'-3')	Description
BS-040	GTGATATTATTGACACGCCCTGAACTGAGTACATGATCGAG	Amplification of TS2 for pBs-11
BS-029	GGGATCACCATCCGTCGCCCTACCTTCTATGCCGCAGAG	Amplification of TS1 for pBs-9
BS-030	CACCTTTACTAAGCGCAGGACATTAGTTTG	Amplification of TS1 for pBs-9
BS-031	TCCTGCGCTTAGTAAAGGTGTGGTCTGATG	Amplification of TS2 for pBs-9
BS-032	GTGATATTATTGACACGCCCGCTCGACTACCCTACTGC	Amplification of TS2 for pBs-9
BS-053	GGGATCACCATCCGTCGCCCTGCAGTTTCTCATGTAAGTCG	Amplification of TS1 for pBs-14
BS-054	TCCGCATCTTGACGAATGGCAGGCATCAC	Amplification of TS1 for pBs-14
BS-055	GCCATTCGTCAAGATGCGGAATATCAGATTAGAGG	Amplification of TS2 for pBs-14
BS-056	GTGATATTATTGACACGCCCGCGTCTGAACAGGGAAGC	Amplification of TS2 for pBs-14

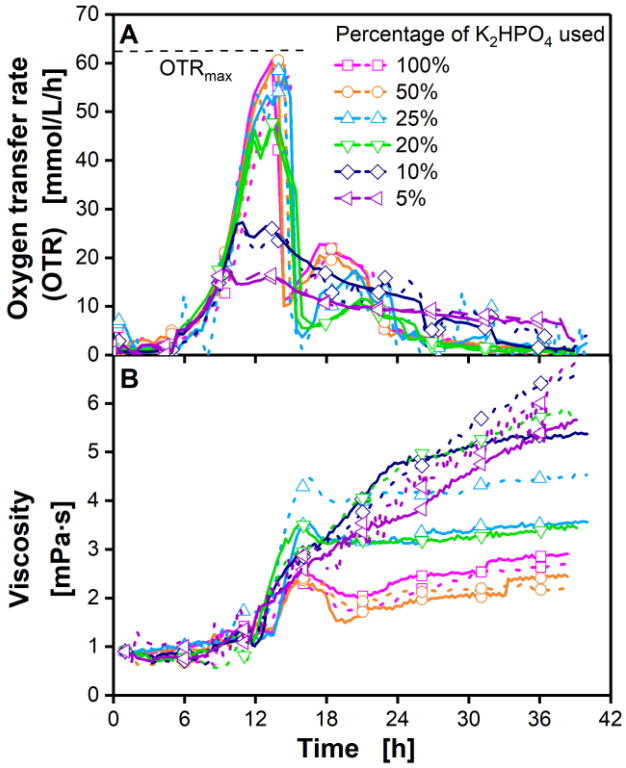

Figure A 1 Determination of the limiting phosphate concentration during shake flask cultivations of *B. subtilis* P_{pst} Δspo. Duplicates of experiment shown in Figure 1.3

The oxygen transfer rate (OTR) (A) and the online viscosity measurements (B) of a *B. subtilis* P_{pst} Δspo cultivation in a modified V3 glucose minimal medium with varying phosphate concentrations are shown: pH_{start} = 8.1, 20 g/L glucose, phosphate: 100% ≙ 3.4 g/L K_2HPO_4, 0.2 M MOPS; inoculation from pre-culture (OD_{start} = 0.1), T = 37 °C, 250 mL shake flask, V_L = 10 mL, n = 350 rpm, d_0 = 50 mm. Oxygen transfer rates (A) were measured with a RAMOS device. Online viscosity (B) was determined with a new system for parallel online measurement of viscosity in eight shake flasks (ViMOS), described by Sieben et al. 2019. The dashed horizontal line (A) indicates the maximum oxygen transfer capacity (OTR_{max}) at 62.4 mmol/L/h, calculated according to Meier et al. 2016. The cultivations were carried out in duplicates in three experimental runs (run 1: 100%, 50%, run 2: 25%, 10%, run 3: 20%, 10%, 5%). For clarity, only every ninth (A) and twentieth (B) measuring point is marked as a symbol.

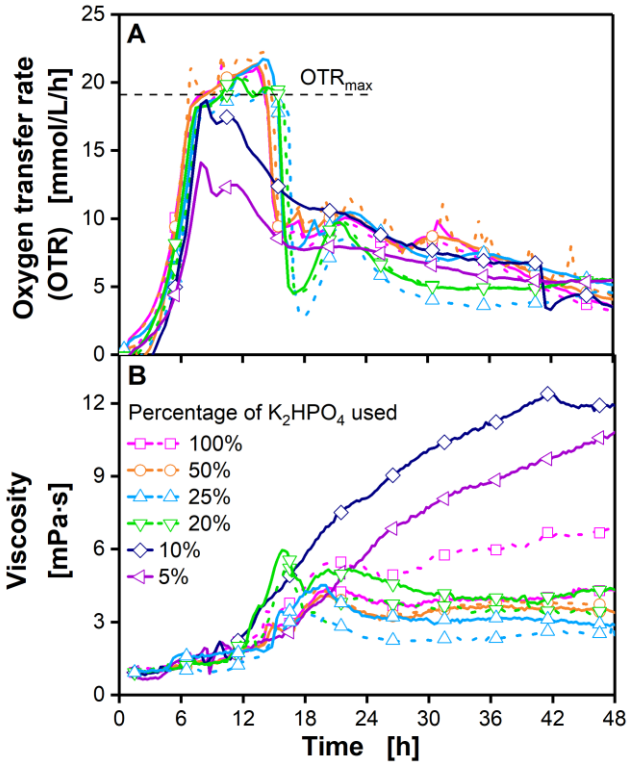

Figure A 2 Determination of the limiting phosphate concentration during shake flask cultivations of *B. subtilis* P_{pst} Δspo at oxygen limited conditions by reduced shaking frequency and enlarged filling volume. Duplicates of experiment shown in Figure 1.4

The oxygen transfer rate (OTR) (A) and the online viscosity measurements (B) of a *B. subtilis* P_{pst} Δspo cultivation in a modified V3 glucose minimal medium with varying phosphate concentrations are shown. In comparison to Figure 1 the shaking frequency was reduced and filling volume increased: pH_{start} = 8.1, 20 g/L glucose, phosphate: 100% ≙ 3.4 g/L K_2HPO_4, 0.2 M MOPS; inoculation from pre-culture (OD_{start} = 0.1), T = 37 °C, 250 mL shake flask, V_L = 30 mL, n = 250 rpm, d_0 = 50 mm. Oxygen transfer rates (A) were measured with a RAMOS device. Online viscosity (B) was determined with a new system for parallel online measurement of viscosity in eight shake flasks (ViMOS), described by Sieben et al. 2019. The dashed horizontal line (A) indicates the maximum oxygen transfer capacity (OTR_{max}) at 19.1 mmol/L/h, calculated according to Meier et al. 2016. The cultivations were carried out in duplicates in two different experimental runs (run 1: 100%, 50%, run 2: 25%, 20%, 10%, 5%). Due to experimental problems during run 2, only single data sets are available for 10% and 5%.

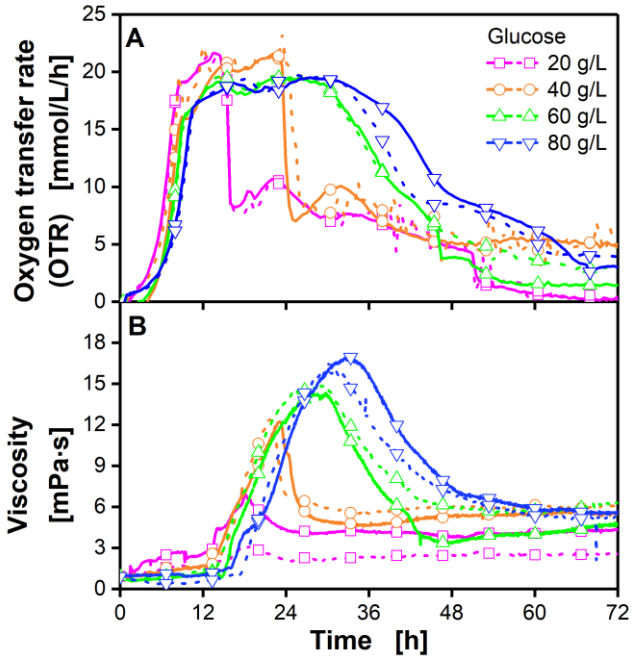

Figure A 3 Enhanced γ-PGA production with increasing glucose concentrations. Duplicates of experiment shown in Figure 1.5

The oxygen transfer rate (OTR) (A) and the online viscosity measurements (B) of a *B. subtilis* P_{pst}Δspo cultivation with varying amounts of glucose from 20 g/L to 80 g/L in the medium are shown. The cultivations were performed in a modified V3 glucose minimal medium: pH_{start} = 8.1, phosphate: 25 % of the original concentration ≙ 0.85 g/L K_2HPO_4, 0.2 M MOPS, inoculation from pre-culture (OD_{start} = 0.1), T = 37 °C, 250 mL shake flask, V_L = 30 mL, n = 250 rpm, d_0 = 50 mm. Oxygen transfer rates (A) were measured with a RAMOS device. Online viscosity (B) was determined with a new system for parallel online measurement of viscosity in eight shake flasks (ViMOS), described by Sieben et al. 2019. The lag phases of cultures with higher glucose concentrations are longer due to increased osmotic pressure. The cultivations were carried out in duplicates. In contrast to Figure 1.5 time data of 40 g/L, 60 g/L, and 80 g/L were not shifted. For clarity, only every fifteenth (A) and eightieth (B) measuring point is marked as a symbol.

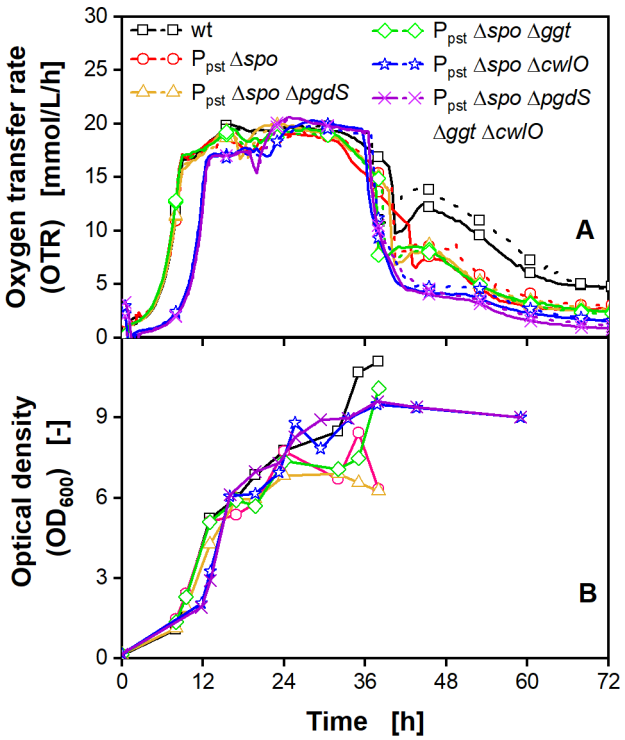

Figure A 4 Duplicates of the oxygen transfer rate (OTR) from Figure 1.7a and the associated optical densities of the cultivations are shown

B. subtilis strains were cultivated in a modified V3 glucose minimal medium: pH_{start} = 8.1, 60 g/L glucose, phosphate: 25% ≙ 0.85 g/L K_2HPO_4, 0.2 MOPS, inoculation from pre-culture (OD_{start} = 0.1), T = 37 °C, 250 mL shake flask, V_L = 30 mL, n = 250 rpm, d_0 = 50 mm. Data were generated in two experimental runs (run 1: wt, P_{pst} Δspo, P_{pst} Δspo Δ*ggt,* P_{pst} Δspo Δ*pgdS*; run 2: P_{pst} Δspo Δ*cwlO*, P_{pst} Δspo Δ*ggt* Δ*pgdS* Δ*cwlO*). Duplicates of the OTR are shown in A. In contrast to Figure 1.7 time data of run 2 were not shifted. For clarity, only every fifteenth measuring point in A is marked as a symbol. B shows the optical densities from offline measurements at 600 nm.

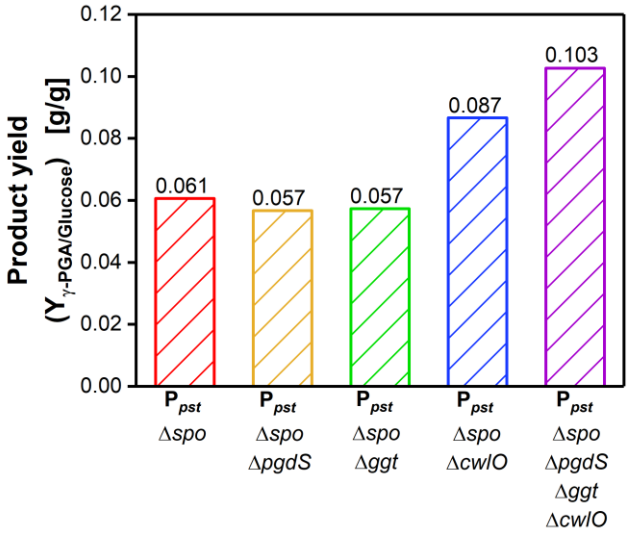

Figure A 5 Comparison of the specific γ-PGA product yield of four different *B. subtilis* γ-PGA depolymerase gene deletion mutants.

B. subtilis strains were cultivated in a modified V3 glucose minimal medium: pH_{start} = 8.1, 60 g/L glucose, phosphate: 25% ≙ 0.85 g/L K_2HPO_4, 0.2 MOPS, inoculation from pre-culture (OD_{start} = 0.1), T = 37 °C, 250 mL shake flask, V_L = 30 mL, n = 250 rpm, d_0 = 50 mm. Data were generated in two experimental runs (run 1: wt, P_{pst}Δspo, P_{pst}Δspo Δ*ggt,* P_{pst}Δspo Δ*pgdS*; run 2: P_{pst} Δspo Δ*cwlO*, P_{pst} Δspo Δ*ggt* Δ*pgdS* Δ*cwlO*). Raw data are taken from Figure 1.7. γ-PGA concentration was measured via GPC and glucose via HPLC. Maximum γ-PGA values were taken as basis for the calculation.

Calculation of μ_{max} from OTR data

The correlation of OTR and growth rate is shown in Sieben et al.[129]. The mass balance of oxygen can be described by the following equation S1.

$$\frac{dc_{O2}}{dt} = -\frac{1}{Y_{X/O}} \cdot \mu \cdot X - \frac{1}{Y_{P/O}} \cdot r_P \cdot X - m_O \cdot X + OTR \qquad \text{Eq. A 1}$$

Dc_{O2}	Oxygen concentration in the liquid	[mol/L]
$Y_{X/O}$	Yield coefficient of the biomass per oxygen	[$mol_{biomass}/mol_{oxygen}$]
μ	Growth rate	[1/h]
X	Biomass	[mol/L]
$Y_{P/O}$	Yield coefficient of product per oxygen	[$mol_{product}/mol_{oxygen}$]
r_p	Product formation rate	[$mol_{product}/mol_{biomass}$/h]
m_O	Maintenance coefficient of oxygen	[$mol_{oxygen}/mol_{biomass}$/h]
OTR	Oxygen transfer rate	[mol/L/h]
OUR	Oxygen uptake rate	[mol/L/h]

Under the assumption of $\mu = \mu_{max}$ during the exponential growth phase, the maintenance metabolism ($-m_O \cdot X$) can be neglected. With the additional assumption of no product and just biomass formation, the term $-\frac{1}{Y_{P/O}} \cdot r_P \cdot X$ is neglected, too. The differential on the left side of the above equation is much smaller than the remaining terms on the right, resulting in the simplification: $\frac{dc_{O2}}{dt} \approx 0$.

This leads to the following equation S2, which shows the direct proportionality of the OTR to the biomass:

$$OTR = \frac{\mu_{max}}{Y_{X/O}} \cdot \qquad \text{Eq. A 2}$$

A more detailed correlation of the growth rate and the OTR, respectively OUR, can be found in Wechselberger et al.[130]. The correlation of the oxygen transfer rate and scattered light was described by Mühlmann et al.[131]. The derivative of the scattered light has been shown to be in good agreement with OTR curves measured by the RAMOS technique in shake flasks.

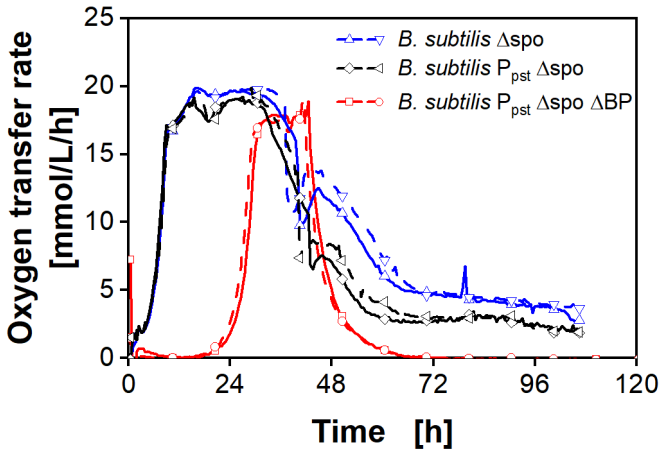

Figure A 6 Impact of by-product knock outs on OTR. Original progression of the OTR over time of experiment shown in Figure 1.8

The OTR of a *B. subtilis* P_{pst} Δspo ΔBP cultivation (red line) are compared to a *B. subtilis* P_{pst} Δspo (black line) cultivation. Negative control was a *B. subtilis* Δ*spo* culture without γ-PGA production (blue line). Cultivation conditions: modified V3 glucose minimal medium, pH_{start} = 8.1, 60 g/L glucose, phosphate: 25% ≙ 0.85 g/L K_2HPO_4, 0.2 M MOPS; inoculation from second pre culture (initial $OD_{600,\ start}$ = 0.1), T = 37 °C, 250 mL shake flask, V_L = 30 mL, n = 250 rpm, d_0 = 50 mm. Oxygen transfer rates (a) were measured with a RAMOS device. The cultivations were carried out in duplicates in two experimental runs (run 1: *B. subtilis* P_{pst} Δspo and *B. subtilis* Δspo, run2: *B. subtilis* P_{pst} Δspo ΔBP. For clarity, only every twentieth is marked as a symbol.

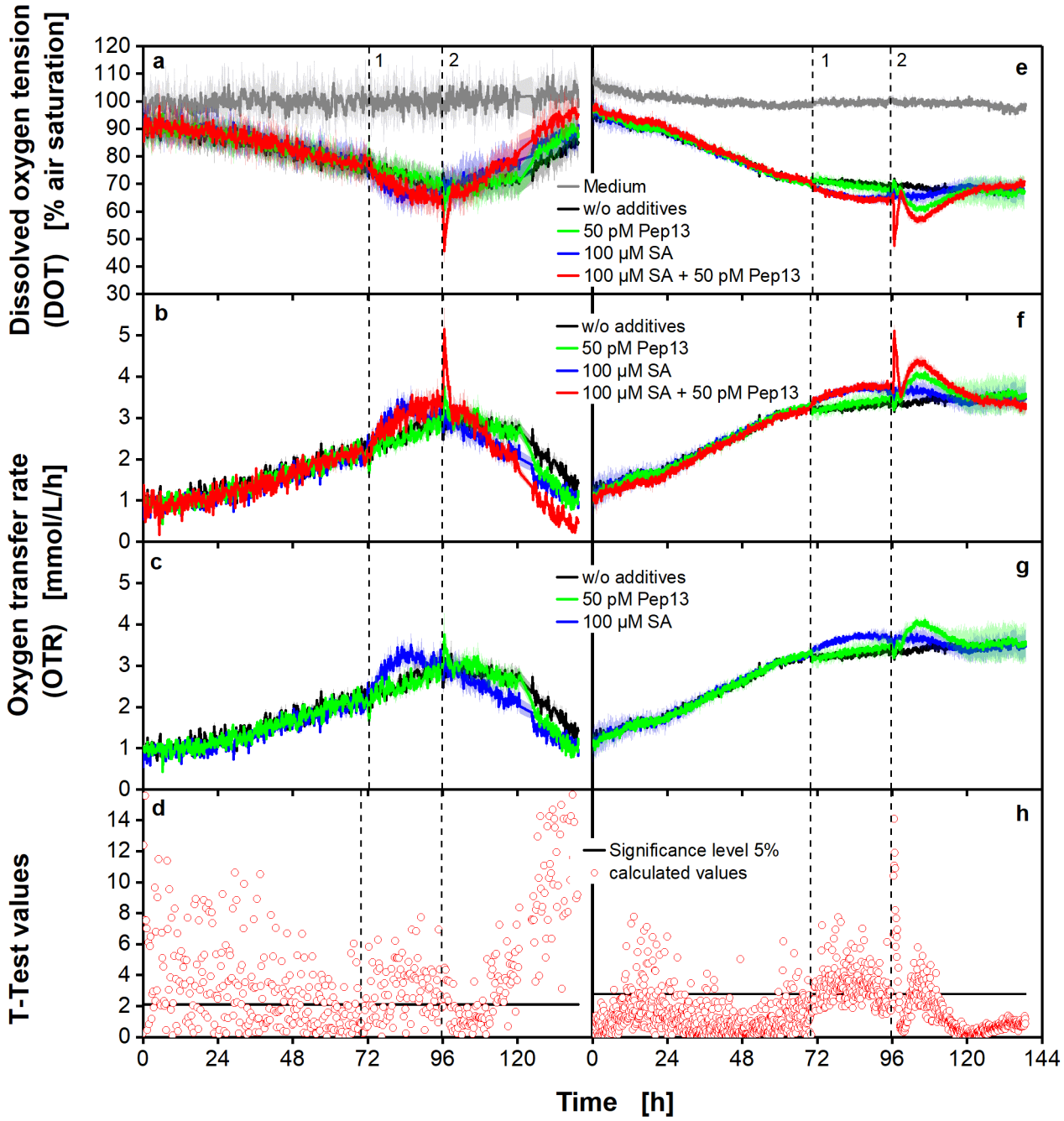

Figure A 7 DOT and calculated OTR of parsley cell cultures measured with two different sensor spot systems.

Parsley cell cultures aerated with air (p_{O2} = 0.21 bar) were cultivated in 48-deep-round-well MTPs with PreSens sensor spots using a custom made industrial BioLector device (**a**) and in 48-deep-round-well MTPs with PyroScience sensor spots using an in-house built BioLector (**e**). The OTR in **b** and **f** was calculated from the DOT (**a** and **e**) according to Equation 3. Since the red curve in **b** and **f** partly covers the other curves, the graphs **b** and **f** are shown again without the red curve in **c** and **g**, respectively. Dashed vertical lines indicate the addition of salicylic acid (SA) (1) and Pep13 (2). Mean values were calculated from 10 wells in **a** and **b** and from three wells in **e** and **f**, respectively. The SD in **a**, **b**, **c**, **e**, **f** and **g** is indicated by colored shadows. The data were normalized as described

in Material and Methods. MTP cultivation conditions: V_L = 2 ml, n = 600 rpm, d_0 = 3 mm and 25 °C in modified Gamborg's B5 medium. **d** and **h** show the T-test values for the comparison of the Pep13 treated cultures (**b**,**c**, **f** and **g** green line) and the SA and Pep13 treated experiments (**b** and **f** red line). The black dashed horizontal lines in **d** and **h** show the 5% quantile of the t_n-distribution.

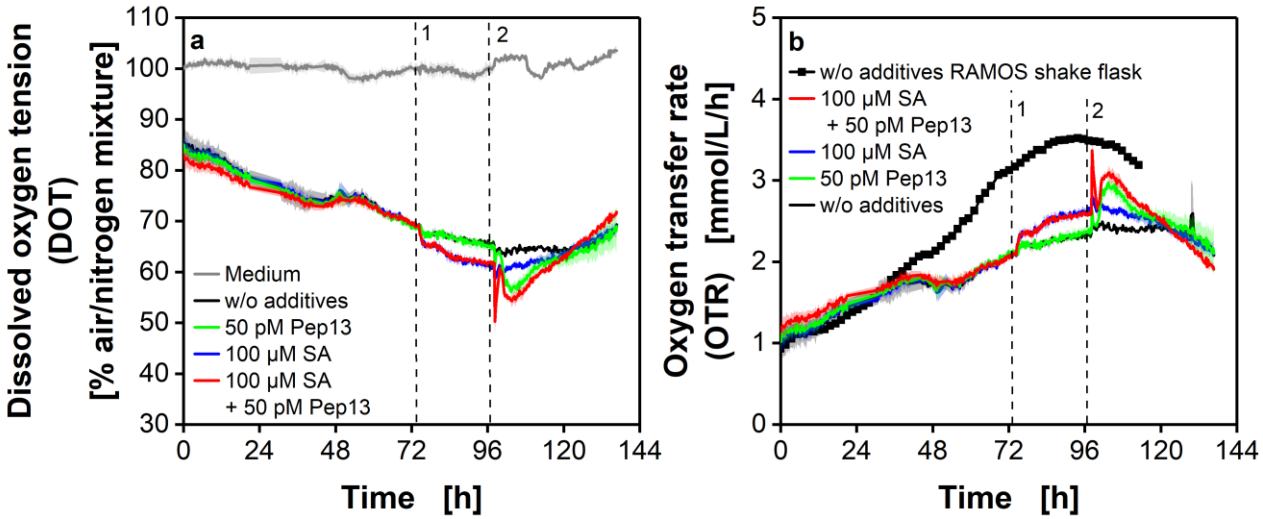

Figure A 8 DOT and OTR of parsley cell cultures in a MTP aerated with an air/nitrogen mixture.

Parsley cell cultures aerated with an air/nitrogen mixture (partial pressure of oxygen in supplied gas mixture p_{O2} = 0.15 bar) were cultivated in 48-deep-round-well MTPs. PyroScience sensor spots were used to measure the DOT with an in-house built BioLector (**a**). The OTR was calculated from the DOT according to Equation 3 and is shown in **b**, compared to a reference cultivation from shake flasks. Dashed vertical lines indicate the addition of salicylic acid (SA) (1) and Pep13 (2). MTP cultivation conditions: V_L = 2 ml, n = 600 rpm, d_0 = 3 mm and 25 °C in modified Gamborg's B5 medium. Mean values were calculated from three wells and the SD is indicated by colored shadows. The data were normalized as described in Material and Methods. Parameters for OTR calculation: k_La = 37 1/h, L_{O2} = 1.22 mmol/L/bar, p_{O2} = 0.15 bar. Shake flask cultivation conditions p_{O2} = 0.21 bar, 250 mL RAMOS flasks, V_L = 50 mL, n = 180 rpm, d_0 = 50 mm and 25 °C.

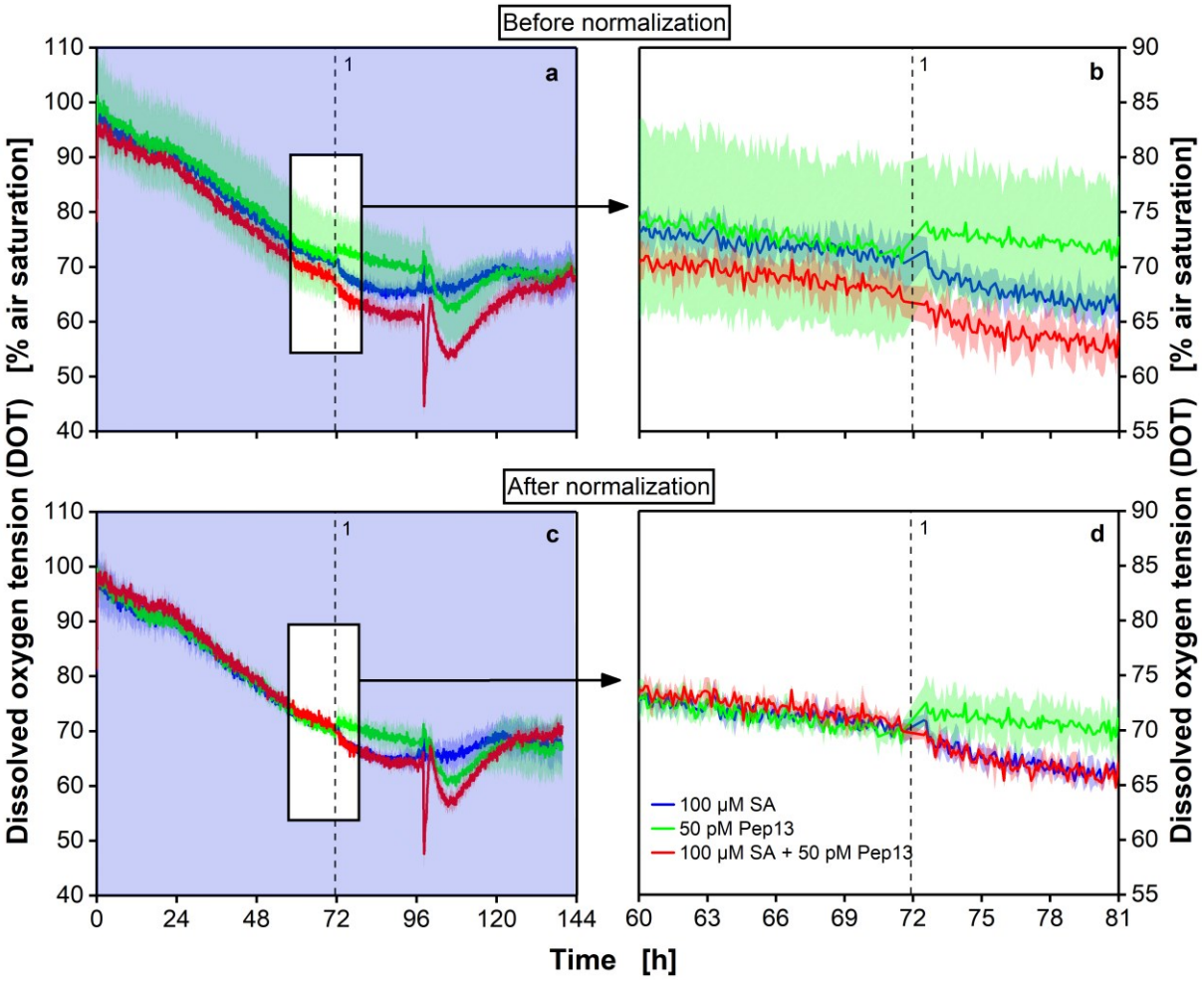

Figure A 9 DOT of parsley cell cultures before (a and b) and after (c and d) normalization.

Normalization was performed before the addition of salicylic acid (SA) after 72 h (Material and Methods: Normalization of DOT and OTR data). The data are drawn from the cultivation shown in Fig. 3**e.** In **a** and **c** inserts are depicted, which are enlarged in **b** and **d**. In **c** and **d** it is shown, how curves are aligned on top of each other after normalization. Parsley cell cultures were cultivated in 48-deep-round-well MTPs. 100 µM SA was added after 72 h and 50 pM Pep13 after 96 h. PyroScience sensor spots were used to measure the DOT with an in-house built BioLector. The dashed vertical lines indicate the addition of SA after 72 h. MTP cultivation conditions: V_L = 2 ml, n = 600 rpm, d_0 = 3 mm and 25 °C in modified Gamborg's B5 medium. Mean values were calculated from three wells. The standard deviation is indicated by colored shadows.